THE SOMATOSENSORY AND VESTIBULAR INTERACTION IN HUMAN
POSTURAL CONTROL

A THESIS SUBMITTED TO
THE GRADUATE SCHOOL OF NATURAL AND APPLIED SCIENCES
OF
MIDDLE EAST TECHNICAL UNIVERSITY

BY

MUSTAFA EMRE AKÇAY

IN PARTIAL FULFILLMENT OF THE REQUIREMENTS
FOR
THE DEGREE OF DOCTOR OF PHILOSOPHY
IN
MECHANICAL ENGINEERING

SEPTEMBER 2015

Approval of the thesis:

THE SOMATOSENSORY AND VESTIBULAR INTERACTION IN HUMAN POSTURAL CONTROL

submitted by **MUSTAFA EMRE AKÇAY** in partial fulfillment of the requirements for the degree of **Doctor of Philosophy in Mechanical Engineering Department, Middle East Technical University** by,

Prof. Dr. Gülbin Dural Ünver
Dean, Graduate School of **Natural and Applied Sciences** ⎯⎯⎯⎯⎯⎯

Prof. Dr. R. Tuna Balkan
Head of Department, **Mechanical Engineering** ⎯⎯⎯⎯⎯⎯

Prof. Dr. Mustafa Kemal Özgören
Supervisor, **Mechanical Engineering Department, METU** ⎯⎯⎯⎯⎯⎯

Assoc. Prof. Dr. Senih Gürses
Co-supervisor, **Engineering Sciences Department, METU** ⎯⎯⎯⎯⎯⎯

Examining Committee Members:

Prof. Dr. Bülent Emre Platin
Mechanical Engineering Department, METU ⎯⎯⎯⎯⎯⎯

Prof. Dr. Mustafa Kemal Özgören
Mechanical Engineering Department, METU ⎯⎯⎯⎯⎯⎯

Prof. Dr. Hakan Işık Tarman
Engineering Sciences Department, METU ⎯⎯⎯⎯⎯⎯

Assist. Prof. Dr. Ergin Tönük
Mechanical Engineering Department, METU ⎯⎯⎯⎯⎯⎯

Prof. Dr. Metin Uymaz Salamcı
Mechanical Engineering Department, Gazi University ⎯⎯⎯⎯⎯⎯

Date: 15.09.2015

I hereby declare that all information in this document has been obtained and presented in accordance with academic rules and ethical conduct. I also declare that, as required by these rules and conduct, I have fully cited and referenced all material and results that are not original to this work.

Name, Last Name: MUSTAFA EMRE AKÇAY

Signature   :

ABSTRACT

THE SOMATOSENSORY AND VESTIBULAR INTERACTION IN HUMAN POSTURAL CONTROL

Akçay, Mustafa Emre

Ph.D., Department of Mechanical Engineering

Supervisor : Prof. Dr. Mustafa Kemal Özgören

Co-Supervisor : Assoc. Prof. Dr. Senih Gürses

September 2015, 188 pages

Human upright posture is essential for people during daily activities. Upright posture is a skill, which is acquired before walking during the human development. Classically defined five senses (as the sense of kinesthesia is not included) are not enough to obtain this difficult and important skill. Thus, the humans need another group of senses; i.e., proprioception, vestibular sensor, joint receptors etc. to achieve the upright posture. In this thesis, two distinct stimulations were given to the subjects to identify the two different kinematic frames of reference. The first perturbation was above the vestibular threshold (high angular velocity) so gravity vertical has been expected to be the reference frame. The second stimulation was below the vestibular threshold thus, the somatosensory system has been proposed to dominate the postural behavior where the reference frame was hypothesized to be the platform normal. A tilt platform was developed and manufactured to check this hypothesis. The experiments were performed in complete darkness. We have shown that the subjects demonstrated a vestibular dominated postural behavior for the high frequency perturbation (kinematics data revealed that postural corrections were performed with respect to gravity vertical) whereas, subjects' behavior for the low frequency perturbation presented a habitual postural sway-like behavior on the platform. The findings were mathematically modeled by using a 3-DoF inverted pendulum including vestibular and somatosensory dynamics (optimizing the system parameters), where

joint control torque compensated for gravity vertical for the high frequency whereas, control strategy used for the low frequency depended on compensation for CoP deviations.

ÖZ

İNSAN DİK DURUŞ KONTROLÜNDE SOMATOSENSORİYEL VE VESTİBÜLER ETKİLEŞİM

Akçay, Mustafa Emre

Doktora, Makina Mühendisliği Bölümü

Tez Yöneticisi   : Prof. Dr. Mustafa Kemal Özgören

Ortak Tez Yöneticisi : Doç. Dr. Senih Gürses

Eylül 2015 , 188 sayfa

İnsan dik duruşu günlük aktiviteler sırasında insanlar için çok önemlidir. Dik duruş insan gelişimi sırasında yürüyüşten önce edinilen bir beceridir. Klasik olarak tanımlanan beş duyu (kinestezi duygusu dahil değildir), bu zor ve önemli beceriyi elde etmek için yeterli değildir. Bu nedenle, insanlar dik duruşu sağlamak için başka bir grup duyuya; propriyosepsiyon (derin duyu), vestibüler sensör, eklem reseptörleri v.b., ihtiyaç duyarlar. Bu tezde, iki farklı kinematik referansı belirlemek için iki farklı uyaran deneklere verildi. İlk örseleme vestibüler eğişiğin üzerindeydi (yüksek açısal hız); böylece, yerçekimi düşeyinin referans olması bekleniyordu. İkinci uyaran vestibüler eşiğin altındaydı; bu nedenle, somatosensorial (beden duyusal) sistemin postural davranışı yönettiği öne sürülmüştür (platform normalinin referans olduğu hipotezi kurulmuştur). Bu hipotezi kanıtlamak için bir örseleme platformu geliştirilmiş ve imal edilmiştir. Deneyler tam karanlıkta gerçekleştirilmiştir. Denekler yüksek frekanslı örseleme için vestibüler hakim bir postur davranışı göstermiştir. Kinematik veriler, postur düzeltmelerinin yerçekimi normaline göre yapıldığını göstermiştir. Diğer yandan, düşük frekans uyaranında, denekler platformun üzerinde alışageldikleri postur salınımlarına benzer davranış göstermişlerdir. Bulgular, yüksek frekans uyaranı için eklem torklarının yerçekimi düşeyine göre telafi edildiğini göstermiştir. Bulguların, vestibüler ve beden duyusal sensör dinamikleri kullanılarak, 3 serbestlik dereceli ters sarkaçlar ile matematiksel modeli geliştirilmiştir. Modeldeki sistem parametreleri op-

timize edilmiştir. Diğer taraftan, deneklerin düşük frekans uyaranı için kullandıkları stratejinin ağırlık vektörlerinin iz düşümünü ayak altındaki basınç merkezi (CoP) ile öpüştürmek (sakin duruş stratejisi) olduğu ve bu merkezin de gezindiği gösterildi.

Anahtar Kelimeler: İnsan Dik Duruş Kontrol Sistemi, Vestibüler Sistem, Somatosensöriyel Sistem, Sensör eşikleri ve kinematik referans, Sensör Füzyonu

To my wife
Şafak

and my family
Safiye, Abdülkadir, Tuğçe

ACKNOWLEDGMENTS

I would like to express the deepest appreciation to my supervisor Prof. Dr. Kemal Özgören and my co-supervisor Assoc. Prof. Dr. Senih Gürses. Without their guidance and persistent help this dissertation would not have been possible.

I would like to present my thanks to the members of the thesis supervising committee, Prof. Dr. Bülent E. Platin and Prof. Dr. Hakan I. Tarman, for their insightful advice.

I owe the greatest thanks to my dear family for their endless support througout my education.

Finally, I express my deepest gratitude to my wife, for their continuous encouragement, understanding, and support.

TABLE OF CONTENTS

xiii

LIST OF TABLES

TABLES

LIST OF FIGURES

FIGURES

xvii

LIST OF SYMBOLS AND ABBREVIATIONS

F_x Force in x direction

F_y Force in y direction

F_z Force in x direction

G_{xx} One Sided Power Spectral Density Function

M_x Moment in x direction

M_y Moment in y direction

M_z Moment in x direction

R_{xx} Auto-correlation Function

Ψ Root Mean Square

θ Angular Displacement

A Cross-sectional area of the cylinder

P Pressure

Q Flow Rate

T Torque

CAD   Computer Aided Drawing

CCR   Cervico-collic Reflex

CNS   Central Nervous System

CoM   Center of Mass

CoP   Center of Pressure

DoF   Degree of Freedom

FFT   Fast Fourier Transform

PID   Proportional Integral Derivative

RMS   Root Mean Square

VCR   Vestibulo-collic Reflex

CHAPTER 1

INTRODUCTION

This chapter is devoted to introduce the motivation of the thesis and to define the hypothesis. The objective and scope of this thesis are also stated.

1.1 Motivation

Human postural control is the ability to maintain body orientation and stability against the gravitational force [3], which is gained prior to walking and even talking of the babies [4]. Thus, humans should succeed to manage their body orientation and stability while performing many daily activities such as standing, walking, driving or talking [5]. On the other hand, human can encounter many postural positions in their daily life; for instance, driving a car while on a seat is an example of a sitting posture or waiting on a tail that is an upright stance position. Especially, the human upright stance is a very unstable task due to the gravitational forces. Humans should achieve to keep their center of body mass projection (center of pressure (CoP)) within their base of support which is related to their feet. This stability and orientation should be accomplished in two planes that are the frontal plane and the sagittal plane. These planes are the front view and side view of a human, respectively. Figure 1.1 illustrates these planes.

Body Planes

| Sagittal/Anteroposterior Plane | Frontal/Lateral Plane | Horizontal/Transverse Plane |
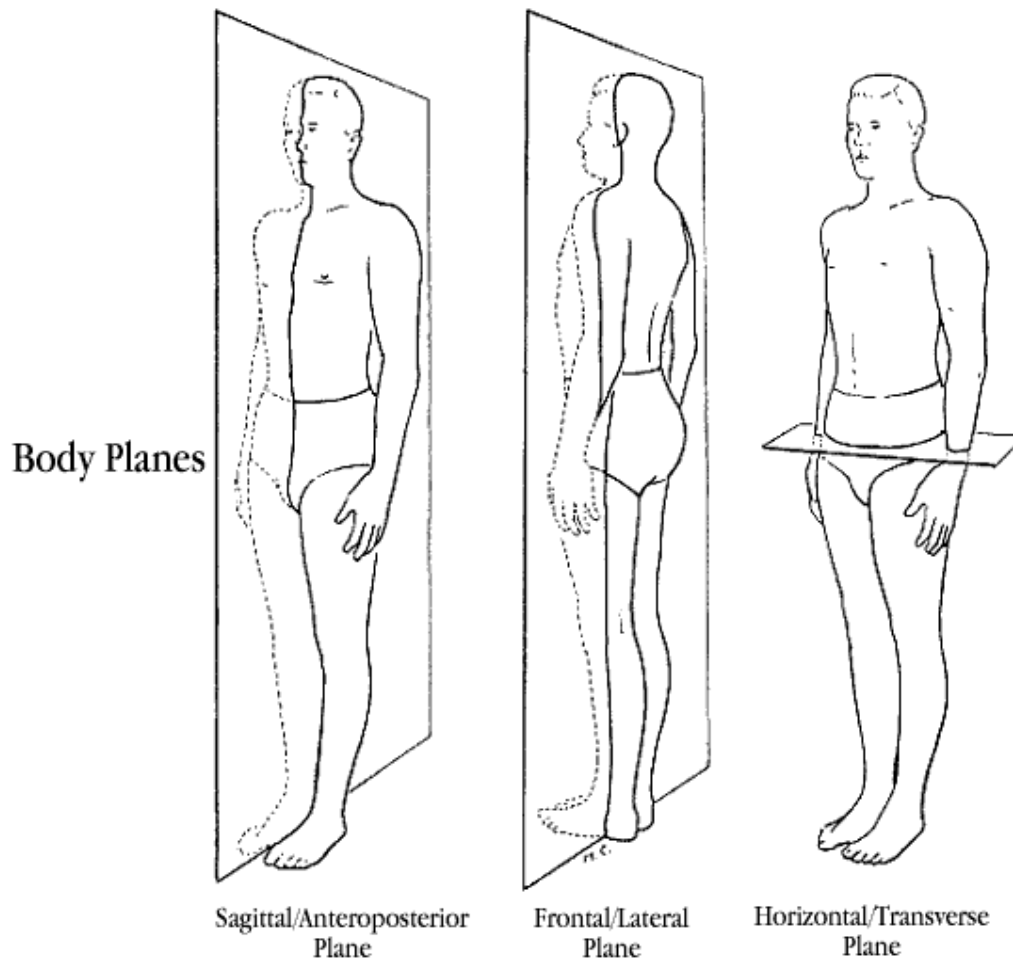
Figure 1.1 Three planes of motion for the human body [1]

The human erect posture in the sagittal plane is inherently unstable because the human body movements in the sagittal plane are similar to the motion of inverted pendulums. Therefore, to obtain the stability in the sagittal plane is the most difficult among these two planes.

The human erect posture is a very challenging and a crucial task for human daily activities. There are many defense mechanisms against the malfunction of the erect posture. The most basic mechanism (primary) is related to the reflexes. The second one is the autonomous movements that take place after the reflexes in time (temporal) and is accomplished through modulation of the reflexes, which are task depended and adaptable to different physical environments. On top of those mechanisms (the third stage), there are also the voluntary movements; which as a whole (with the previous

2

two stages) constitute the human behavior.

Two approaches are widely used for understanding the adaptive movements. These are static postural control and dynamic postural control approaches. The disturbances (i.e. tilt or linear movements) are applied to the human for the latter one. The former one is also called quiet stance at which external disturbances are not applied to human.

Figure 1.2 An example of dynamic posture system [1]

Humans are equipped for sustaining postural stability over a wide range of complex scenarios and configurations. There are basically two scenarios of special interest to clinical and engineering studies: the static posture and the dynamic posture during standing. Different postural control strategies can be selected by the central nervous system depending on the scenario. The two posture regulation scenarios overlap in the necessity for maintaining the balance of the body through a stabilizing postural control process [6, 7].

Human upright stance is inherently unstable without a balance control scheme. This scheme consists of central nervous system (CNS) (sensorimotor processes using the vestibular, joint angle proprioceptive, force sensors and visual perception) and mus-

culoskeletal system. This task will become more difficult due to aging, illness and disabilities. The neural mechanisms that determine control patterns during quiet standing postural regulation are still not well understood.

Postural sway during standing is detected by three sensory systems (the visual, vestibular sensors and the somatosensory system), and upright posture is stabilized by feedback mechanisms from these systems (Figure 1.3). It is, therefore, important to analyze the posture control system from a viewpoint of feedback control. In fact, many researchers treat the posture control system as a feedback system [8, 9, 10, 11, 12, 13, 14, 15, 16, 17]. Feedback information from each sensory system is integrated within the central nervous system, and the contribution of each system is modulated according to environmental conditions. In order to understand the basic mechanisms of sensory feedback, it is essential to investigate the characteristics of all sensors.
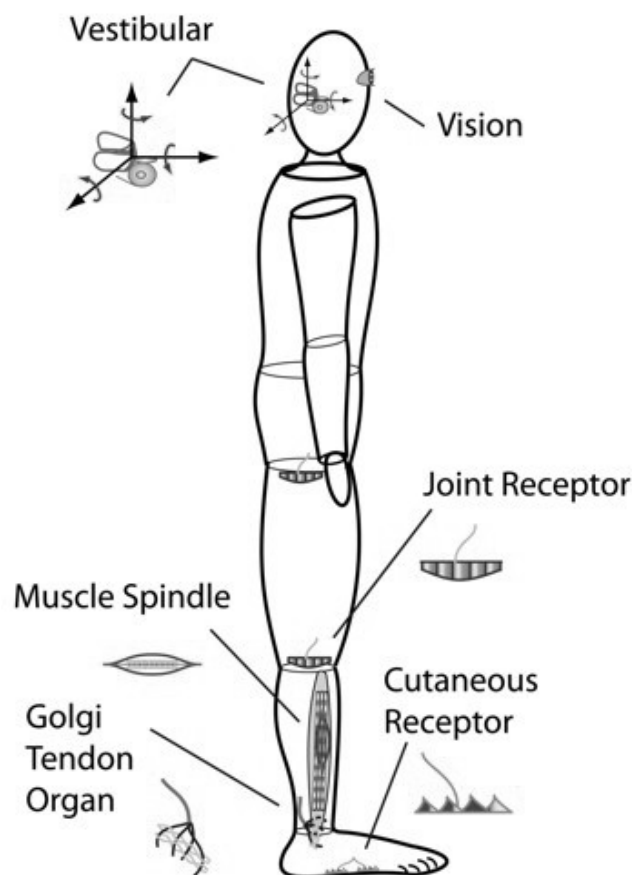
Figure 1.3 Sensors of human postural control system

1.1.1 The Somatic Senses in Different Biological Phyla

The somatosensory system is very important for postural control [18, 19, 20]. Figure 1.4 shows the interior structure of the dermis. Here, the receptors sensitive to light touch are located in dermal papillae. On the other hand, the receptors sensitive to deep pressure and vibration are in the reticular layer. Although the somatosensory system is the most wide spread part of the central nervous system (it is ubiquitous), it is the least known part of it with its relations to human postural dynamics and control.
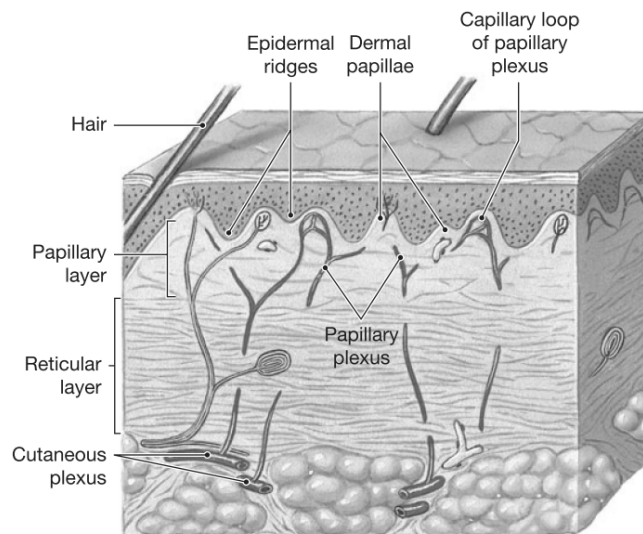
Figure 1.4 Dermal circulation shown are the cutaneous and papillary plexuses

Every organism has an external skin or other covering that encloses its body and separates it from the environment [21]. Through this covering, the animal receives information about the presence of objects, other organisms, or physical changes in its environment. The Greek word for body is *soma*, and the sensory modalities that are signaled by receptors in and near the body surface are referred as *the somatic senses*.

The most basic and primitive somatic sense is the *noxious sens*e, which is the reception of stimuli that are harmful or signal potential harm to the organism. A second modality is the ability to sense the *ambient temperature*. A third category may be referred to as *crude touch*; this includes *light touch* and *pressure*, which are distinct in some organisms and mixed in others. Finally, there is the *fine tactile sense*, the ability to make precise surface discrimination in space and time.

These sensory modalities can also be grouped according to the nature of the stimulus energy. Thus, stimuli that effect the body may be classed as chemical (some kinds of noxious stimuli), radiant (temperature, sometimes noxious), and mechanical (some noxious stimuli, crude touch, and tactile). Chemical stimuli require chemical transduction by chemoreceptor mechanisms in the sensory membrane; temperature is transduced by *temperature receptors*; and various kinds of mechanical stimuli are transduced by *mechanoreceptors*.

1.1.1.1 Invertebrates

Invertebrates (above the sponges) characteristically have tough outer covering, called a cuticle. In worms and molluscs, the cuticle is soft. Leech sensory system (e.g., Hirudo medicinalis).

1.1.1.2 Arthropod Sensory Receptors

In arthropods the integument forms a hard skeleton. This step in the evolution requires suitable adaptations of sensory receptor, so that they can detect mechanical and other forms of stimuli through the hard outer coating. The simplest and most common type of structure for achieving this task is the sensillum trichodeum, or sensory hair [21]. Sensory hairs are scattered widely over the body surface. Any force that displaces the hair, such as touch, air movement, or changes in pressure, causes stimulation of the sensory cell. Sensory hair acts as a force transducer.

1.1.1.3 Vertebrates

By far the greatest amount of information about the general somatosensory system in vertebrates has been obtained in the mammal, much of it in primates and humans. This is partly because the mammalian skin is a relatively general, unspecialized covering.

There are two main types of skin. One type, found our palms and fingertips, is called glabrous, or hairless skin. The other type, found over most of the rest of our body, is

called hairy skin [21].

1.1.2 The Somatic Senses in Different Receptors

1.1.2.1 Pacinian Corpuscle

Pacinian corpuscle is associated with a special end organ, and the end organ is of medium-sized myelinated fiber, the A-beta (Aβ) type (6-12 μm in diameter). It is one of the largest of the end organs, situated deepest in the dermis. The Pacinian corpuscle has a wide spread distribution, in the connective tissue of muscles, the periosteum of bones, and the mesentery of the abdomen.

The Pacinian corpuscle is composed, like an onion, of concentric layers of cellular membranes alternating with fluid-filled spaces. The picture that has emerged from electron microscopic studies is the naked ending of the nerve fiber surrounded by an inner core of incomplete shells of cell processes and collagen fibers. Making up the bulk of the corpuscle are outer complete lamellae [21].

The receptor response of the Pacinian corpuscle has been shown to be a rapidly adaptive receptor response. Experiments performed on the desheated Pacinian corpuscle revealed that the lamellae act as a filter, to absorb slow changes impressed upon them, while still passing on rapid changes to the nerve endings.

The Pacinian corpuscle is thus constructed to signal rapid changes in touch pressure; this is presumably why our sensation of a steady pressure applied to the skin soon fades away. This organ is well suited for signaling rapid vibratory *stimuli* [21]. The maximum sensitivity is in the range of 200-300 Hz. This form of stimulation may be important in our tactile perception of objects and textures. Note the extremely high sensitivity of the corpuscle; less than a 1 - μm displacement at its surface is sufficient to give a threshold response.

1.1.2.2   Tactile End Organs

Most of the other end organs are located superficially in the skin, near the junction between the dermis and epidermis. These are specialized to be sensitive to different types of tactile stimuli.

A systematic study has been carried out in humans to identify different receptor types and relate them to sensory perception. Using the method called microneurography, Vallbo and Johansson have been able to study different types of responses in the awake human and relate them to psychophysical functions [21]. Two of the basic response properties of any receptor are its size of receptive field and its rate of adaptation. With regard to the adaptation, the tactile receptors in the glabrous skin of the hand fall into two groups, fast or slowly adapting [21]. The rapidly adapting type includes the Meissner corpuscle and the Pacinian corpuscle. Within this type, the adaptation shows interesting differences. The Meissner corpuscle is not quite as rapidly adapting as the Pacinian corpuscle, and therefore has a lower range for signaling vibratory frequency. In addition, the threshold for activation of the Meissner corpuscle is much higher than the threshold of the Pacinian corpuscle. Pacinian and Meissner corpuscles thus provide an interesting comparison. The Pacinian corpuscle has an extremely low threshold, high temporal resolution, and low spatial resolution; by contrast, the Meissner corpuscle has a higher threshold, lower temporal resolution, but higher spatial resolution.

The slowly adapting type of response arises in Merkel's discs and Ruffini endings. Here also there are differences. Both receptors respond to a steady indentation of the skin with a sustained discharge, but the Merkel's disc shows an overshoot during the initial phasic part of the indentation. It can thus provide information about changes in stimulus intensity as well as steady-state values. Similar differences have been found between the two types of slowly adapting receptors: the Merkel's disc receptors have small receptive fields, whereas the Ruffini ending receptors have very broad receptive fields.

A vibrating probe is very effective stimulus for Meissner's corpuscles, at 30-50 Hz. In life, this kind of receptor is probably most often activated by our fingers moving over

rough or irregular objects. If two points on an object are 2 mm apart, and our finger moves past them at a rate of 80 mm/sec, the second point will excite a given site on the finger at a frequency of 40 Hz.-just right for a Meissner corpuscle. Although as physiologists and neurologists tend to apply a given stimulus at a single site to study receptor responses or sensations, in natural behavior the fingers and hand take an active part by moving over and exploring surfaces in order to give rise to our sensory perceptions. This is called the active touch.

1.1.3   The Vestibular System

The vestibular system is the sensory system that provides the angular velocities and linear acceleration information of the head to CNS. Figure 1.5 shows the anatomy of vestibular system. The vestibular system contains three semicircular canals in each labyrinth. They are approximately orthogonal (right angles) to each other, and are called the horizontal (or lateral), the anterior semicircular canal (or superior) and the posterior (or inferior) semicircular canal. Anterior and posterior canals may be collectively called vertical semicircular canals. The semicircular canal is sensitive to rotation of the head. The movement of fluid pushes on a structure called the cupula, which contains hair cells that transduce the mechanical movement to electrical signals [22].
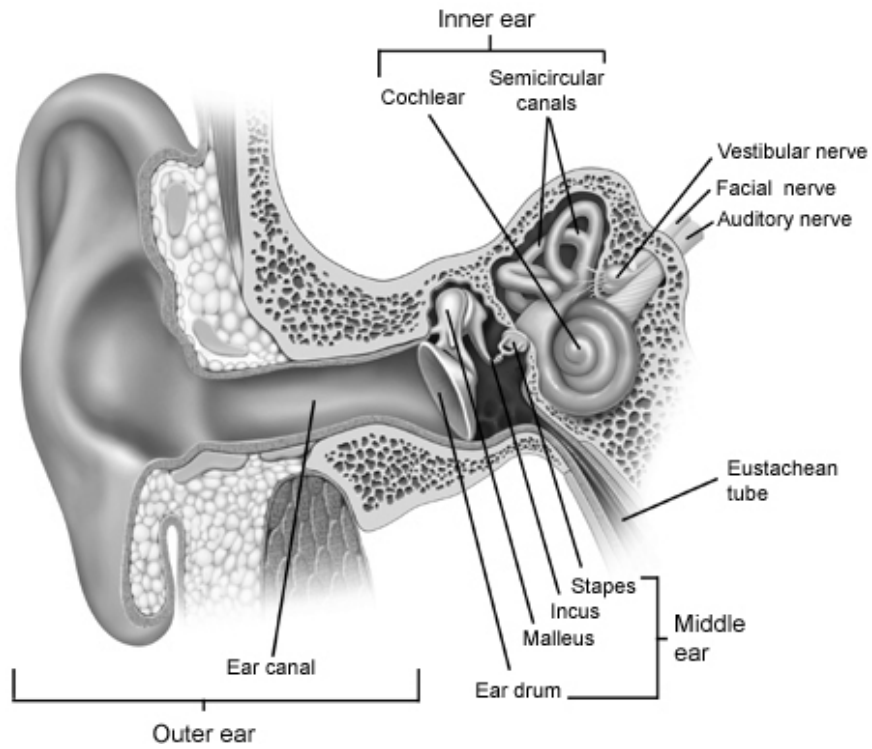
Figure 1.5 Human vestibular system [21]
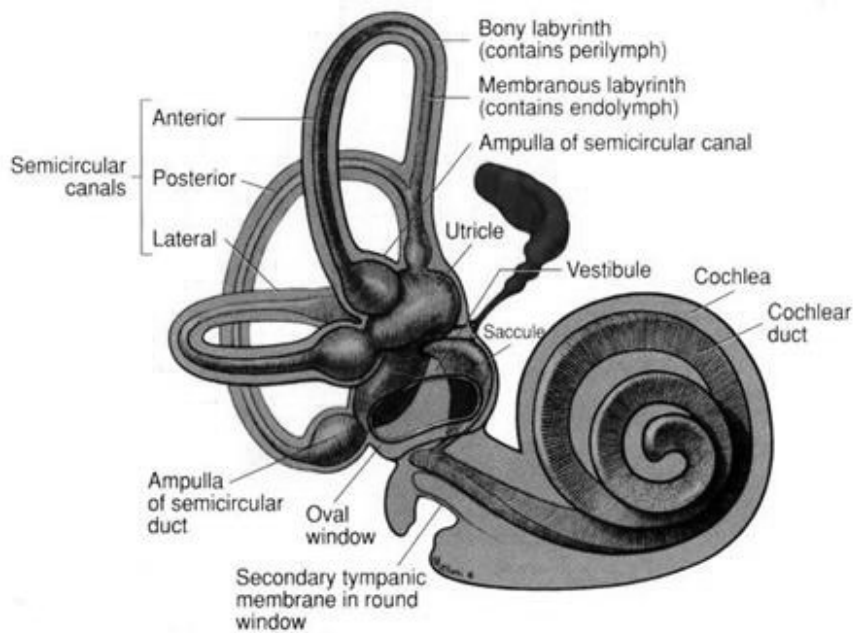
Figure 1.6 Internal structure of the vestibular system [21]

In general, these special organs fall into two categories. One is the statocyst. This

characteristically takes the form of a fluid-filled pocket that has, in its wall, a patch (called a macula) of sensory cells (Figure 1.5). The cells have fine hairs which support, at their tips, some dense crystals glued together with a jelly like material. When the statocyst is tilted, the heavy crystals weigh on the hairs, making them bend, which leads to an increased discharge of impulses in the sensory fibers. This arrangement is sensitive to velocity. Since the mechanism is sensitive to the force gravity, the statocyst is a gravireceptor. Gravity is a universal force on all organisms, and it is not surprising that nearly all active organisms should have gravireceptors. The statocyst must be an effective organ for this purpose, because, with the conspicuous exception of the insects, most animals have gravireceptors.

The other type of organ contributing to the sense balance is the canal. As shown in Figures 1.5, and 1.6, it is fluid-filled canal with a patch of sensory cells in the wall. These cells also have hairs, which project into the lumen, and are embedded in a structure called the cupula, a jelly like matrix composed of glycoprotein, which stretches across the lumen of the canal. The patch of cells forms a raised protuberance which is called a crista. When the head rotates, the fluid in the affected canal is displaced, which causes a shearing force on the hairs projecting into the cupula, and this is converted into a burst of impulses. As long as the body movement is changing (either accelerating or decelerating) the cupula will be displaced, but when constant velocity is attained, the fluid of the canal moves at the same rate as the body, and the cupula returns to its original position. Thus, the canal type of organ is especially adapted to detect angular acceleration. There are a few examples of this type of organ in invertebrates (e.g., lobster, octopus) but they are a constant feature of the vertebrates, where they are called the semicircular canals.

1.1.4 Postural Representation in the CNS (Body Schema)

There are two main aspects of human posture; first one being the anti-gravity function maintaining an erect posture for a multi-segmented body through creating ground reaction forces which are used by a complex neuro-muscular-skeletal control system for balancing the body under a variety of tasks, while the second function is for serving as an interphase in-between the environment (exterior) and the "self" for acting

11

and perceiving in a behavioral context which generally has an ecological meaning [19, 38, 23]. The first function has been adapted to the earth through unique phylogenetic pathways which has a rigorous spatial organization in the nervous system maintaining a stable backbone to movement involved in the motion repertoire of the organism [21, 24], while the second function is much more universal and evolves through ontogenesis for the semantics of a sequence of postural actions in a self-realized postural language.

In order to achieve these two tasks simultaneously it has been proposed by Gurfinkel's group that the human erect posture is organized in the human cortex at two distinct levels; i.e., the lower level (operative level) surrounding the projection of the center of gravity within a bounded region (center of pressure) at the horizontal plane (base of support) at around the equilibrium point while the higher level (second level) is prescribing the equilibrium [25]. The higher level (body postural schema) is supposed to represent the postural configurations (self) with its relations to the external world. The existence of such a kind of postural representation (body schema) has been checked against illusions (static and/or dynamic) created through sensory ambiguities caused by delivering vibration to tendons [26], electric stimulation to vestibular system [27], motion to visual scenes [28], auditory signals [29], and very slow tilt/translation stimulation (below vestibular threshold) to mechanical receptors (mainly somatosensory) at foot, finger, etc [29]. It is important to note specially (because of pointing to the adaptability of the schema) the experiments performed at microgravity conditions (rescaling the weight vector adapted to the earth) to investigate the contribution of the putative receptors signaling about the load to the body schema [30].

In order to show the existence of the second level representation (higher level) Gurfinkel et al used a superslow tilt paradigm (0.007 Hz with 1.5^0 amplitude sinusoidal stimulation which is below vestibular threshold) trying not to activate the inherent reflex mechanisms, where they came across with a paradoxical picture of motion control such that large deviations of center of pressure (projection of the center of gravity to the plane of support) from the equilibrium point were compensated (due to the ankle stiffness adjustment through modulation of the stretch reflex [31]) very slowly (comparable to the very low frequency of the stimulation) while quick and small oscillations (like in the quiet stance around 1 Hz) were corrected very fast [25].

12

This paradigm seems to be a modulation of the quiet stance with a very low frequency of perturbation. Later, they discussed that maintenance of the current equilibrium continues working not with respect the habitual vertical, but rather accomplishing the task according to a slowly and continuously changing set-point. They proposed the ability to change the set-point as the indication of the existence of a higher level of (representation of the postural body schema) postural control (in the sense of decision maker for the reference signal for equilibrium) however the source/reason of the very slow excursion of the equilibrium point (or the set-point) has not been thoroughly explained.

1.1.5 Nonlinear Postural Dynamics

Erratic motion of the complex quiet stance dynamics have been studied by a number of researchers such as Collins and De Luca [32, 33] by using diffusion plots' analysis that revealed a fractional stochastic process with at least two scaling regions (a bounded, correlated random walk); a short term region (<1s) with positive correlations in center of pressure (CoP) suggesting an open-loop control mechanism which allow a certain amount of sloppiness (CoP to drift for some time and/or displacement) while long-range negative correlations in the CoP data suggesting a close loop control mechanisms utilized over long-term intervals of time (>1s - <10s). Later Duarte and Zatsiorsky have shown the existence of long-range correlations (negative correlations resembling 1/f noise characteristics) in postural dynamics with single scaling exponents (through detrended fluctuation analysis) over a broad range, from 10 seconds to 10 minutes during prolonged human standing [34]. Furthermore fractal properties of human quiet standing has been shown to exist quantified by computing Hurst exponent [35] and revealed through correlation dimension estimates using ergodic system theory [36]. It is very important to show the existence of a fractal structure for a complex (nonlinear) dynamics, which points to a self-organizing self-similarity in different time and length scales (eg, human postural dynamics and control can be accepted a complex neuro-musculo-skeletal system which is hierarchically structured with a considerable number of nonlinear sources like motor redundancy and polyarticularity [37] being driven by different senses relying on coming information from different sources with different delays and frequency responses and even working in different

domains [38]) that may give rise to a deterministic behavior out of chaos depending on the input and system parameters [39]. Thus in the light of nonlinear behavior, we can recall the paradoxical motion observed in Gurfinkel's very slow tilt perturbation paradigm (from the point of nonlinear postural dynamics) in order to investigate how quiet stance can demonstrate a modulated behavior with respect to the frequency of perturbation.

Indeed, Zatsiorsky and Duarte decomposed CoP trajectories into rambling and trembling dynamics (in antero-posterior direction) such that, while trembling trajectories were related to correcting the postural deviations from instant equilibrium points (through restoring forces whose source is unidentified) prescribed by the rambling trajectory whose reason is unknown (although discussed as being the noisy character of the sensory fusion and decision making in the central nervous system (CNS) and/or lacking accurate enough proprioceptive originated information to CNS) [40]. Phase plane analysis of this decomposition revealed multi-poles for slowly wandering instantaneous equilibrium points due to where limit cycle like attraction takes place through trembling action. On the other hand, the possible nonlinear dynamical mechanisms behind the coupled dynamical subsystems in quiet standing have been studied by a couple of researchers; e.g.; Bottaro et al proposed postural sway as being a sequence of incipient falls stabilized by intermittent bursts (a weaker stability than asymptotic stability), Gurses et al [39, 41] used a threshold (may be a sensory threshold) driven nonlinear set of control equations for generating the ankle torque where the phase plane dynamics presented hyperbolic trajectories around an unstable equilibrium throwing the body (rambling-like trajectory) to stable equilibrium points around which body oscillates like a limit cycle (trembling-like trajectory). Later (in the same study) it has been shown that (through computing the largest Lyapunov exponent of the system) the dynamics presents deterministic chaos (through bifurcations) where it can be changed to periodic motion by tuning the system and/or the perturbation parameters [39].

14

1.1.6 Postural Control Strategies

There are three main strategies for human postural control system. These are ankle, hip and stepping strategies. Figure 1.7 shows these strategies.

Ankle strategy   Hip strategy   Stepping strategy
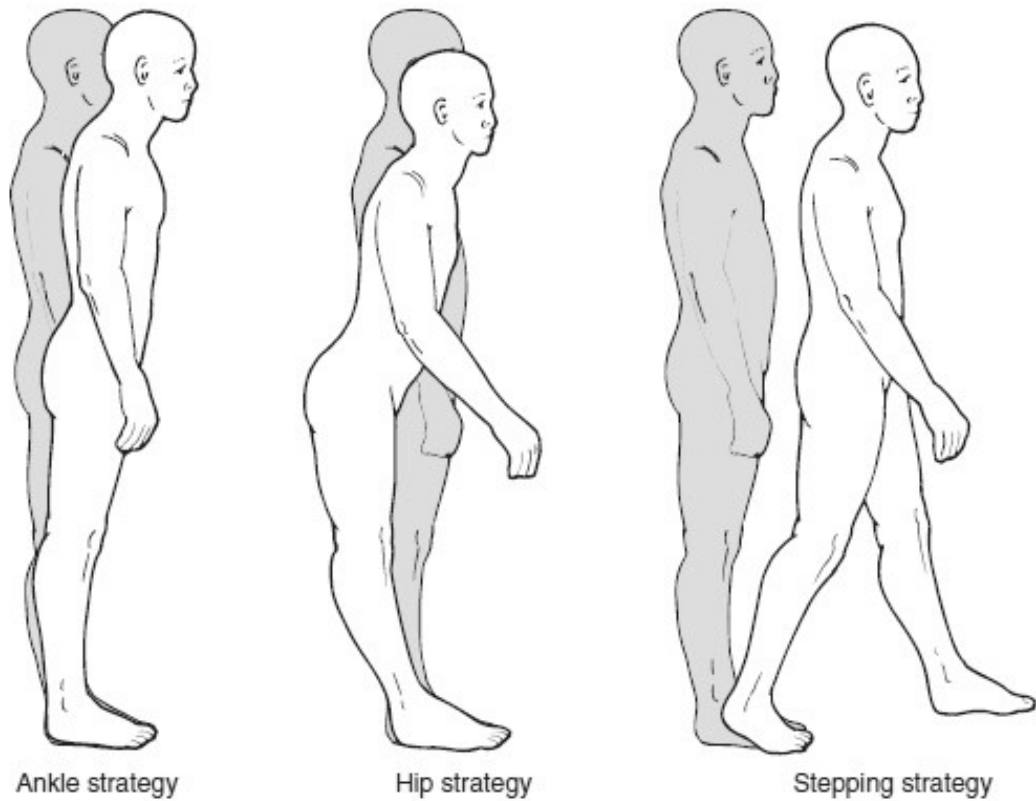
Figure 1.7 Three strategies of human postural control system

The ankle strategy was characterized by body sway resembling a single degree of freedom (DoF) inverted pendulum. In contrast, the hip strategy was characterized by body sway resembling a double DoF inverted pendulum divided at the hip. On the other hand, the stepping strategy was the transition from standing to walking [42, 43, 44, 45, 46].

The merits of biological control have always been highlighted and discussed from an engineering perspective. A properly designed biomechanical model and its computer implementation could quantitatively reproduce the corresponding human performance and help the researchers to understand the core principles of human postural control. At the clinical level, it would be particularly useful for diagnosis and treat-

ment of motor control disorders, and the development of functional electrical stimu-
lation for recovery of lost motor functions. In the practical engineering level, this also
provides insights and inspiration for humanoid robot design [47, 48, 49, 50, 51].

1.2   A Brief Review of Dynamic Postural Control

The prior research about dynamic posture was performed in early 70's. Nashner used
a sway platform in his experiments [8, 52]. Upright postural balancing describes
the dynamics of body posture to prevent falling over a relatively small base of sup-
port under gravitational field. Several experimental methods have been employed to
study human balance control, and a major method was to investigate human postural
response to backward platform translations [53, 54]. Humans have been noted to ex-
hibit characteristically different balancing kinematics that emphasizes either ankle or
hip motion depending upon the magnitude and speed of the platform translation. The
postural strategy being implemented can be characterized by assessing the determi-
nants of body's center of mass (CoM) control.

The fist strategy is ankle strategy. Slow disturbances result in comparable peak ex-
cursions at the ankle and hip. In this case, because the CoM is much farther from the
ankle than the hip, the ankle motion has dominant control over the CoM positioning.
This type of motion is considered "ankle strategy" [53]. For low disturbance veloci-
ties, there is extremely little activation of ventral musculature while the dorsal mus-
cles are activated in ascending sequence, despite the shorter long-loop reflex times of
the knee and hip musculature. This is a recognized pattern in ankle strategy motions
[54]. The second strategy is mixed (ankle and hip) strategy. Rapid disturbances yield
progressively greater hip motion until both joints contribute more equally to balance,
especially later within the recovery motion. This pattern is termed as mixed ankle and
hip strategy. It enables the body to remain within the feasible balance configuration
region by limiting ankle movement, and restricting ankle torque to levels consistent
with maintaining heel contact with the platform. The flexion at the hip and extension
at the ankle that promote CoM recovery are aided by the abrupt deceleration of the
platform at all translational velocities [55]. At higher velocities, there is early activa-
tion of ventral muscles at the knee and hip, and late activation of the dorsal muscles

16

at these joints. This is the characteristic muscle activation pattern associated with the mixed ankle-hip strategy [54].

Human erect posture in reality is maintained a few degrees forward tilt from the vertical [56]. This helps to keep the CoM closer to the center of the stable support area that is located at front of the body. Therefore, ankle flexor activities are rare while ankle extensors are considerably activated. Ankle extensors mostly contribute to control of the ankle joint torque and therefore the body posture during quiet stance. Activity of gastrocnemius lateralis is closely correlated with postural micro-sway [56]. The actual postural control system during quiet stance adopts a control strategy that relies notably on velocity information and that such a controller can modulate muscle activity in an anticipatory manner without using a feed-forward mechanism [57]. The velocity information is most accurate among proprioceptive sensor inputs [58].

Some mathematical models of upright postural control have been developed. For instance, Peterka showed that principally a Proportional Integral Derivative (PID) controller can describe human sensorimotor control system of maintaining postural balance involving primarily ankle motion, which is represented by a link inverted pendulum, and the force feedback is influential at motion of low frequencies [14]. The force feedback primarily influences postural behavior, a gain decline and phase advance by scaling proportionally to the integral of the sensed signal [14]. A gain decline means smaller steady error with respect to the gravitational vertical line. The force-related signal input may arise from the pressure distribution on the feet or muscle tension by Golgi tendon organs. However, balance maintenance in reaction to rapid external disturbances necessitates multi-joint, e.g., mixed hip and ankle, responses. In addition, rapid disturbances may excite high-frequency dynamics that give rise to undesirable oscillations or destabilize a nonlinear system with delays or other phase lags. Peterka's model included neural transmittance delays, but did not provide the confidential details on neuroanatomical structure.

The engineering analysis and modeling of the neuromuscular system is an exciting and challenging area of research where we may learn something about the principles of controlling large, complex systems. In the literature, there were many different approximations for modeling the postural control. One DoF inverted pendulum model

is the most common mathematical modeling approach for mechanical part of the postural control [59, 60, 61, 62, 63, 64]. On the other hand, there were some linear and reflex model studies for the vestibular system [65, 66, 67, 68, 69, 70]. However, the somatosensory system has not been studied as well as the vestibular system. Thus, there has not been found a mathematical model for somatosensory system in the literature. When one looks at the central processing part (brain) of the postural control, two major approaches popped up. These were PID control and the Kalman filter method [14, 59, 71]. The main purpose of the Kalman filter models is that constructing the sensory integration center to centrally generated information. Therefore, these solutions were not related to the physiological of the postural control system. On the other hand, it is suspicious that the human brain is capable of handling numerous and complicated computation for balance estimation that the Kalman filter method needs. In the literature, the frequently used method to model the balance system then comes out to be PID control.

1.3   Hypothesis

The dynamic balance control of human is a highly integrated task. The CNS integrates sensory information, makes decisions based on this information, and then directs the ensemble of muscles during the task. The human sensorimotor system is also a system with the capability of learning, developing, and adapting to improve performance.

The human might be solving the dynamic balance problem by representing the environment and the body (self) in the cortex. Different coordinate systems, which are triggered by different senses (i.e. the somatosensory versus the vestibular system), might happen to be used to create *the body in the space* perception.

We hypothesized that the postural control system (as being nonlinear depending on the sensory thresholds) demonstrates different quality dynamics (from deterministic chaos to periodic motion) depending on the experimental design parameters for perturbation frequency and amplitude. Furthermore, we proposed that the subject will demonstrate a postural behavior (modulation of the joint stiffness, especially the ankle joint) depending on the kinematic frame of reference with respect to which the body

18

is controlled due to the stimulation parameters. The postural behavior is proposed to be a vestibular driven control when the perturbation frequency and the amplitude is above the vestibular threshold; i.e., joint torques generated will compensate due to the gravity vertical. On the other hand, when the stimulation (angular velocity) is below the vestibular threshold the subject's behavior will present a somatosensory driven (adapted to the tilting platform) postural control, where the joint torques will compensate due to the normal direction of the platform.

1.4   Objective and Scope of the Thesis

The main objective is to find some clues for the defined hypothesis whether there exists a perturbation based reference system versus an inertial based reference system that triggers different postural control strategies and/or postural behavior. The other objective of the thesis is to develop a model of human upright stance that is descriptive of the experimentally observed postural response, physiologically relevant, and straightforward to interpret.

A hydraulics tilt platform was produced for investigating these objectives. Moreover, a three degrees of freedom inverted pendulum model with vestibular, joint angle proprioceptive and force sensors are developed.

1.5   Thesis Outline

This dissertation is organized in seven chapters. Following the introduction chapter (the physiological background about human posture regulation), Chapter 2 presents design and production of the hydraulics tilt platform (system identification, modeling and control). Chapter 3 covers the equipments and the setup that are used in the experiments and data acquisition method. In Chapter 4, the protocol for performing the experiments, knowledge about the subjects involved in the experiments, and methods for data analysis are introduced. Chapter 5 presents the mathematical model developed for human balance control system using three degrees of freedom inverted pendulum. In Chapter 6, experimental and simulated results are presented. Finally,

Chapter 7 covers the summary of the main findings of this study and considers further prospects in the research field.

CHAPTER 2

HYDRAULIC TILT PLATFORM

2.1   Introduction

Mechanical perturbation is a must condition for the dynamic posture researches. In this work, human postural control system was studied under dynamic conditions. Therefore, a hydraulic tilt platform, which can perform pitch and roll rotations as mechanical perturbation was developed to study human posture. Two hydraulic cylinders and a proportional valve were used to control the platform. The tilt platform can follow sine waves in the range of 0.5 -10 degrees of amplitude and 0.01 to 1 Hz of frequency. In order to tune the control parameters of the platform a mathematical model of the hydraulics tilt platform has been developed. Afterwards, system parameters in the mathematical model of the platform have been identified by performing some experiments. Figure 2.1 shows the hydraulic tilt platform.
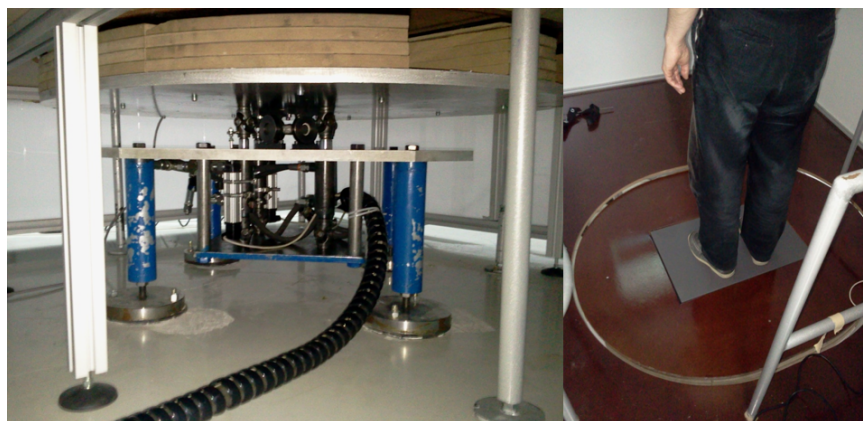
Figure 2.1 Hydraulic tilt platform

2.2 Mathematical Modeling of the Hydraulic Tilt Platform

Figure 2.2 illustrates the hydraulic tilt platform mechanical and hydraulic parts. In this figure, P_1 and P_2 are the hydraulic pressure values inside the cylinders. A is the cross-sectional area of the cylinder and r is the distance between a cylinder and point, O, which is the rotation axis of the platform. Thus, the moment with respect to point, O can be found as:

$$(P_1 - P_2)Ar = T \tag{2.1}$$
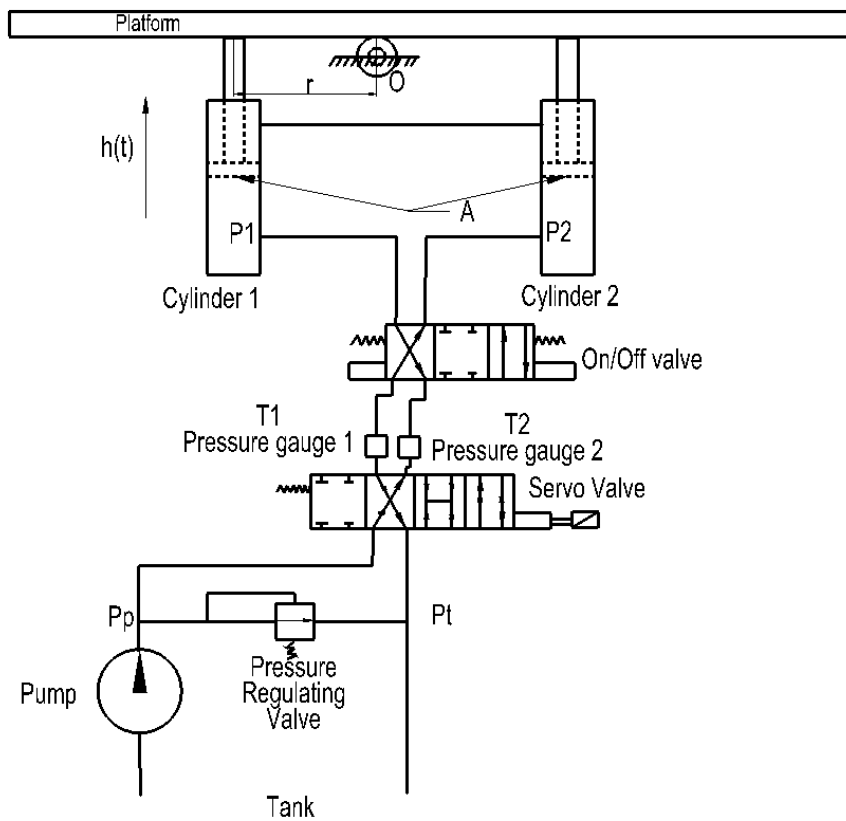
Figure 2.2 Hydraulic tilt platform mechanical and hydraulic scheme

The mechanical equation of motion for the movable platform is

$$I\ddot{\theta} + b\dot{\theta} = T \tag{2.2}$$

22

where I is the moment of inertia about point O. b is the viscous friction in rotation axis. Finally, θ is the rotation angle with respect to a transverse axis passing through point, O.

From equations 2.1 and 2.2

$$I\ddot{\theta} + b\dot{\theta} = (P_1 - P_2)Ar \tag{2.3}$$

The hydraulic equation (conservation of mass) is

$$Q = A\dot{h} \tag{2.4}$$

where Q is the flow rate in m^3/s. h is the linear motion of the hydraulic cylinder and A is the cross-sectional area of the cylinder.

For small angles, $h = r\theta$. Therefore,

$$Q(t) = Ar\dot{\theta}(t) \tag{2.5}$$

The dynamical equation for proportional valve is given in equation 2.6 [72].

$$Q(t) = K_1 x(t) - K_2 \Delta P(t) \tag{2.6}$$

where x is the linear motion of the valve spool. In addition,

$$
\begin{aligned}
K_1 &= C^* \sqrt{\frac{P_p}{2}} \\
K_2 &= C^* \frac{x_0}{4\sqrt{2}\sqrt{P_p}}
\end{aligned}
\tag{2.7}
$$

where x_0 is the leakage value under system maximum pressure. P_p is the maximum pressure supplied by the pressure valve. Equation 2.6 is the linearized equation about $x_0 = 0, \Delta P_0 = 0$ and $Q_0 = 0$ which is the neutral position of the valve spool. C^* is the constant value related to the physical and geometrical properties of the valve.

From equations 2.6 and 2.5

$$K_1 x(t) - K_2 \Delta P(t) = A r \dot{\theta}(t) \tag{2.8}$$

From equations 2.8 and 2.3

$$K_1 A r x = K_2 I \ddot{\theta} + (A^2 r^2 + K_2 b) \dot{\theta} \tag{2.9}$$

From equations 2.9 and K_1 and K_2

$$A^2 r^2 \theta = C^* (\sqrt{\frac{P_p}{2}} A r x - \frac{x_0}{4\sqrt{2P_p}} (I \ddot{\theta} + b \dot{\theta})) \tag{2.10}$$

2.3 Parameter Identification and Simulation

First, the parameters *A* and *r* were calculated from designed Computer Aided Drawing (CAD) studies. These are 804.25 mm^2 and 0.1395 m, respectively. Then, the maximum flow rate was calculated. The valve spool was opened to maximum position and all the hydraulic flow was directed to the one cylinder. Figure 2.3 shows the angular position with respect to time for the platform.

24
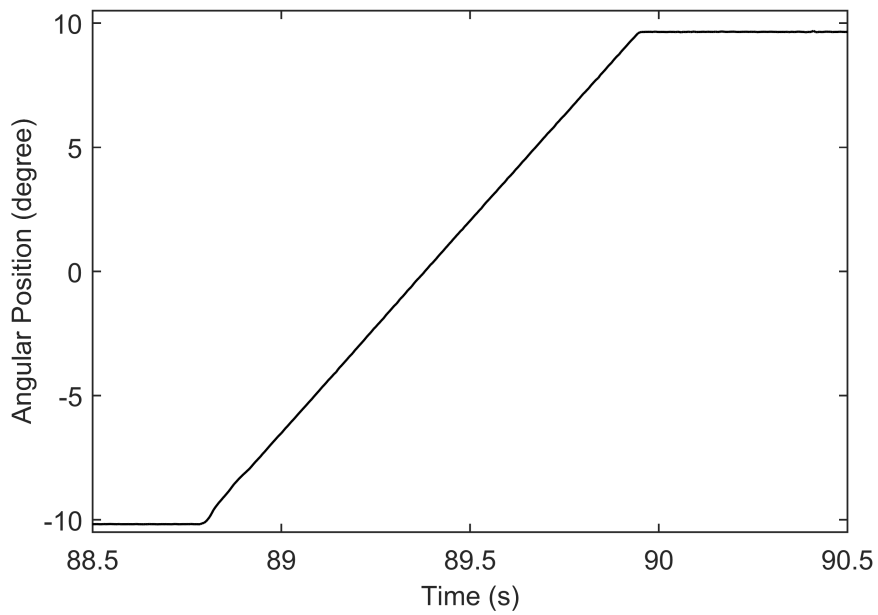
Figure 2.3 The angular position of the platform for max spool opening

The angular velocity was calculated using the ramp of the figure 2.3. Thus, the angular velocity is 0.2954 rad/s for maximum flow rate. Then, the flow rate is 1.9885 l/s from equation 2.5. In addition, the angular acceleration data was calculated from figure 2.3. This data is shown in figure 2.4.
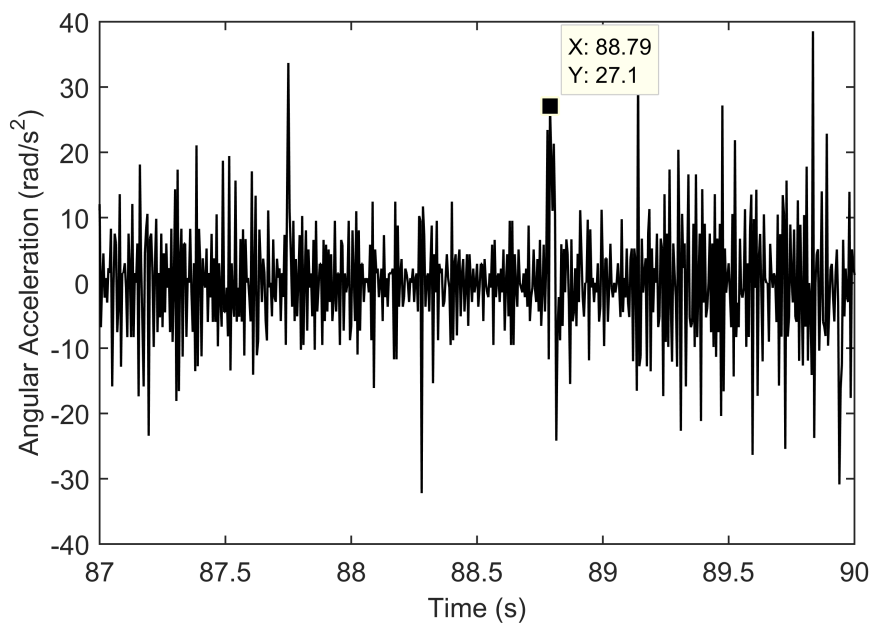
Figure 2.4 The angular acceleration of the platform
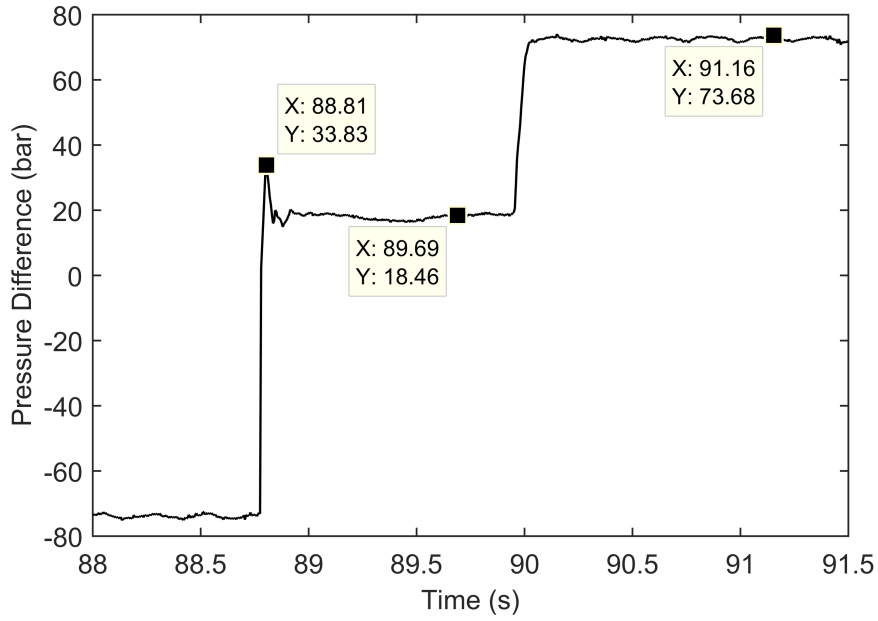
Figure 2.5 The pressure differences between two cylinders

Also, the pressure differences between two cylinders are measured and shown in figure 2.5. Applied torque to the platform can be calculated using the equation $T = Ar\Delta P$. The calculated torque curve is shown in figure 2.6.
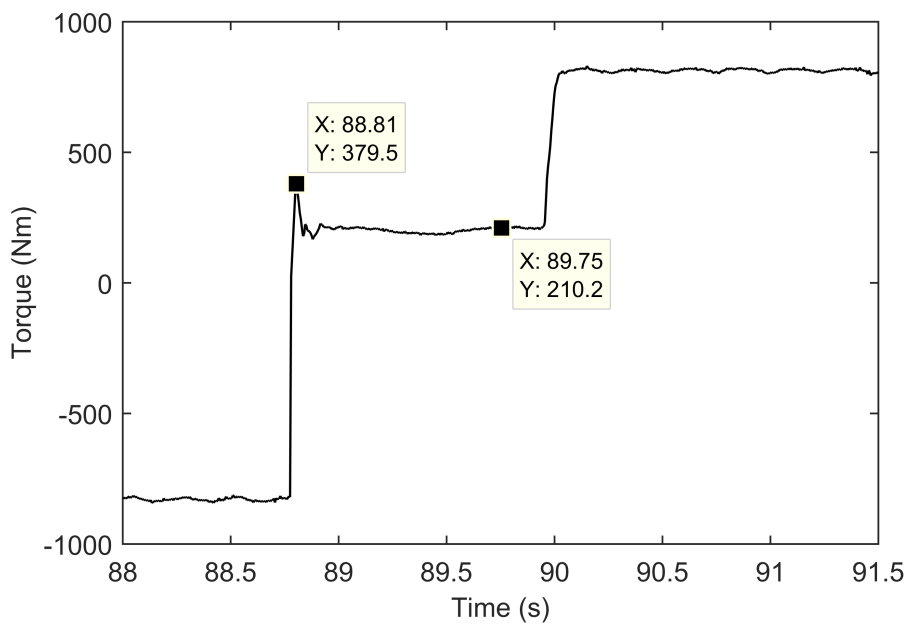
Figure 2.6 Applied torque to the platform while performing figure 2.3 movement

26

The selected values from Figure 2.6 are the starting point of the platform and after reaching the constant angular velocity of the platform. Thus, $T = b\dot{\theta}$ covers the dynamical equation for the platform for latter selected point and $T = I\ddot{\theta} + b\dot{\theta}$ covers for former selected point in figure 2.6. Finally, I and b were calculated using above equations and selected point on figure 2.6. These are 6.24 kgm^2 and 711.92 Nms, respectively.

Next, the platform was moved to the end of the cylinder. Therefore, the hydraulic flows over pressure security valve.

$$x = \frac{K_2}{K_1}\Delta P \tag{2.11}$$

Equation 2.11 can be found using equation 2.6 where $Q = 0$. Also, the following equation can be derived from K_1 and K_2.

$$\frac{K_2}{K_1} = \frac{x_0}{4P_p} \tag{2.12}$$

From equations 2.11 and 2.12,

$$x = \frac{x_0}{4P_p}\Delta P \tag{2.13}$$

X_0 can be calculated after the platform hits the end point of the cylinder and reaching the pressure difference being equal to the maximum supplied pressure value. This value is 0.08 mm for the valve spool and P_p equals to 73.68 *bar*. From equation 2.13,

$$x_0 = 4x \tag{2.14}$$

So, x_0 equals to 0.32 mm. In addition, some experiments were performed for finding the maximum spool movements for maximum flow rate. Figure 2.7 shows these experiments. The lines of platform tilt angle velocity for different spool openings saturated in figure 2.7. Thus, this saturation value for the spool opening is x = 0.21 mm for maximum angular velocity.
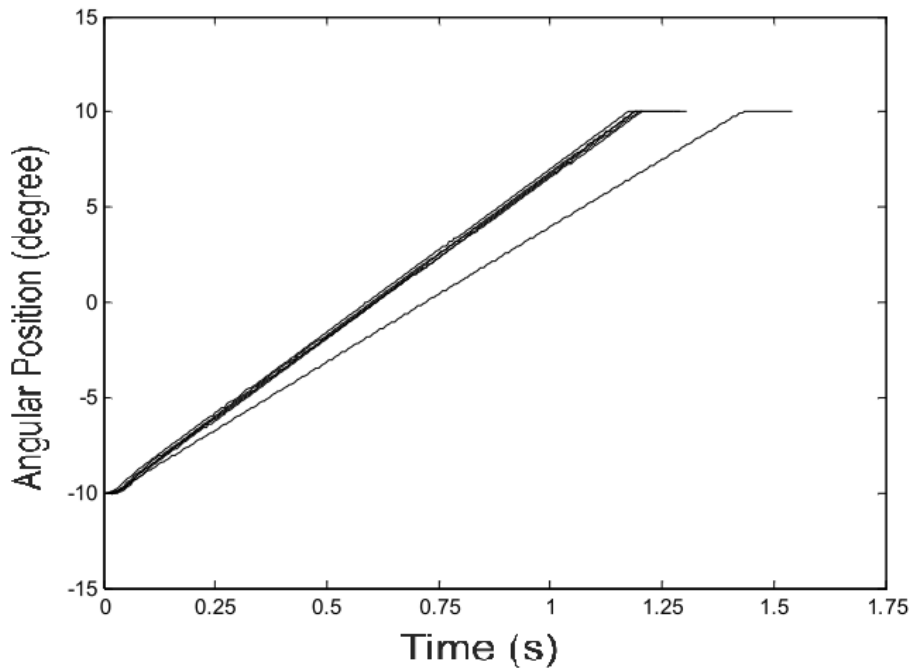
Figure 2.7 Maximum angular velocity for different spool displacements

Using these information and equation 2.10 , C^* can be calculated which is $9.9651 \times 10^{-5} \ m^{5/2}kg^{-1/2}$. K_1 and K_2 can be calculated using C^* which are $0.1912 \ m^2/s$ and $2.0767 \times 10^{-12} \ m^4s/kg$, respectively.

The block diagram of the hydraulic tilt platform is shown in figure 2.8. The transfer function is given in equation 2.15 through Laplace Transformation of equation 2.8.
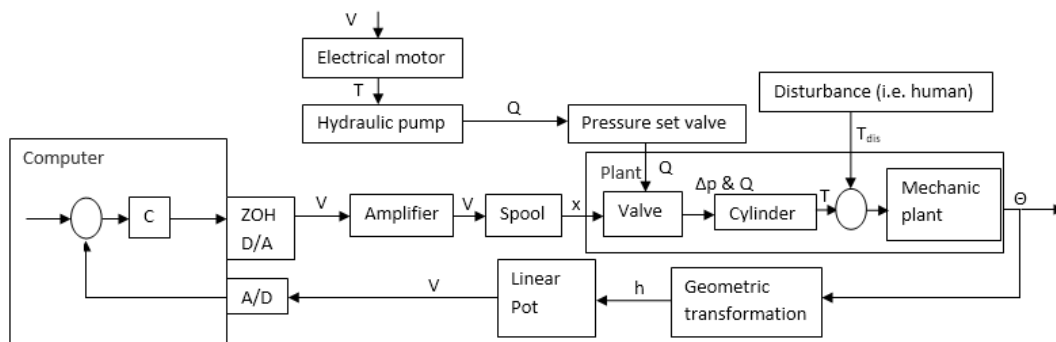
Figure 2.8 The block diagram of the hydraulic tilt platform

28

$$\frac{\theta(s)}{x(s)} = \frac{K_1 A r}{K_2 I s^2 + (A^2 r^2 + K_2 b)s} \qquad (2.15)$$

The Simulink diagram of the hydraulic tilt platform is given in figure 2.9.
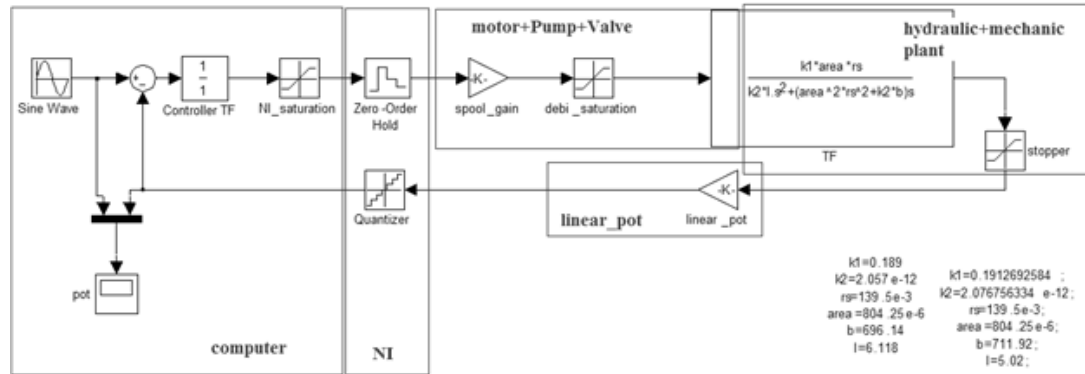
Figure 2.9 The Simulink diagram for the hydraulic tilt platform

2.4 Results

The simulation results and collected data are given in figures 2.10 and 2.11. In addition, figure 2.12 shows the Bode diagram of the simulation and real platform data.
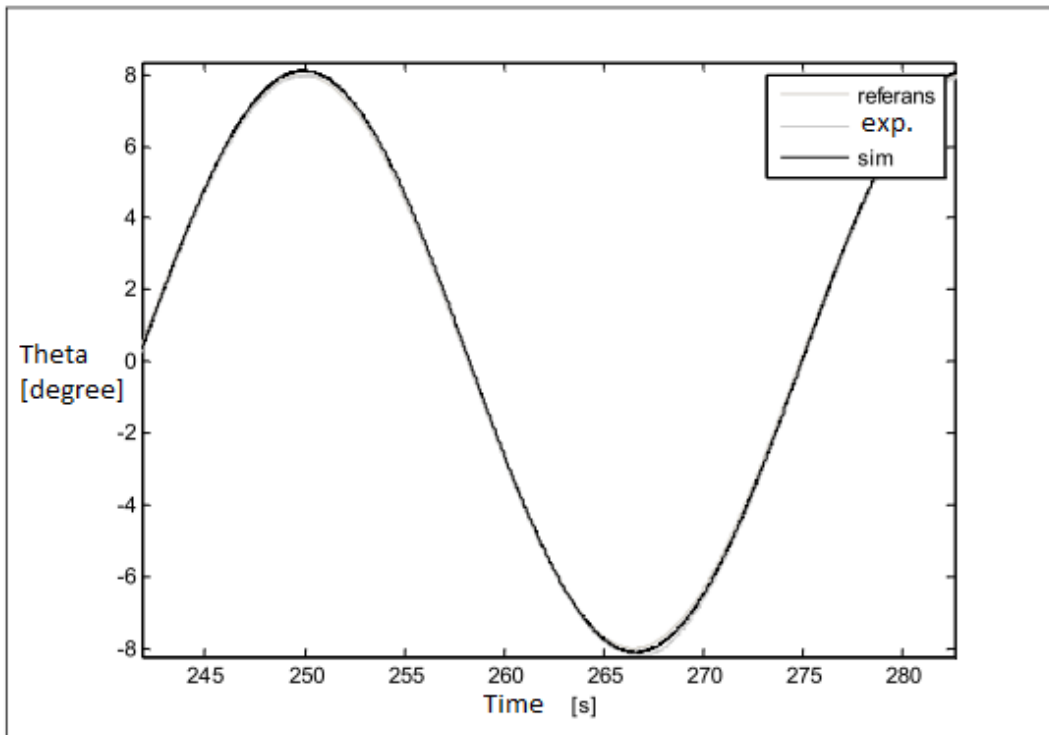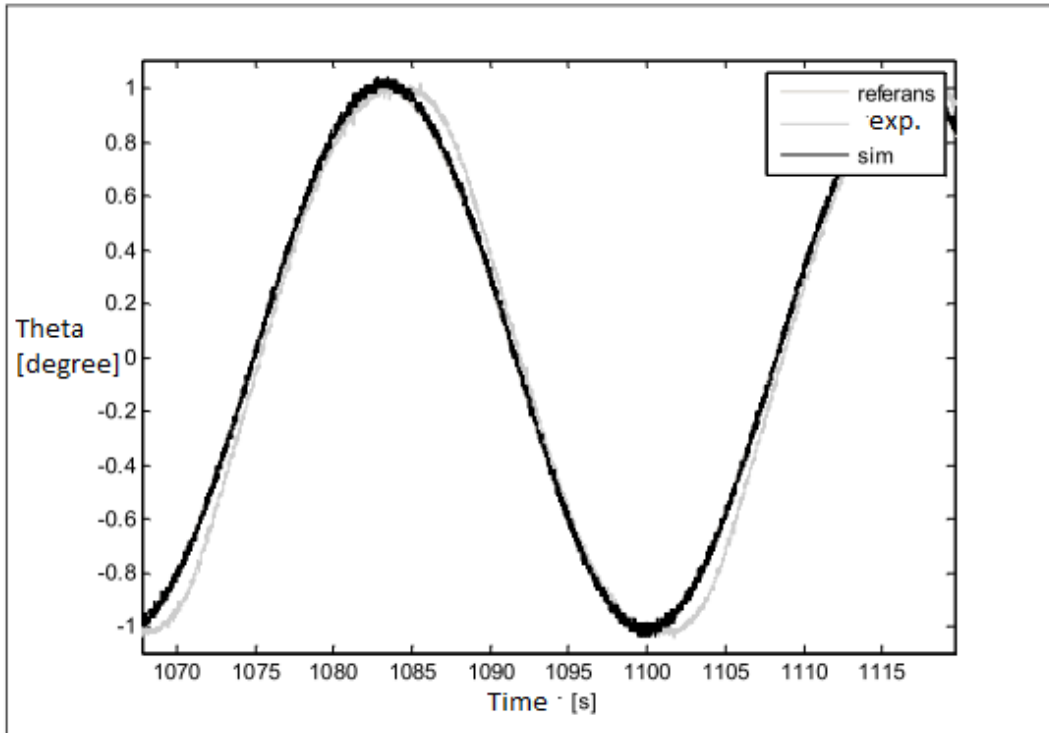
Figure 2.10 The results for the 1 and 8 degrees 0.03 Hz sinus wave
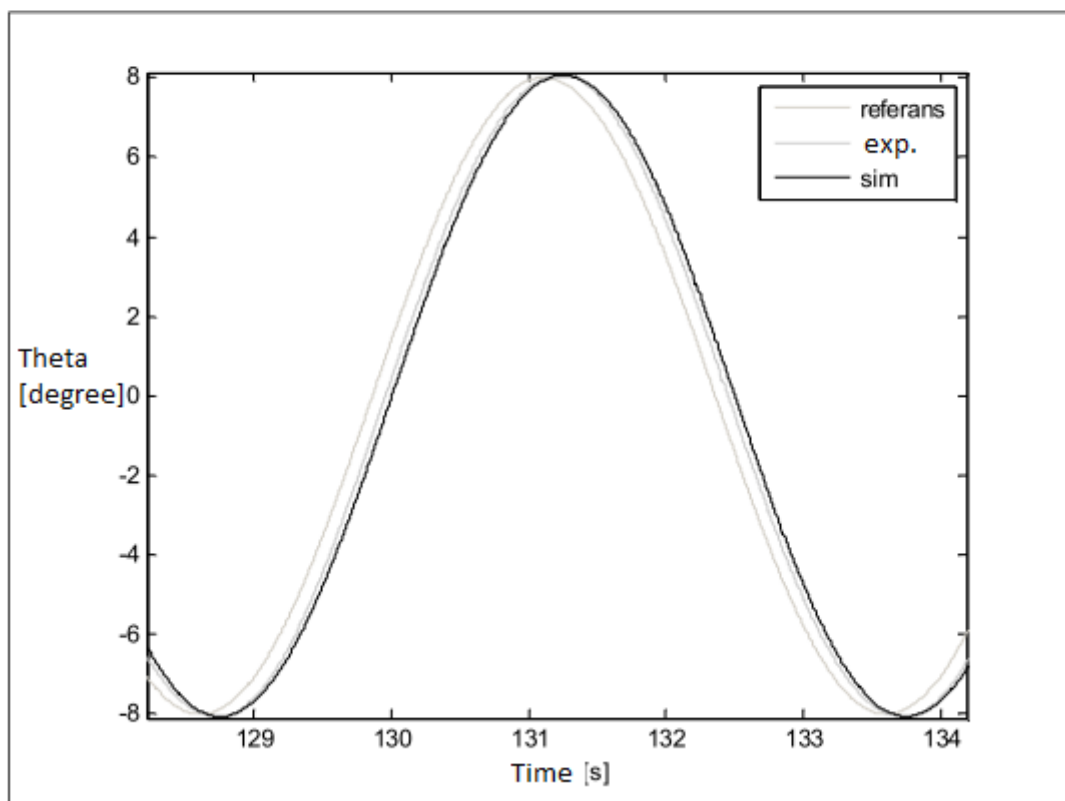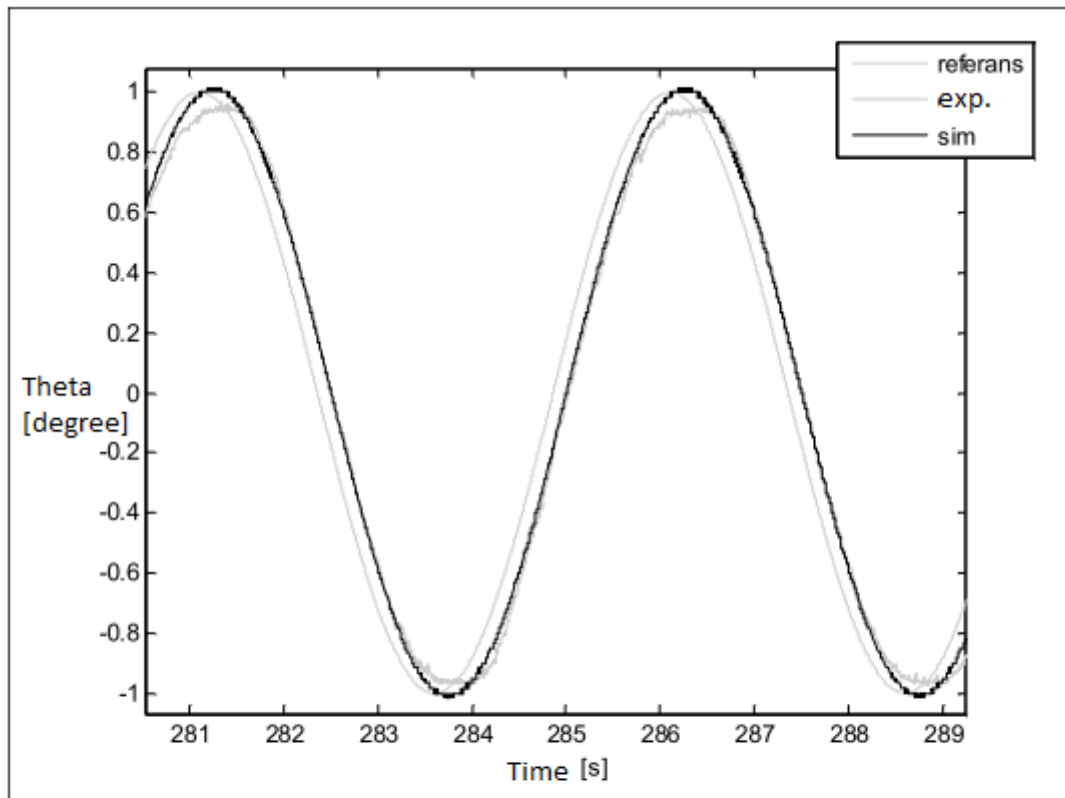
Figure 2.11 The results for the 1 and 8 degrees 0.2 Hz sinus wave
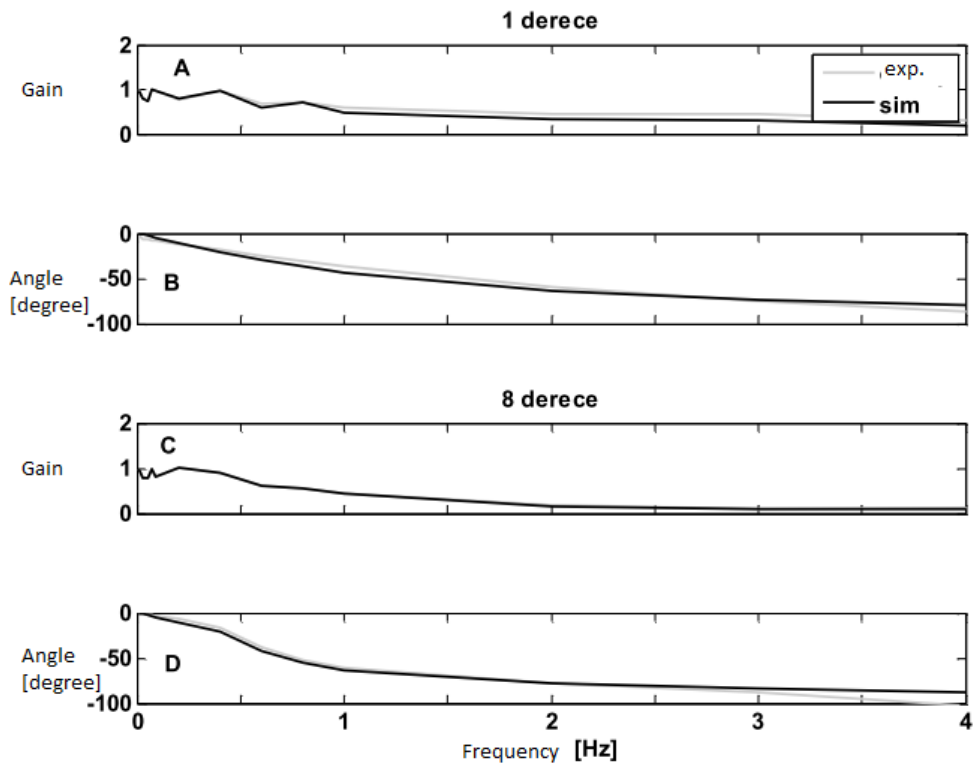
Figure 2.12 The Bode diagram of the simulation and real platform data

2.5 Conclusion

The hydraulic tilt platform was developed, modeled and controlled. The simulation results and the actual platform data are close to each other. Thus, the hydraulic tilt platform can be used for the dynamical posture researches.

CHAPTER 3

EXPERIMENTAL EQUIPMENTS AND DATA ACQUISITION

In this chapter, experimental equipments ere introduced. Besides, the structure of data acquisition was presented.

3.1 Experimental Equipments

Subjects were tested by using a hydraulic tilt platform while kinematic and kinetic data from the subjects were collected through a motion capture system, ground reaction forces measurement system (force plate), and pressure distribution measurement system, respectively.

3.1.1 Motion Capture System

Xsens MVN BIOMECH$^{\textcircled{C}}$ is an easy-to-use, cost efficient system for full-body human motion capture. MVN BIOMECH is based on unique, state-of-the-art miniature inertial sensors, biomechanical models and sensor fusion algorithms. Figure 3.1 shows Xsens MVN BIOMECH motion capture system (see Appendix E).

Figure 3.1 Xsens MVN BIOMECH motion capture system

Inertial sensors, also known as inertial measurement units, measure acceleration, angular rate and the magnetic field vector in their own three-dimensional local coordinate system. With proper calibration, the axes of this local coordinate system represent an orthonormal base that is typically well aligned with the outer casing of the sensor. In addition to the mentioned inertial measurement signals, MVN BIOMECH incorporates some algorithms that provide estimates of the sensor's orientation with respect to a global fixed coordinate system. This orientation can be represented by a quaternion, a rotation matrix or Euler angles.

Figure 3.2 shows the joint axis direction (green arrows) and the joint position (blue arrows). A fundamental problem in inertial measurement units based human motion analysis is that the inertial measurement units local coordinate axes are not aligned with any physiologically meaningful axis. Xsens MVN BIOMECH uses the static posture to identify the coordinates of physically meaningful axes in the upper and lower sensor coordinate system.
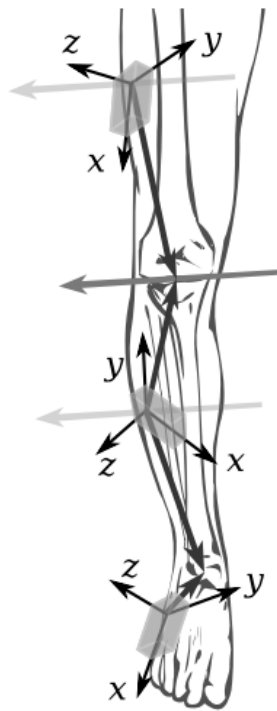
Figure 3.2 The placement of inertial sensors on the human body

Xsens MVN BIOMECH motion capture system is fully ambulatory and consists only of body worn sensors. The system is unique in its approach to estimate body segment orientation and position changes by integration of gyroscope and accelero-meter signals which are continuously updated by using a biomechanical model of the human body. This allows for tracking of dynamic motion. By facilitating the constraints of the model, notably, the segments are connected by joints, the kinematics of body segments are corrected for drift and other errors. The system runs in real-time with a maximum update rate for all kinematics of 100 Hz.

Figure 3.3 shows the global and local coordinate frames for the subject. The orientation outputs with respect to the joint axis direction are represented using quaternions for Xsens MVN BIOMECH.
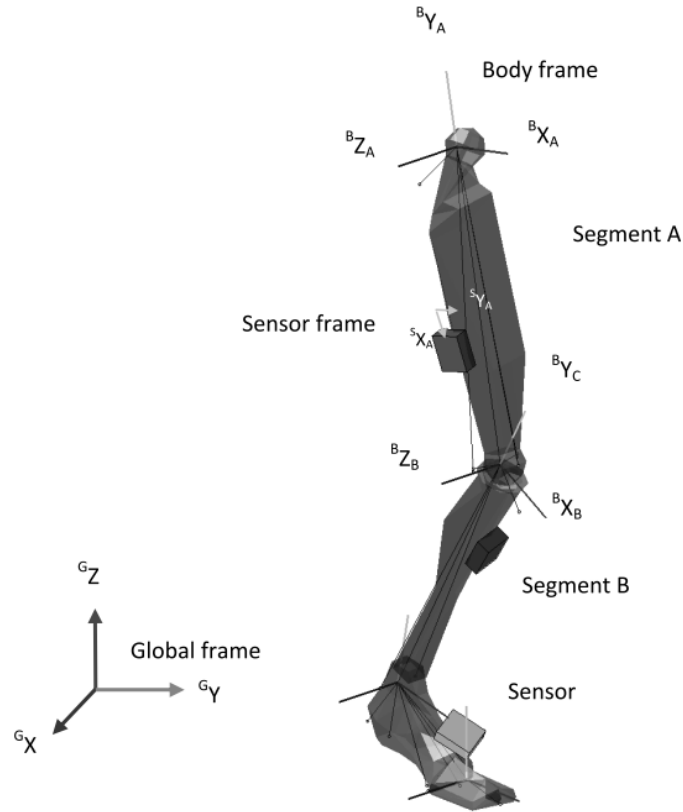
Figure 3.3 Global and local coordinate frames

The orientation of segment A with respect to the global frame was shown as ^{GB_A}q. A joint rotation is defined as the orientation of a distal segment ^{GB_B}q with respect to a proximal segment ^{GB_A}q.

$$^{B_A B_B}q = {}^{GB_A}q^* \otimes {}^{GB_B}q \tag{3.1}$$

where $\otimes$ denotes a quaternion multiplication and * is the complex conjugate of the quaternion. Figures 3.4 and 3.5 show the sample data for Xsens MVN BIOMECH software.

36
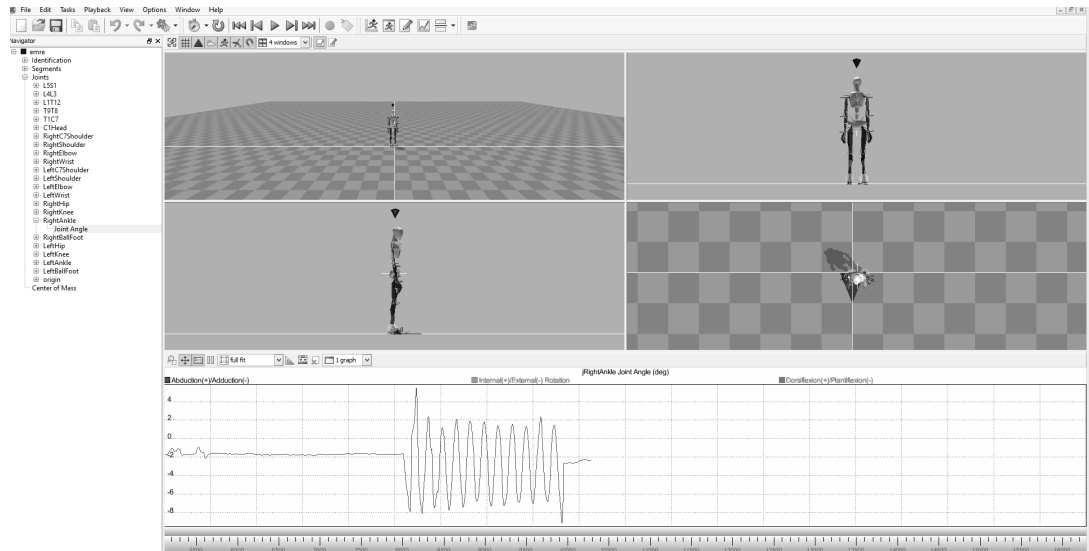
Figure 3.4 Data from Xsens MVN BIOMECH
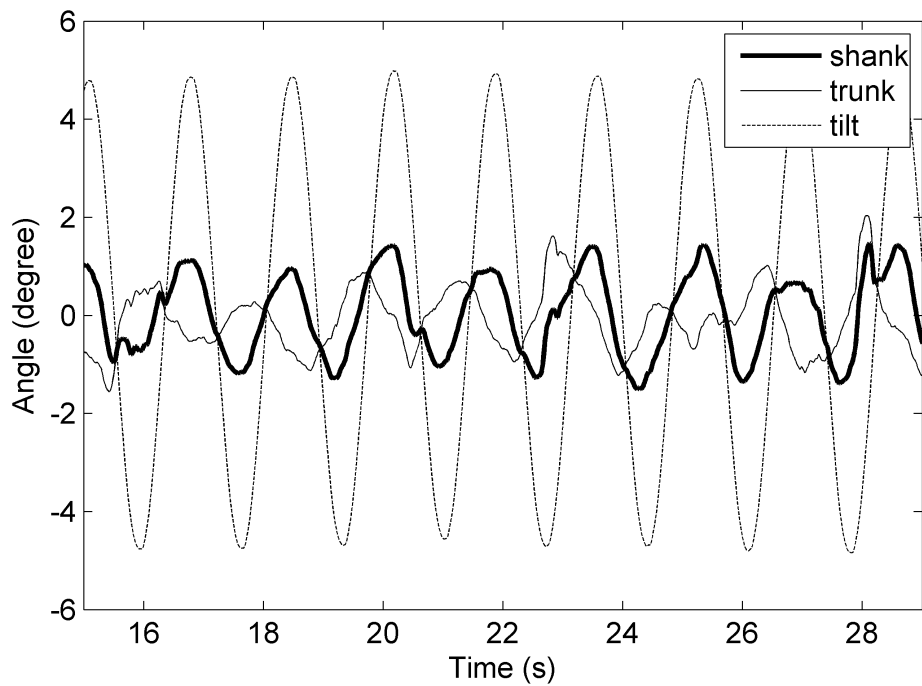
Figure 3.5 Measurements for 5 degrees 0.59 Hz absolute limb's angle

3.1.2 Ground Reaction Forces Measurement System

Accurate measurements of ground reaction forces are important in postural control research, as these forces under the feet are unique to create motion of the body. Bertec

force plate measures three force and three moment components about x,y, and z axes for a total of six outputs. Figure 3.6 shows Bertec© force plate (see Appendix F).

Figure 3.6 Bertec force plate

Figure 3.7 illustrates the schematic diagram of ground reaction forces. Bertec force plate measures the ground reaction forces using strain gauges on four locations and in three axes. These four locations are shown on figure 3.7 as numbers 1 to 4.
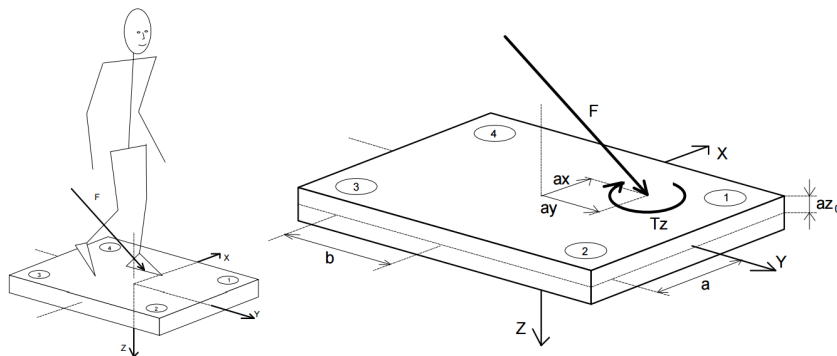
Figure 3.7 The schematic diagram of ground reaction forces

In figure 3.7, a and b are the sensor offsets with respect to x and y axes, respectively. In addition, az_0 is the top plane offset with respect to the origin of the coordinate system. The center of pressure (CoP) is widely used in posture research to understand the postural control system. CoP is the point of application for ground reaction forces.

In this point, there are only three forces (F_x, F_y, and F_z) and a twisting moment (M_z). On the other hand, the force plate measures the ground reaction forces with respect to the coordinate system that is shown in figure 3.7. Therefore, some calculations could be performed to calculate the CoP. Following equations were used to calculate the CoP. First of all, three force components were measured by the force plate using following force and moment equations.

$$F_x = fx_{12} + fx_{34} \tag{3.2}$$

where, fx_{12} are the forces in x direction measured by sensors 1 and 2. fx_{34} are the forces in x direction measured by sensors 3 and 4.

$$F_y = fy_{14} + fy_{23} \tag{3.3}$$

where, fy_{14} are the forces in y direction measured by sensors 1 and 4. fy_{23} are the forces in y direction measured by sensors 2 and 3.

Finally,

$$F_z = fz_1 + fz_2 + fz_3 + fz_4 \tag{3.4}$$

where, fz_1 to fz_4 are the forces in z direction measured by sensors 1 to 4.

Next, the moments were calculated.

$$M'_x = b * (fz_1 + fz_2 - fz_3 - fz_4)$$
$$M'_y = a * (-fz_1 + fz_2 + fz_3 - fz_4) \tag{3.5}$$
$$M_z = b * (-fx_{12} + fx_{34}) + a * (fy_{14} - fy_{23})$$

At the last step, the force plate gives measurements with respect to the top plate surface using the following equations for M_x and M_y.

39

$$M_x = M_x' + F_y * az_0$$
$$M_y = M_y' - F_x * az_0 \tag{3.6}$$

The x and y coordinates of CoP can be calculated using three force and moment signals; i.e., F_z, M_y, and M_x respectively, which are measured by the force plate. Equations 3.7 and 3.8 give x and y coordinates of CoP (ax and ay distances at figure 3.6 respectively).

$$COP_x = -\frac{M_y}{F_z} \tag{3.7}$$

$$COP_y = \frac{M_x}{F_z} \tag{3.8}$$

Ground reaction forces and moments were measured with 100 Hz sampling rate. The anterior-posterior movement of the subjects were studied. Therefore, only COP_x was calculated in this thesis.

3.1.3   Pressure Distribution Measurement System

Tekscan Matscan$^{©}$ system is low-profile floor mat that captures barefoot plantar pressures and forces. The location of the ankle joint with respect to the barefoot's projection on the horizontal plane is crucial to measure for estimating ankle torque produced through somatosensory feedback. This was the basic motivation to use Tekscan Matscan in this thesis. Figure 3.8 shows a sample frame from a subject's foot pressure distribution. The data was collected at 50 Hz frame rate (see Appendix G).
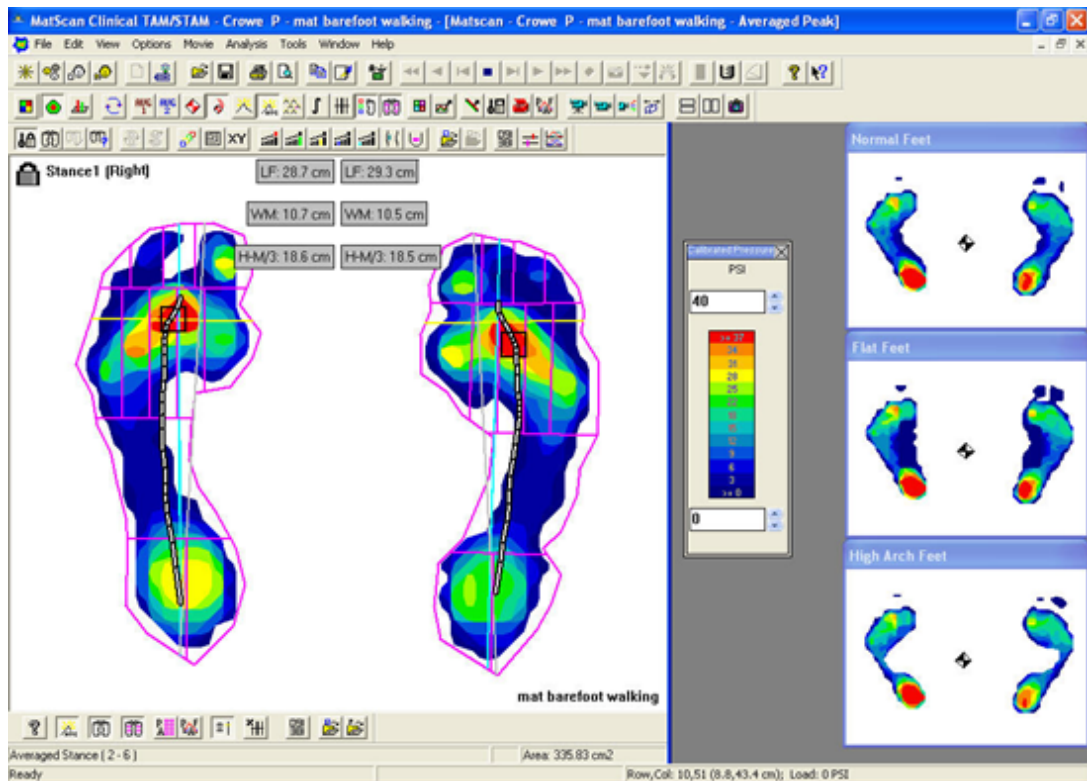
Figure 3.8 One frame data from a subject's pressure distribution

3.2 Data Acquisition

In this section, the physical characteristics of collected signals are proposed. In addition to that, the synchronization sequences of the data collection system are introduced.

3.2.1 The Physical Characteristics of Collected Signals

The kinematic data of the human body were collected. These are all the angular positions, velocities and accelerations of the body segments and the joints. The reaction forces and moments of the human feet. Finally, the pressure distribution of the feet also collected. The synchronization between hydraulic tilt platform, sensors and computers, which were used to gather data from the sensors is shown in Figure 3.9. One main computer is used for synchronization of the other computers and hydraulic tilt platform. One computer collects data from motion capture system and another

computer collects data from the pressure pad.

```
                    ┌─────────────────────┐
              ┌─────┤    Main Computer     ├─────┐
              │     └──────────┬───┬──────┘      │
              │                │   │             │
              ▼                ▼   │ ▼           ▼
        ┌──────────┐  ┌─────────────────────┐ ┌────────────┐ ┌──────────┐
        │ Computer │  │ Hydraulic Tilt Platform │ │ Force Plate │ │ Computer │
        └────┬─────┘  └─────────────────────┘ └────────────┘ └────┬─────┘
             │                                                     │
             ▼                                                     ▼
        ┌──────────┐                                         ┌──────────────┐
        │   MTX    │                                         │ Pressure Pad │
        └──────────┘                                         └──────────────┘
```
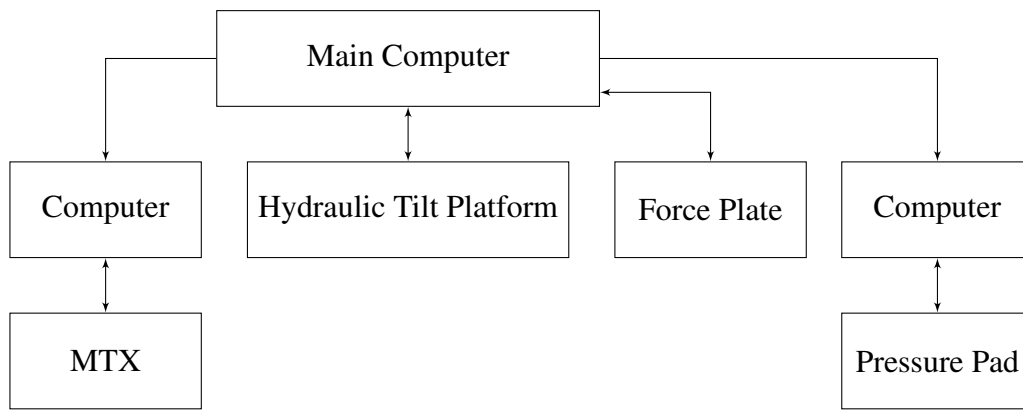
Figure 3.9 Synchronization Block Diagram

CHAPTER 4

EXPERIMENTS AND METHODS

4.1   Subjects and the Testing Procedure

The subjects stood on the force plate sensor, which was explained in Chapter 3. Therefore, all reaction forces that were produced by the subjects were measured. In addition to that, the force plate was connected to the hydraulic tilt platform. The hydraulic tilt platform was tilted at two distinct frequencies and amplitudes. These frequencies and amplitudes were 0.021 and 0.59 Hz with 1 and 5 degree sine waves. These two sine waves were chosen because of the hypothesis of thesis, which was explained in Chapter 1. Main purpose of the thesis has been to understand the interaction between the vestibular and somatosensory systems. The subjects have been chosen from healthy people who have no known vestibular or other significant health problems. The identification of the postural control system is complicated in the sense that the two feedback systems (vestibular and somatosensory) are talking to each other. There has been no known method to eliminate the somatosensory system. In contrast, the vestibular system has a threshold value which has been measured in the literature [5,6,7]. Thus, the experiment has been designed to reveal the vestibular and somatosensory interaction such that, the first sine wave for the stimulus has been chosen as being below the vestibular threshold (0.021 Hz with 1 degree), while the second perturbation was 0.59 Hz with 5 degrees peak amplitude being above the vestibular threshold. Therefore, it has been assumed that there was no sensory feedback available from vestibular system at the low frequency perturbation. Indeed, the subjects confirmed that they have felt only one tilt stimulus throughout all of the data collection period. In addition to that, vision effects the postural control system.

Thus, the tests were performed in complete darkness and eyes open condition (against performing the experiments in eyes closed condition) because, we did not want the subjects to get exposed to an unusual sensory condition which they do not experience during their daily life. Tests were repeated five times in random order. The test duration was about 20 cycles of the stimulus period. (e.g. 180 seconds for test 1 and 40 seconds for test 2). The subjects were chosen from 20-40 age groups. Total test duration was about 35 minutes. Experiments have been performed to 31 people but 11 subjects' data have been used in the thesis for data reliability reasons. The most frequent reason to leave the data outside of the analysis was the stepping response observed during the experiment. Figure 4.1 shows a photo from the experiment.

Figure 4.1 A photo from the experiment

4.2 Data Analysis Methods

Time domain and frequency domain analysis were performed in the collected data.

4.2.1 Analysis in the Time Domain

The root mean square (Ψ) RMS value of the absolute and relative angular movements of the hip and ankle joints were calculated using mean square (Ψ^2). RMS value of a signal gives the total power that the signal carries.

$$\Psi^2 = R_{XX}(\tau = 0) \tag{4.1}$$

where R_{xx} is the auto-correlation function as a function of the delay operator, τ.

$$R_{XX}(\tau) = \frac{1}{T}\int_0^T X(t)X(t+\tau)dt \tag{4.2}$$

where, T is the data collection period of time, X is the time series for the kinematic variable.

On the other hand, cross correlation function between the two kinematic time series (X(t) and Y(t)) is given as:

$$R_{XY}(\tau) = \frac{1}{T}\int_0^T X(t)Y(t+\tau)dt \tag{4.3}$$

4.2.2 Decomposition Method

There are two possible different (distinct) motions of the subjects that can be observed on the hydraulic tilt platform. The first one being the alignment of the subjects with respect to the gravity vertical, while the second motion is the alignment due to the tilt platform's vertical. The second motion is seen in inanimate objects on the tilt platform. When the tilt platform moves, if the friction force between the object and the platform is big enough, the second motion occurs. Therefore, the subject's real

45

(actively controlled) motion is to be separated from the second motion. This is crucial to understand the subject's behavior on the tilt platform. Therefore, a behavioral vestibular model being the subject trying to align himself with respect to the gravity vertical during the experiment is proposed. Alternatively, a behavioral somatosensory model can be defined when the subject allows himself to get tilted by the platform. The signal decomposition method suggests a way to differentiate between these two behavioral models as it compensates for stationary mass effects (detrending statically) of the force plate and human subjects. The equation 4.4 shows the decomposition method that is proposed.

$$COPx_{m/s} = COPx_{m/fp} + COPx_{fp/s} \qquad (4.4)$$

Here, $COPx_{fp/s}$ (force-plate with respect to space) denotes the gravitational effect of the mass which is assumed to be stationary with respect to tilting platform (apparent CoPx). $COPx_{m/s}$ (mass (human) with respect to space) is the measured CoPx signal by the force-plate, where CoPx signal will reflect the gravitational effect of the mass (human) tilted by the platform (Figure 4.2). One can use this method to understand the CoP sway with respect to the tilting platform. In addition, the same method can be also applied to the CoM signal (Equation 4.5). The relation between CoM and CoPx is explained in Appendix B.

$$COM_{m/s} = COM_{m/fp} + COM_{fp/s} \qquad (4.5)$$

46
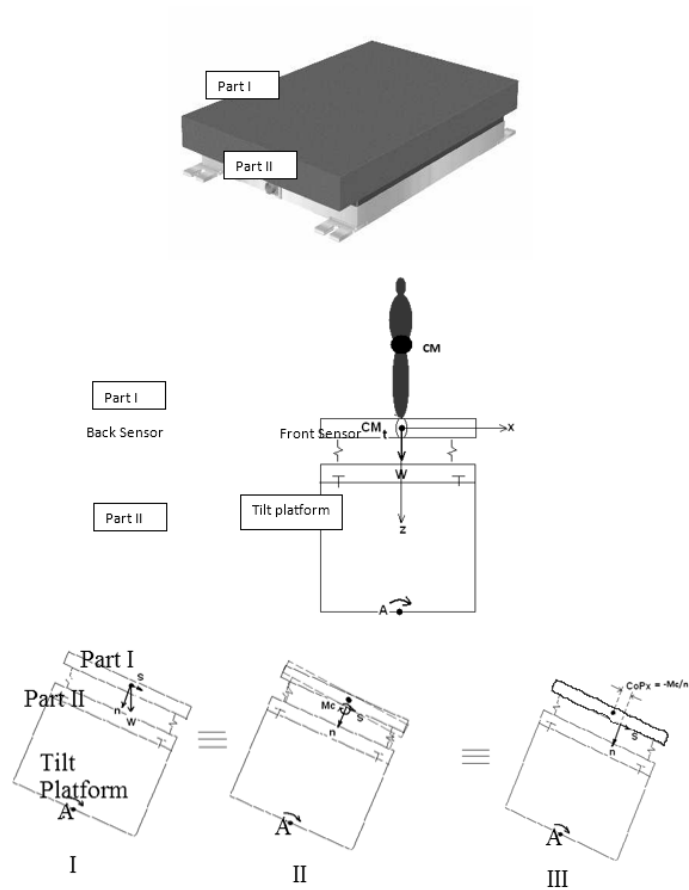
Figure 4.2 Stationary mass on the tilt platform showing equipollent systems, I, II, III

Figure 4.3 demonstrates the absolute and relative angles with respect to the gravity vertical and the platform normal, where θ_1 is the absolute angle of the limbs with respect to the gravity vertical while θ_2 is the relative angle with respect to the platform normal.
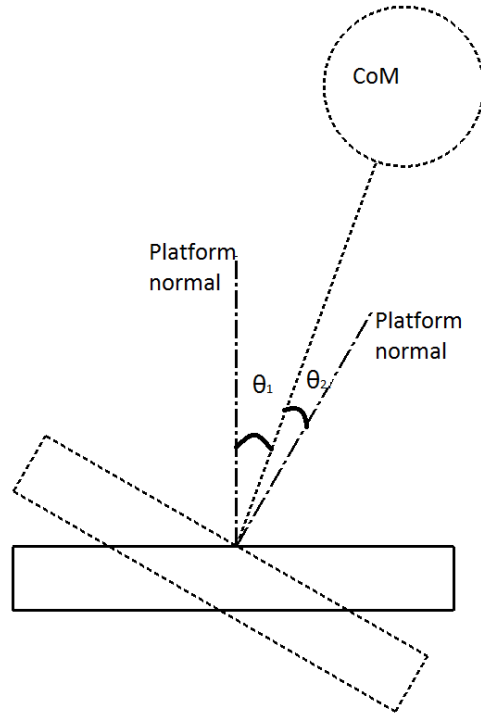
Figure 4.3 Absolute and relative angle with respect to the gravity vertical and the platform normal, respectively

Relative angular displacement of the shank with respect to the foot at the ankle joint (refer to θ_2 in Figure 4.3) has been defined as;

$$\theta_{s/f} = \theta_{s/g} - \theta_{f/g} \qquad (4.6)$$

where, f denotes foot and $\theta_{f/g}$ is the absolute angular displacement of the foot with respect to the ground (gravity vertical, refer to θ_1 in Figure 4.3) and is indeed the platform's angular movement; i.e., is equal to $\theta_{p/g}$ (p stands for the platform) as foot has not been allowed to move with respect to the platform throughout the experiments, s denotes shank angular displacement with respect to gravity vertical in $\theta_{s/f}$.

4.2.3   Analysis in the Frequency Domain

The kinematics data of the subjects' joints (e.g. ankle, hip or neck) have been measured by using Xsens MTX and the reactions forces of the subjects were measured by

the force plate in time. In order to observe the frequency content of the time signals collected, frequency domain analyses were performed.

The Fourier Transform mathematically relates the time domain and the frequency domain. The Fourier transform is given by:

$$G_{XX}(f) = 2 \int_{-\infty}^{\infty} R_{XX}(\tau)e^{-j2\pi f\tau} d\tau \tag{4.7}$$

where $G_{xx}(f)$ is the one-sided power spectral density function estimate, $R_{XX}(\tau)$ is the auto correlation function of the related kinematic signal and f is the frequency in Hz. The total power of the signal can now be given as

$$\Psi^2 = \int_{0}^{\infty} G_{XX}(f) df \tag{4.8}$$

The frequency domain analysis shows how much of the power of the kinematic signal is presented at each frequency. For a simple signal such as a sine wave, the frequency domain representation does not usually show us much additional information. However, with more complex signals like the kinematics data of the subjects' joints or the CoPx data, the frequency domain analysis is crucial to understand the different control strategies discussed through decomposition method.

4.2.4   Cross Spectral Density Function

Cross spectral density function ($G_{XY}(f)$, one-sided power spectrum) searches for the common power distribution over the frequency spectrum for the two time series (X and Y);

$$G_{XY}(f) = 2 \int_{-\infty}^{\infty} R_{XY}(\tau)e^{-j2\pi f\tau} d\tau \tag{4.9}$$

where $R_{XY}(\tau)$ is the cross correlation function

Here in equation 4.9, the first input which is the data x is always the input of the platform while the second input is the absolute or relative movements of the body segments (see Figure 4.3).

Cross spectral density function is generally a complex number such that

$$G_{XY}(f) = C_{XY}(f) - jQ_{XY}(f) \tag{4.10}$$

where the real part, $C_{XY}(f)$ and the imaginary part, $Q_{XY}(f)$ are known as the coincident spectral density function (co-spectrum) and quadrature spectral density function (quad-spectrum) respectively.

Thus, Cross spectral density function ($G_{XY}(f)$) can also be expressed in complex polar notation such that,

$$G_{XY}(f) = |G_{XY}(f)|e^{-j\theta_{XY}(f)} \tag{4.11}$$

where the magnitude ($|G_{XY}(f)|$) and the angle ($\theta_{XY}(f)$) of cross spectral density function, $G_{XY}(f)$ are related to real and imaginary part of equation according to equations 4.10 and 4.11

$$|G_{XY}(f)| = \sqrt{C_{XY}^2(f) + Q_{XY}^2(f)} \tag{4.12}$$

$$\theta_{XY}(f) = tan^{-1}[\frac{Q_{XY}(f)}{C_{XY}(f)}] \tag{4.13}$$

Finally, a real-valued quantity, γ_{XY}^2 (the coherence function) between the two kinematic signals (X and Y) estimating the normalized correlated behavior in the frequency domain is defined as

$$\gamma_{XY}^2(f) = [\frac{|G_{XY}|^2}{G_{XX}(f)G_{YY}(f)}] \tag{4.14}$$

Here, the value of the coherence will always satisfy $0 \leq \gamma_{xy}(f) \leq 1$. This measure

can be used for identifying of how much the output signal (e.g. hip and ankle angle) is correlated with the input signal that is the platform tilt input in the frequency domain.

4.2.5 Area Ratio in Frequency Domain

The area under the FFT plots are also calculated and the ratio of the area of the perturbation frequency area over the total FFT area is calculated using the equation 4.15.

$$A_{ratio} = \frac{\int\limits_{f_s - 2\Delta f}^{f_s + 2\Delta f} A(f)df}{\int\limits_{0}^{50} A(f)df} \tag{4.15}$$

where f_s is the stimulation frequency.

CHAPTER 5

MATHEMATICAL MODELING

In this chapter, the mathematical model of human postural control system was derived. First of all, the equations of the mechanical model of the human body were produced. Then, the vestibular system's equations were added to the mathematical model.

5.1 Mechanical Model

$OA = h$

$AH = b_1$

$HN = b_2$

$NB = b_3$

$AK = c_1$

$HT = c_2$
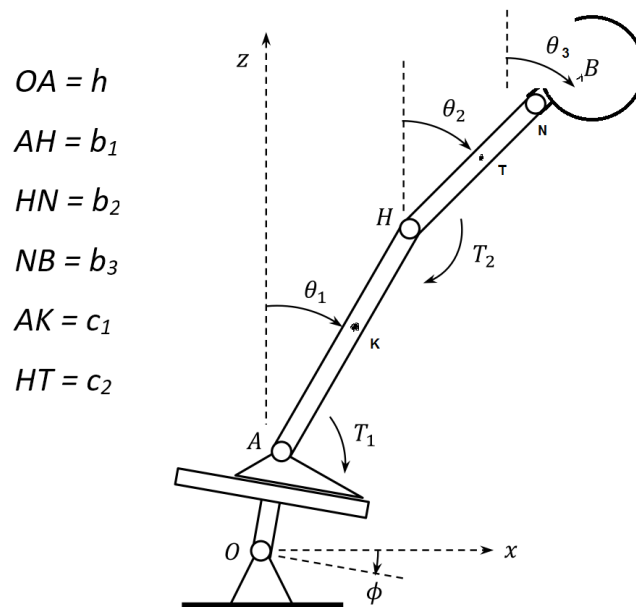
Figure 5.1 A Subject Standing on the Hydraulic Tilt Platform

Figure 5.1 shows a subject trying to keep his balance on the hydraulic tilt platform. The subject modeled as a triple inverted pendulum with his mass as m_1, m_2 and m_3,

respectively. The subject uses the ankle torque T_1, the hip torque T_2 and the head torque T_3.

The kinematic expressions are written below:

$$\vec{r}_K = \overrightarrow{OK} = h\vec{u}(\phi) + c_1\vec{u}(\theta_1) \tag{5.1}$$

$$\vec{r}_T = \overrightarrow{OT} = h\vec{u}(\phi) + b_1\vec{u}(\theta_1) + c_2\vec{u}(\theta_2) \tag{5.2}$$

$$\vec{r}_B = \overrightarrow{OB} = h\vec{u}(\phi) + b_1\vec{u}(\theta_1) + b_2\vec{u}(\theta_2) + b_3\vec{u}(\theta_3) \tag{5.3}$$

$$\vec{v}_K = \frac{d\vec{r}_K}{dt} = h\dot{\phi}\vec{u}'(\phi) + c_1\dot{\theta}_1\vec{u}'(\theta_1) \tag{5.4}$$

$$\vec{v}_T = \frac{d\vec{r}_T}{dt} = h\dot{\phi}\vec{u}'(\phi) + b_1\dot{\theta}_1\vec{u}'(\theta_1) + c_2\dot{\theta}_2\vec{u}'(\theta_2) \tag{5.5}$$

$$\vec{v}_B = \frac{d\vec{r}_B}{dt} = h\dot{\phi}\vec{u}'(\phi) + b_1\dot{\theta}_1\vec{u}'(\theta_1) + b_2\dot{\theta}_2\vec{u}'(\theta_2) + b_3\dot{\theta}_3\vec{u}'(\theta_3) \tag{5.6}$$

Here, θ_1, θ_2 and θ_3 are the unspecified generalized coordinates, whereas $\phi = \phi(t)$ is specified. The differential equations for θ_1, θ_2 and θ_3 can be derived as described below by means of the Lagrangian formulation.

The potential energy of the subject is

$$U = m_1 g z_K + m_2 g z_T + m_3 g z_B$$
$$= m_1 g(h\cos(\phi) + c_1\cos(\theta_1)) + m_2 g(h\cos(\phi) + b_1\cos(\theta_1) + c_2\cos(\theta_2)) \tag{5.7}$$
$$+ m_3 g(h\cos(\phi) + b_1\cos(\theta_1) + b_2\cos(\theta_2) + b_3\cos(\theta_3))$$

The virtual work equation is

$$\delta W = T_1 \delta\theta_1 + T_2(\delta\theta_2 - \delta\theta_1) + T_3(\delta\theta_3 - \delta\theta_2)$$
$$= (T_1 - T_2)\delta\theta_1 + (T_2 - T_3)\delta\theta_2 + T_3\delta\theta_3 \tag{5.8}$$

Note that $\delta\phi = 0$ because ϕ is specified. Hence, the generalized forces are seen to be

$$Q_1 = T_1 - T_2 \tag{5.9}$$

$$Q_2 = T_2 - T_3 \tag{5.10}$$

$$Q_3 = T_3 \tag{5.11}$$

The kinetic energy of the subject is

$$K = K_1 + K_2 + K_3 \tag{5.12}$$

$$K_1 = \frac{1}{2}m_1 v_K^2 + \frac{1}{2}I_1\dot\theta_1^{\,2} = \frac{1}{2}m_1(c_1^2\dot\theta_1^{\,2} + h^2\dot\phi^2)$$
$$+ m_1 h c_1 \dot\phi\dot\theta_1 cos(\theta_1 - \phi) + \frac{1}{2}I_1\dot\theta_1^{\,2} \tag{5.13}$$

$$K_2 = \frac{1}{2}m_2 v_T^2 + \frac{1}{2}I_2\dot\theta_2^{\,2} = \frac{1}{2}m_2(c_2^2\dot\theta_2^{\,2} + b_1^2\dot\theta_1^{\,2} + h^2\dot\phi^2)$$
$$+ m_2(h c_2 \dot\phi\dot\theta_2 cos(\theta_2 - \phi) + h b_1 \dot\phi\dot\theta_1 cos(\theta_1 - \phi)$$
$$+ b_1 c_2 \dot\theta_1\dot\theta_2 cos(\theta_2 - \theta_1)) + \frac{1}{2}I_2\dot\theta_2^{\,2} \tag{5.14}$$

$$K_3 = \frac{1}{2}m_3 v_B^2 + \frac{1}{2}I_3\dot\theta_3^{\,2} = \frac{1}{2}m_3(b_3^2\dot\theta_3^{\,2} + b_2^2\dot\theta_2^{\,2} + b_1^2\dot\theta_1^{\,2} + h^2\dot\phi^2)$$
$$+ m_3(h b_3 \dot\phi\dot\theta_3 cos(\theta_3 - \phi) + h b_2 \dot\phi\dot\theta_2 cos(\theta_2 - \phi) + h b_1 \dot\phi\dot\theta_1 cos(\theta_1 - \phi)$$
$$+ b_1 b_3 \dot\theta_1\dot\theta_3 cos(\theta_3 - \theta_1) + b_1 b_2 \dot\theta_1\dot\theta_2 cos(\theta_2 - \theta_1)$$
$$+ b_2 b_3 \dot\theta_2\dot\theta_3 cos(\theta_3 - \theta_2)) + \frac{1}{2}I_3\dot\theta_3^{\,2} \tag{5.15}$$

The generalized momenta are

$$p_1 = \frac{dK}{d\dot{\theta}_1} = m_1 c_1^2 \dot{\theta}_1 + m_1 h c_1 \dot{\phi} \cos(\theta_1 - \phi) + I_1 \dot{\theta}_1 + m_2 b_1^2 \dot{\theta}_1$$

$$+ m_2 h b_1 \dot{\phi} \cos(\theta_1 - \phi) + m_2 b_1 c_2 \dot{\theta}_2 \cos(\theta_2 - \theta_1) + m_3 b_1^2 \dot{\theta}_1 \qquad (5.16)$$

$$m_3 h b_1 \dot{\phi} \cos(\theta_1 - \phi) + m_3 b_1 b_3 \dot{\theta}_3 \cos(\theta_3 - \theta_1) + m_3 b_1 b_2 \dot{\theta}_2 \cos(\theta_2 - \theta_1)$$

$$p_2 = \frac{dK}{d\dot{\theta}_2} = m_2 c_2^2 \dot{\theta}_2 + m_2 h c_2 \dot{\phi} \cos(\theta_2 - \phi) + m_2 b_1 c_2 \dot{\theta}_1 \cos(\theta_2 - \theta_1)$$

$$+ I_2 \dot{\theta}_2 + m_3 b_2^2 \dot{\theta}_2 + m_2 h b_2 \dot{\phi} \cos(\theta_2 - \phi) + m_3 b_1 b_2 \dot{\theta}_1 \cos(\theta_2 - \theta_1) \qquad (5.17)$$

$$+ m_3 b_2 b_3 \dot{\theta}_3 \cos(\theta_3 - \theta_2)$$

$$p_3 = \frac{dK}{d\dot{\theta}_3} = m_3 b_3^2 \dot{\theta}_3 + m_3 h b_3 \dot{\phi} \cos(\theta_3 - \phi) + m_3 b_1 b_3 \dot{\theta}_1 \cos(\theta_3 - \theta_1)$$

$$+ m_3 b_2 b_3 \dot{\theta}_2 \cos(\theta_3 - \theta_2) + I_3 \dot{\theta}_3 \qquad (5.18)$$

The angle derivatives of K are

$$K_1' = \frac{dK}{d\theta_1} = -m_1 h c_1 \dot{\phi} \dot{\theta}_1 \sin(\theta_1 - \phi) - m_2 h b_1 \dot{\phi} \dot{\theta}_1 \sin(\theta_1 - \phi)$$

$$+ m_2 b_1 c_2 \dot{\theta}_1 \dot{\theta}_2 \sin(\theta_2 - \theta_1) - m_3 h b_1 \dot{\phi} \dot{\theta}_1 \sin(\theta_1 - \phi) \qquad (5.19)$$

$$+ m_3 b_1 b_3 \dot{\theta}_1 \dot{\theta}_3 \sin(\theta_3 - \theta_1) + m_3 b_1 b_2 \dot{\theta}_1 \dot{\theta}_2 \sin(\theta_2 - \theta_1)$$

$$K_2' = \frac{dK}{d\theta_2} = -m_2 h c_2 \dot{\phi} \dot{\theta}_2 \sin(\theta_2 - \phi) - m_2 b_1 c_2 \dot{\theta}_1 \dot{\theta}_2 \sin(\theta_2 - \theta_1)$$

$$- m_3 h b_2 \dot{\phi} \dot{\theta}_2 \sin(\theta_2 - \phi) - m_3 b_1 b_2 \dot{\theta}_1 \dot{\theta}_2 \sin(\theta_2 - \theta_1) \qquad (5.20)$$

$$+ m_3 b_2 b_3 \dot{\theta}_2 \dot{\theta}_3 \sin(\theta_3 - \theta_2)$$

$$K_3' = \frac{dK}{d\theta_3} = -m_3 h b_3 \dot{\phi} \dot{\theta}_3 \sin(\theta_3 - \phi) - m_3 b_1 b_3 \dot{\theta}_1 \dot{\theta}_3 \sin(\theta_3 - \theta_1)$$

$$- m_3 b_2 b_3 \dot{\theta}_1 \dot{\theta}_3 \sin(\theta_3 - \theta_2) \qquad (5.21)$$

The angle derivative of the potential energy

$$G_1 = \frac{dU}{d\theta_1} = -m_1 g c_1 sin(\theta_1) - m_2 g b_1 sin(\theta_1) - m_3 g b_1 sin(\theta_1) \qquad (5.22)$$

$$G_2 = \frac{dU}{d\theta_2} = -m_2 g c_2 sin(\theta_2) - m_3 g b_2 sin(\theta_2) \qquad (5.23)$$

$$G_3 = \frac{dU}{d\theta_3} = -m_3 g b_3 sin(\theta_3) \qquad (5.24)$$

The Lagrange's equations are

$$\dot{p}_1 - K_1' + G_1 = Q_1 \qquad (5.25)$$

$$\dot{p}_2 - K_2' + G_2 = Q_2 \qquad (5.26)$$

$$\dot{p}_3 - K_3' + G_3 = Q_3 \qquad (5.27)$$

Hence, the differential equations are obtained as follows:

$$\mathbf{M}\ddot{\theta} = \mathbf{Q} + \mathbf{S} \qquad (5.28)$$

In equation 5.28, bold letters are matrices and expanded forms are shown in the next page.

$$\begin{bmatrix} m_1c_1^2 + I_1 + m_2b_1^2 + m_3b_1^2 & m_2b_1c_2cos(\theta_2 - \theta_1) + m_3b_1b_2cos(\theta_2 - \theta_1) & m_3b_1b_3cos(\theta_3 - \theta_1) \\ m_2b_1c_2cos(\theta_2 - \theta_1) + m_3b_1b_2cos(\theta_2 - \theta_1) & m_2c_2^2 + I_2 + m_3b_2^2 & m_3b_2b_3cos(\theta_3 - \theta_2) \\ m_3b_1b_3cos(\theta_3 - \theta_1) & m_3b_2b_3cos(\theta_3 - \theta_2) & m_3b_3^2 + I_3 \end{bmatrix} \begin{bmatrix} \ddot{\theta}_1 \\ \ddot{\theta}_2 \\ \ddot{\theta}_3 \end{bmatrix} = \begin{bmatrix} T_1 - T_2 \\ T_2 - T_3 \\ T_3 \end{bmatrix} + \begin{bmatrix} S_1 \\ S_2 \\ S_3 \end{bmatrix}$$

$$S_1 = -m_1hc_1\ddot{\phi}cos(\theta_1 - \phi) - m_2hb_1\ddot{\phi}cos(\theta_1 - \phi) - m_3hb_1\ddot{\phi}cos(\theta_1 - \phi) - m_1hc_1\dot{\phi}^2 sin(\theta_1 - \phi) - m_2hb_1\dot{\phi}^2 sin(\theta_1 - \phi)$$
$$- m_3hb_1\dot{\phi}^2 sin(\theta_1 - \phi) + m_3b_1b_3\dot{\theta}_3^{\,2} sin(\theta_3 - \theta_1) + m_3b_1b_2\dot{\theta}_2^{\,2} sin(\theta_2 - \theta_1)$$
$$+ m_2b_1c_2\dot{\theta}_2^{\,2} sin(\theta_2 - \theta_1)$$

$$S_2 = -m_2hc_2\ddot{\phi}cos(\theta_2 - \phi) - m_2hb_2\ddot{\phi}cos(\theta_2 - \phi) - m_2hc_2\dot{\phi}^2 sin(\theta_2 - \phi) - m_2b_1c_2\dot{\theta}_1^{\,2} sin(\theta_2 - \theta_1)$$
$$- m_3hb_2\ddot{\phi}cos(\theta_2 - \phi) - m_3b_1b_2\dot{\theta}_1^{\,2} sin(\theta_2 - \theta_1) + m_3b_2b_3\dot{\theta}_3^{\,2} sin(\theta_3 - \theta_2)$$
$$- m_3hb_2\dot{\phi}^2 sin(\theta_2 - \phi)$$

$$S_3 = -m_3hb_3\ddot{\phi}cos(\theta_3 - \phi) - m_3hb_3\dot{\phi}^2 sin(\theta_3 - \phi) - m_3b_1b_3\dot{\theta}_1^{\,2} sin(\theta_3 - \theta_1) - m_3b_2b_3\dot{\theta}_1^{\,2} sin(\theta_3 - \theta_2)$$

The inertial values for the body segments are taken from OpenSim program. One can enter the height and weight of the subject. Thus, OpenSim gives all inertial and other anatomical parameters.

The overall control torque (T_c) for each joint can be divided into two torque components (equation 5.29) as follows;

$$T_c = T_c^1 + T_c^2 \qquad (5.29)$$

Equation 5.30 gives the definition of the first torque partition (proprioceptive originated) where θ_A is an arbitrary relative joint angle; e.g., neck, hip, ankle, θ_{Ao} stands for initial relative joint angle, k is the proprioceptive gain.

$$T_c^1 = k(\theta_{Ao} - \theta_A) \qquad (5.30)$$

Equation 5.31 gives the definition of the second torque partition (somatosensory originated) where CoP is the current CoP position, CoP_o stands for initial CoP position, k is the somatosensory feedback gain.

$$T_c^2 = k(CoP_o - CoP) \qquad (5.31)$$

All the controller for the segments (joint control torque generation) were PD controllers. Figure 5.2 represents the Matlab Simulink model of the overall human upright balance system.
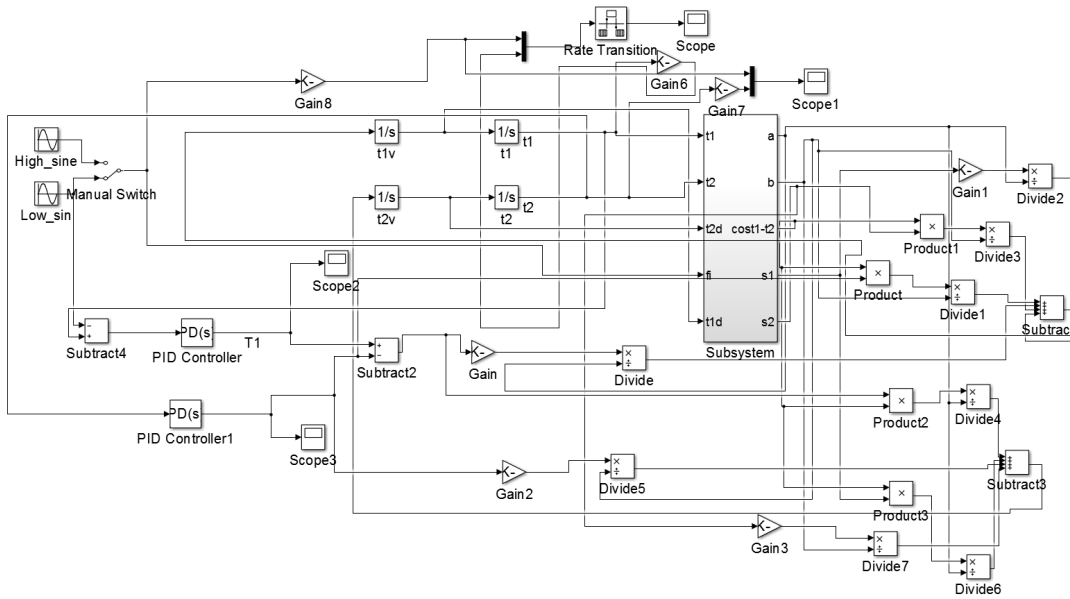
Figure 5.2 Matlab Simulink model of the overall system where the switch in the subssytem changes the postural control startegy from overall body control to modular joint control

5.2 Overall Postural Control Strategy for 2 Stimuli

The overall control of posture for high and low frequency perturbations have been maintained by a piecewise linear model (see Figures 5.2, 5.6, and 5.7), where the essence of the control algorithm depended on tuning the gains for vestibular versus somatosensory system feedbacks. Vestibular feedback system gain has been weighted at around 1 for the high frequency perturbation whereas somatosensory feedback gain has been set to 1 for the low frequency perturbation. Matlab Simulink models' parameters (i.e., PD gains of the controllers) are optimized using the Matlab Simulink design optimization toolbox. The results for the high frequency and low frequency perturbations were given in the next chapter.

5.3 The Vestibular Sensor Model

Figure 5.4 illustrates the vestibular sensor model that is taken from [2]. Angular acceleration in three dimensional space is sensed by three approximately orthogonal

semicircular canals in each inner ear. Figure 5.3 illustrates the vestibular system. The utricle otoliths, one in each inner ear, are multi-dimensional linear accelerometers. They sense specific forces (linear acceleration plus gravity) in a plane rotated 30 degrees with reference to the horizontal plane of the head. Hence, combined canal receptors sense all relevant angular motions of the body; utricle otoliths sense the summation of all linear and gravitational forces. The canals are heavily damped accelerometers, with perceived output corresponding to angular velocity and also the utricle otoliths are heavily damped accelerometers, sensing both tilt angle and linear velocity.
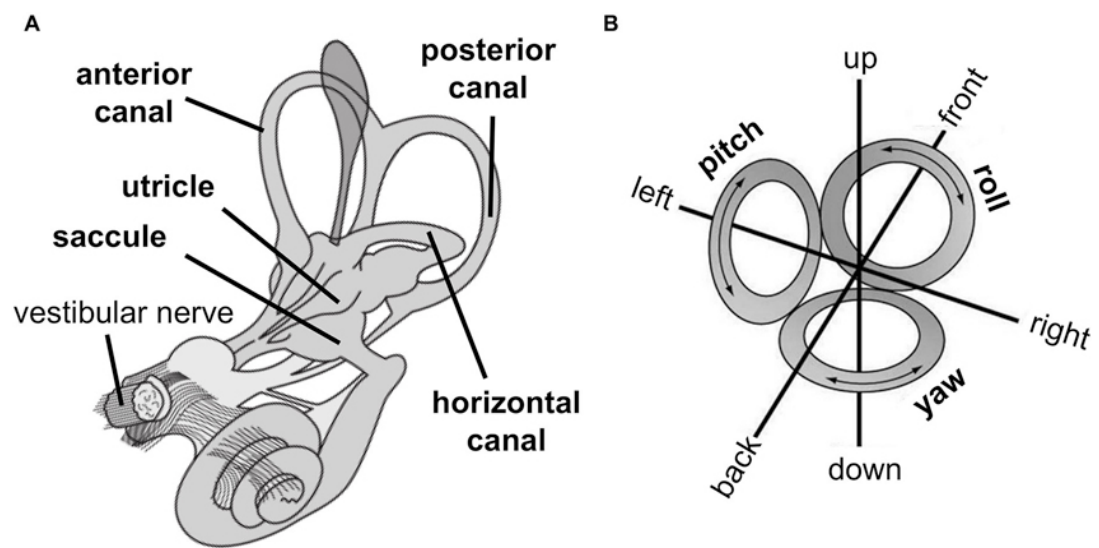
Figure 5.3 The Vestibular System
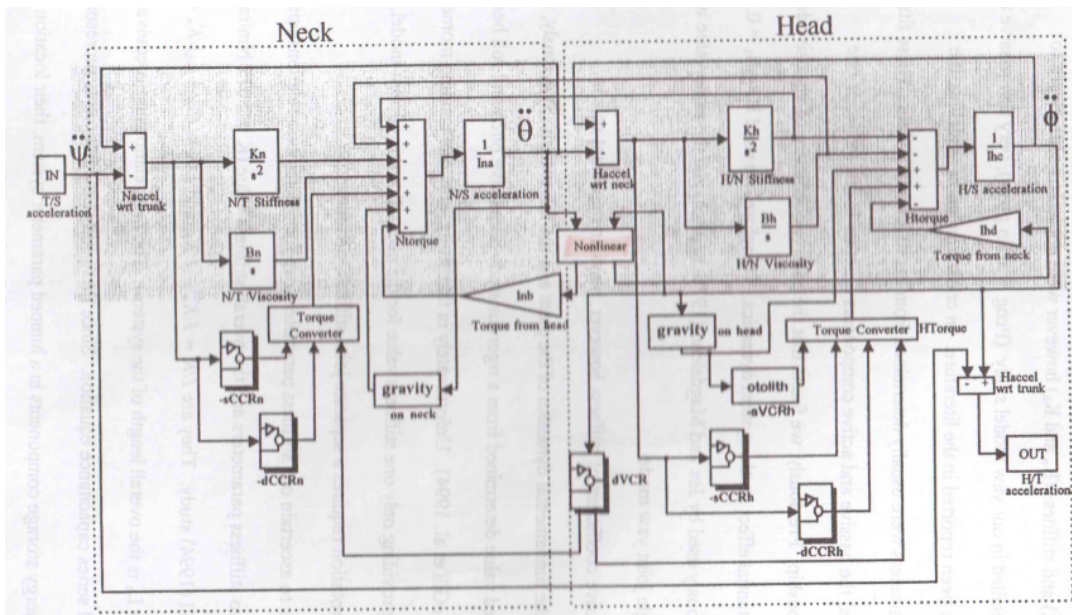
Figure 5.4 The Vestibular Sensor Model [2]
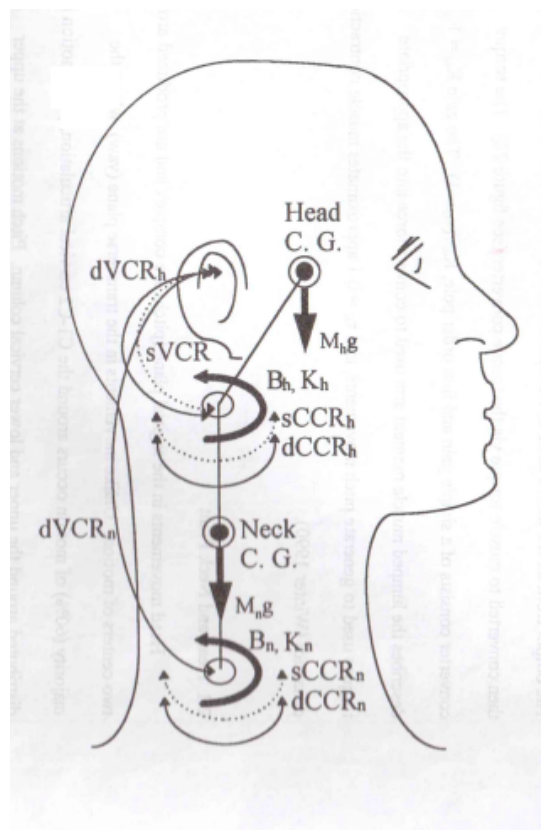
Figure 5.5 The Vestibular Sensor Model [2]

Figure 5.5 shows the two degree of freedom head model. Here, VCR means the

vestibulo-collic reflex and CCR is the cervico-collic reflex. On the other hand, one degree of freedom head model is used in this thesis because of the small movements coming from the tilt platform. In addition to that, there is no method to divide the overall neck control torque created through the CCR and VCR. Thus, it has been assumed that the neck is only controlled by VCR to stabilize head. Equation 5.32 gives the linear model of the vestibular system used in this thesis.

$$\frac{1.5}{(s + 0.19)(s + 1.5)} \tag{5.32}$$

5.4 The Somatosensory Model

Somatosensory feedback is critical for normal motor function (postural control) especially in upright stance. The mathematical model of the somatosensory system in postural control is not available in the literature. The somatosensory system measures pressure under the feet. Therefore, it may be proposed that the somatosensory system feedback generates control torque using CoP information, which has been modeled through a constant gain (see equation 5.31).

5.5 Piecewise linear Control Strategies for High and Low Frequency Perturbations

Figure 5.6 shows the block diagram for simulated human balance system at high frequency perturbation. The proprioception sensor (assumed to be intact throughout this thesis) feedbacks the relative joint angle, however vestibular sensor feedbacks the absolute angle of the head. Therefore, the control strategy at the high frequency starts with estimating the absolute angular position of the head in space through vestibular sensor (top down control strategy). The second step in the control algorithm is to estimate trunk absolute angle for which neck proprioception has been used (sensor dynamics has been assumed to be unity). Control torque for neck joint has then been generated through a PD control strategy (where control parameters of the system have been identified by optimization). The same algorithm has been run for the hip joint.

On the other hand, the control torque for the ankle joint has been estimated depending on proprioceptive and somatosensory (see equations 5.29, 5.30, and 5.31) information whereas, the gains for vestibular and somatosensory feedback contribution have been scheduled (for high frequency versus low frequency perturbation) such that for the high frequency perturbation the vestibular system is weighted against the somatosensory system (total weight of the two control systems adding up to unity). In this case, vestibular system gain has been set almost to 1 while the somatosensory system gain has been set to almost 0; pointing to a vestibular dominant proprioceptive ankle joint control.
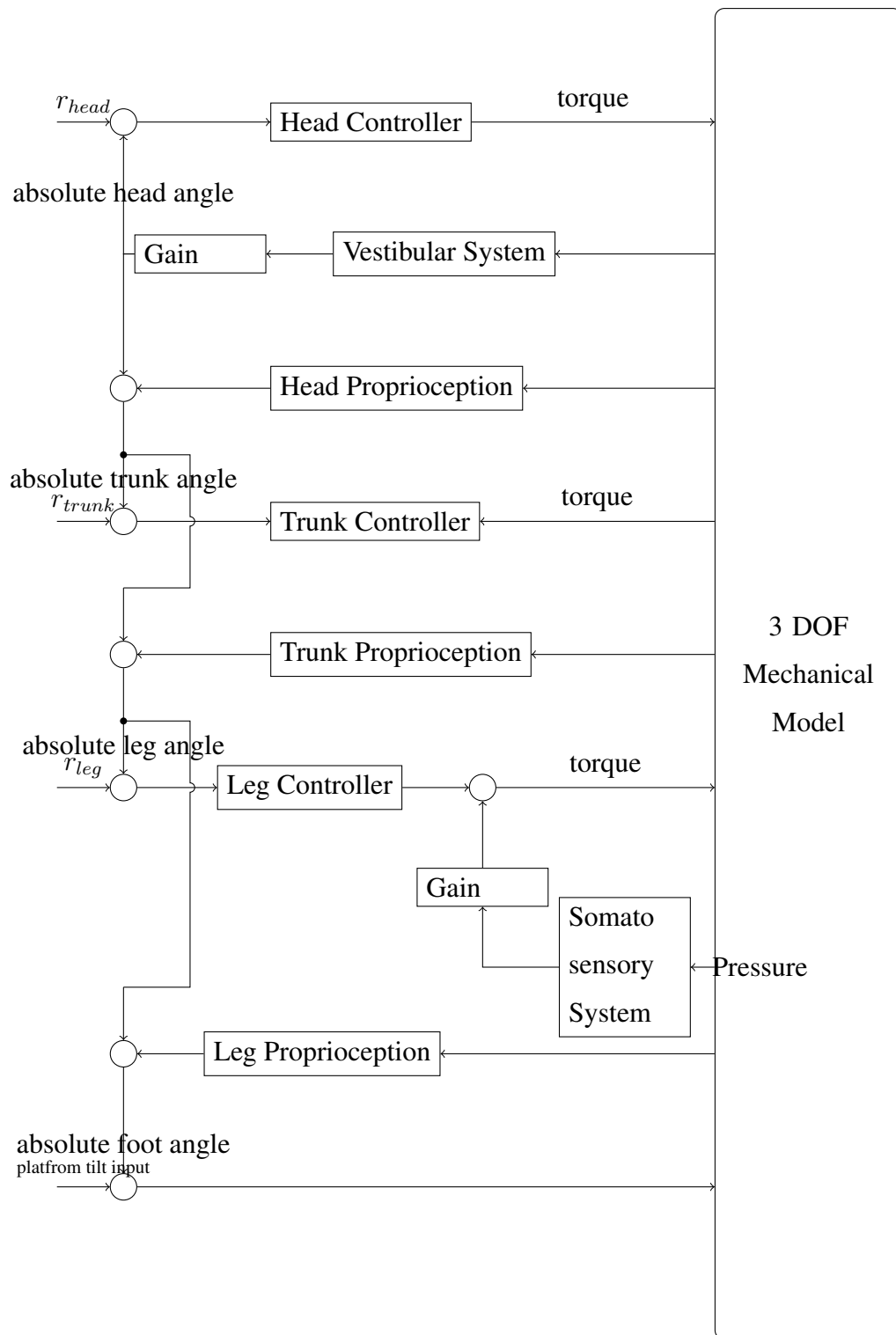
Figure 5.6 The Overall Block Diagram for high freqeuncy perturbation (body control strategy)

Figure 5.7 shows the overall block digram for low frequency input. The gain of the

somatosensory system feedback is set to 1 (because the stimulus is under vestibular threshold). Nevertheless, the control joint torques have been generated with respect to initial relative joint angles (a kind of modular joint control compared to Figure 5.6 where the control strategy depends on body control), because as the absolute head angle is unavailable (the stimulus is vestibular sub-threshold) the top down control algorithm did not work for the low frequency perturbation case. Therefore, the absolute joint angles could not have been estimated. On the contrary, the somatosensory feedback system is set to 1 (see equations 5.29, 5.30, and 5.31, the reference has been shifted to position of CoP), which implies that the control schema is turned to a bottom up control strategy for the low frequency perturbation case.
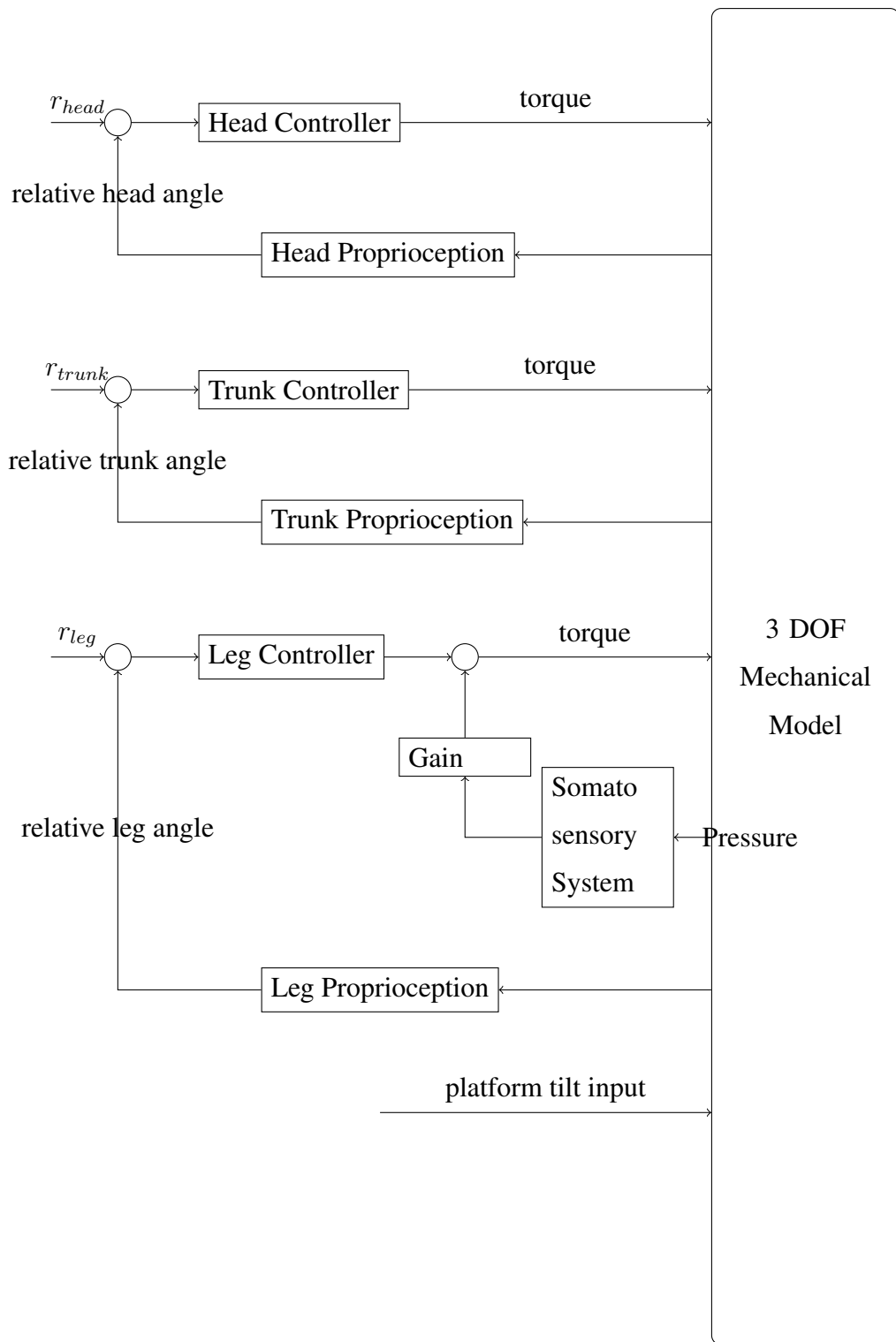
Figure 5.7 The Overall Block Diagram for low frequency input (modular joint control strategy)

CHAPTER 6

RESULTS

The results are given for a representative subject and his first trials for high and low frequency perturbations. The first part of the results is related to experimental data analysis (the statistical analysis). The second part is related to simulated data analysis.

6.1 Experimental Data Analysis Results

In this section, the statistical analysis of time domain and frequency domain results are performed. These are RMS values of absolute motion of shank and trunk with respect to gravity vertical and ankle and hip joint angular displacements. In addition, coherence, magnitude and angle estimations in frequency domain between the input and shank, trunk, ankle, and hip angular displacements. ANOVA test is applied to the signals.
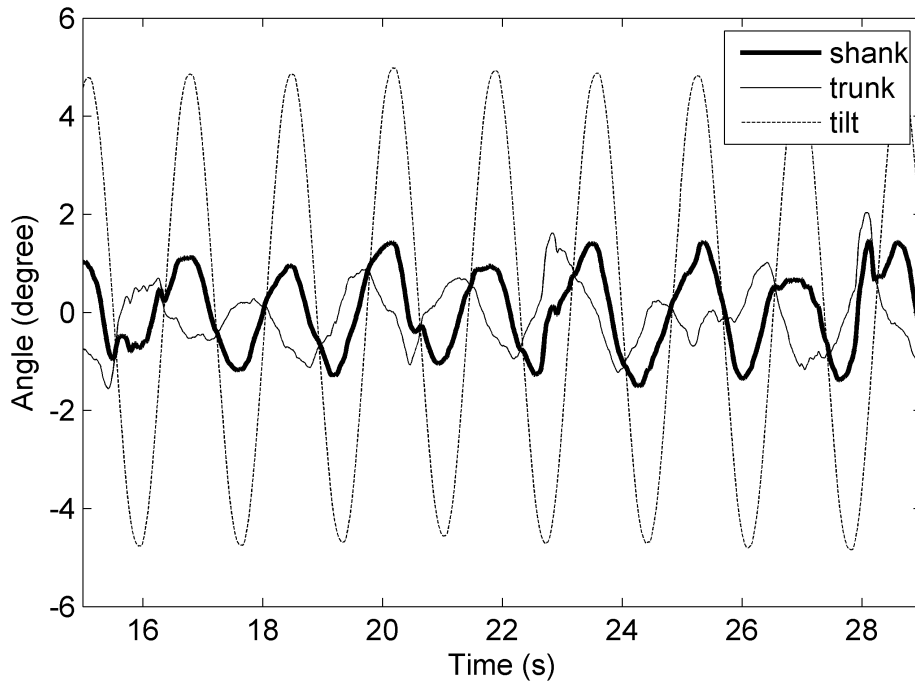
Figure 6.1 5 degrees 0.59 Hz perturbation absolute shank and trunk angular displacements
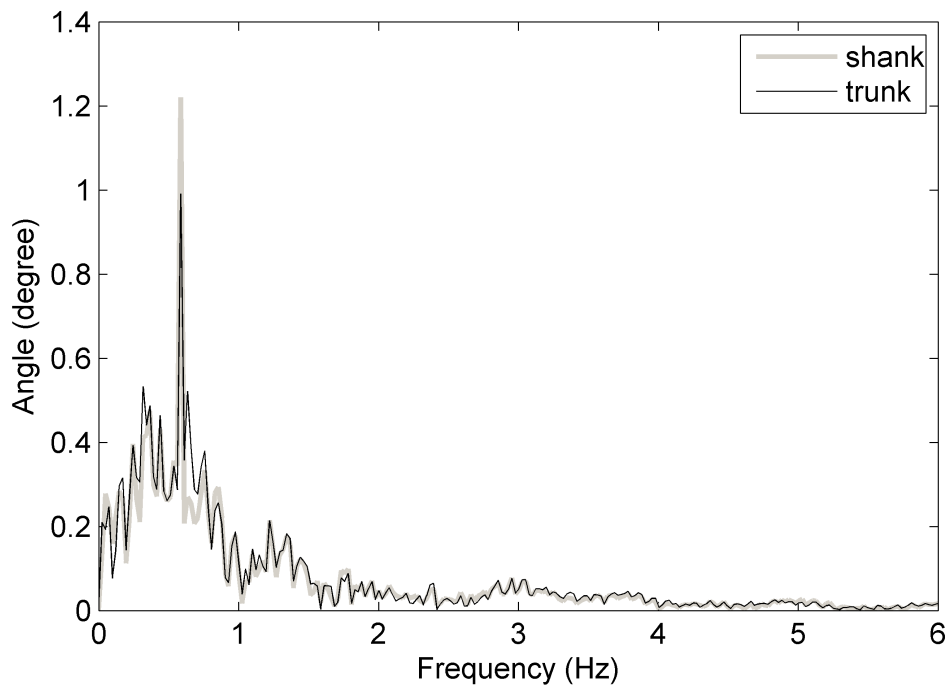
Figure 6.2 FFT of 5 degrees 0.59 Hz absolute shank and trunk angular displacement

Figure 6.1 shows a representative subject's shank and trunk angular displacements as a response to 5 degrees 0.59 Hz sinusoidal perturbation delivered by the hydraulic platform. The angular displacements are due to the gravity vertical (absolute angular displacement).

It is seen that absolute angular displacement of both shank and trunk with respect to gravity vertical did not follow (in time and in space) the platform perturbation perfectly, rather amplitude of the displacements are small compared to the stimulation's amplitude. Frequency domain analysis demonstrated that coherence values for trunk's and shank's absolute motion as a response to 0.59 Hz platform perturbation are 0.76 ± 0.16 and 0.90 ± 0.07 (not significantly different, see Appendix A), respectively. On the other hand, average RMS values for 0.59 Hz 5 degrees in amplitude platform perturbation of absolute angular displacements of trunk and shank have been found as 1.02 ± 0.27 and 1.24 ± 0.41 degrees of amplitude, respectively. Nevertheless, shank's absolute motion at the platform stimulation of 0.59 Hz has been found to be more cohere and in larger amplitude of motion compared to trunk's absolute angular motion with respect to gravity vertical. On the contrary, Figure 6.3 presents a representative subject's response to 1 degrees 0.021 Hz platform stimulation. See Appendix A.
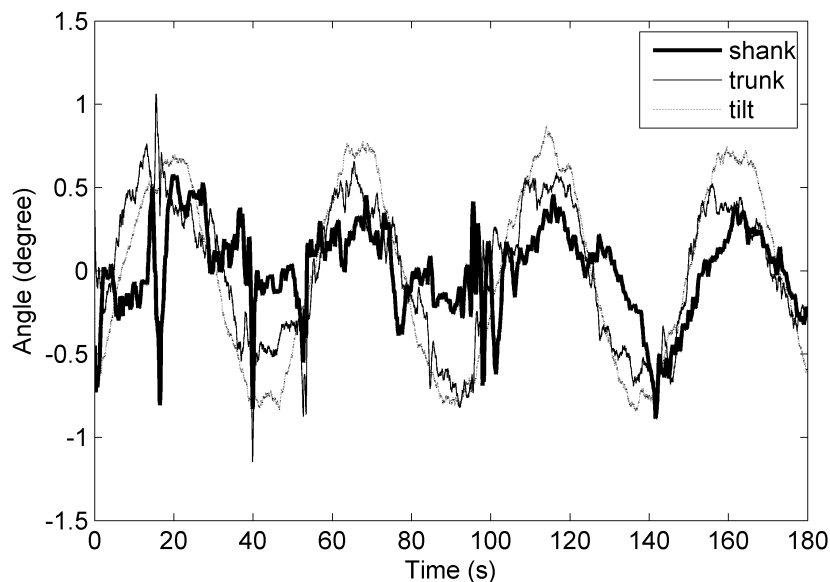
Figure 6.3 Absolute motion of the trunk and the shank as a response to 1 degree 0.021 Hz hydraulic platform stimulation
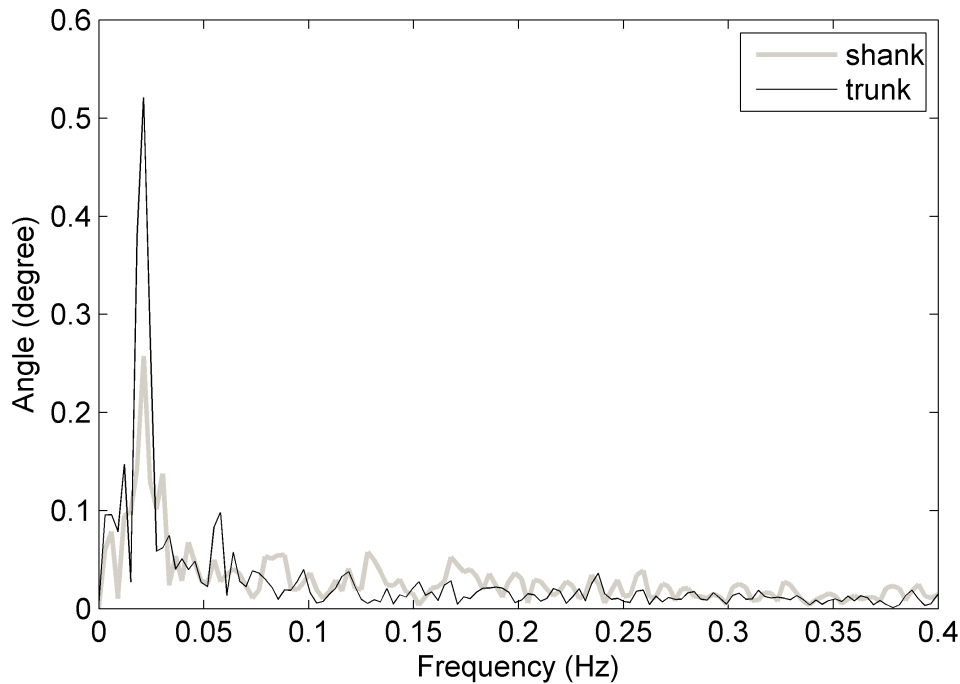
Figure 6.4 FFT of 1 degree 0.021 Hz absolute shank and trunk angular displacement

In this case, it is observed that trunk and shank follows the platform perturbation in relatively higher amplitude (see Table 6.1 magnitude values for 0.59 Hz vs 0.021 Hz). In other words, trunk's and shank's response is much more congruent with the platform perturbation compared to high frequency. Frequency domain analysis demonstrated that coherence values for trunk's and shank's absolute motion as a response to 0.021 Hz platform perturbation are 0.79 ± 0.17 and 0.79 ± 0.17, respectively. On the other hand, average RMS values for 0.021Hz 1 degree platform perturbation of absolute angular displacements of trunk and shank have been found as 0.64 ± 0.23 and 0.53 ± 0.24 degrees of amplitude (significantly different than high frequency p < 0.0000), respectively. See Appendix A.

Magnitude and angle of the cross spectral density function estimates between platform perturbation and angular motion of the trunk and shank with respect to gravity vertical are given in Table 6.1. See Chapter 4 equations 4.12 and 4.13.

Table 6.1 Magnitude and angle values of the cross spectral density function estimates between platform perturbation (P) and absolute angular displacement of trunk (T) and shank (S), respectively.

	f=0.59 Hz	f=0.59 Hz	f=0.021 Hz	f=0.021 Hz
	Magnitude	Angle	Magnitude	Angle
$G_{PT}(f)$	0.15 ± 0.04	110.81 ± 44.82	0.81 ± 0.11	13.95 ± 7.95
$G_{PS}(f)$	0.26 ± 0.10	21.53 ± 13.23	0.66 ± 0.15	12.41 ± 7.54

It can be observed by looking at Table 6.1 that when the platform perturbation is large in amplitude and high at frequency (high velocity perturbation) both absolute trunk and shank displacements are small with respect to the absolute platform motion (p<0.0000), further trunk's motion is out of phase due to the platform's perturbation while shank is in phase with the platform (p<0.0000). However, when the stimulation delivered by the hydraulic platform to the subjects is small in amplitude and low in frequency (low velocity stimulation) both the trunk and the shank follows the platform's motion; trunk's motion is much more congruent to platform rather than shank (in phase) with significantly larger amplitude of movement (p<0.0002, trunk's magnitude has been found to be significantly larger than shank's magnitude for the low frequency perturbation).

In summary, when absolute motion of the trunk and the shank are searched due to the platform input, it has been observed that shank motion (in phase) is much more cohere at the perturbation frequency compared to trunk motion (not in phase) with similar amplitudes (but small magnitudes of related transfer functions in Table 6.1) at high frequency. On the other hand, trunk's and shank's motions are larger in amplitude with a considerable coherence and in phase response for low frequency stimulation. In addition to that, the subjects try not to move the trunk in the higher velocity stimulation compared to the low velocity perturbation where they feel much more free to move the trunk in a congruent way (p<0.0002).

The coherence values of center of mass displacement with respect to the space are found to be 0.77 ± 0.16, 0.54 ± 0.16 for high and low frequency perturbations, respectively (p<0.0024). On the other hand, RMS values for the absolute displacements of the center of mass are found to be 0.018 ± 0.005 and 0.016 ± 0.003 for high and low frequency perturbations, respectively. It is important to note that RMS values of the

absolute movement of center of mass is similar. See Figures 6.5 and 6.7. Table 6.2 demonstrates magnitude and angle values for high and low frequency perturbations of cross spectral density function estimates between the platform motion and the center of mass absolute movement.

Table 6.2 Magnitude and angle values of the Cross spectral density function estimates between platform perturbation (P) and absolute angular motion of the center of mass (CoM)

	f=0.59 Hz	f=0.59 Hz	f=0.021 Hz	f=0.021 Hz
	Magnitude	Angle	Magnitude	Angle
$G_{PCM}(f)$	0.0018 ± 0.005	147.68 ± 19.48	0.017 ± 0.004	29.20 ± 14.90

Figures 6.5 and 6.7 show the time series for absolute motion of COM for 0.59 and 0.021Hz frequencies, respectively and Figures 6.6, 6.8 show their corresponding FFT.
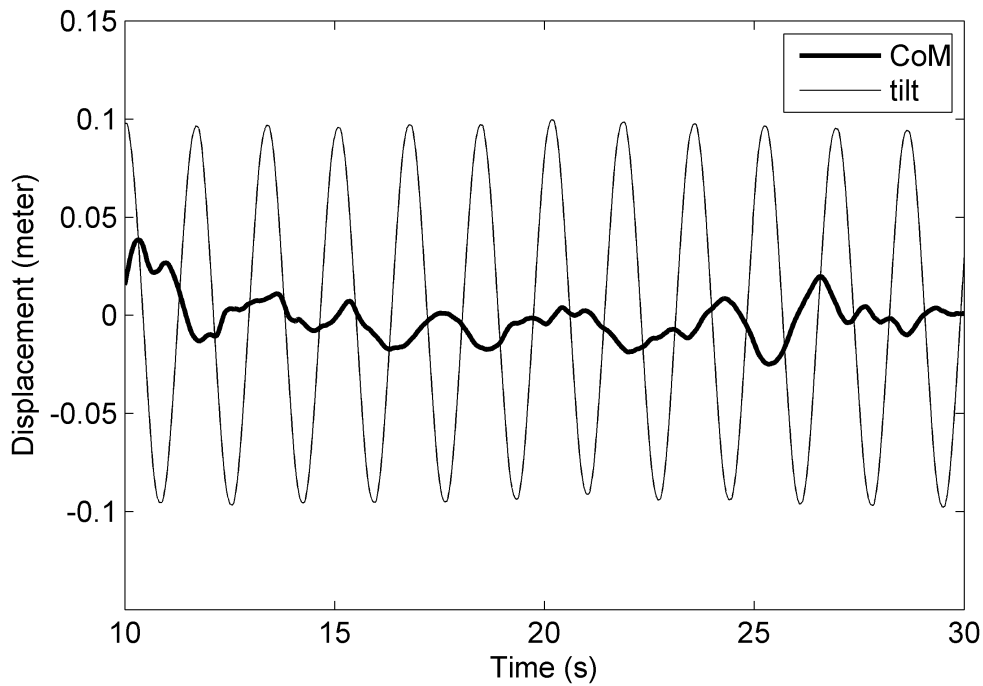
Figure 6.5 Center of mass excursion at 0.59 Hz 5 degrees perturbation with respect to the gravity vertical

74
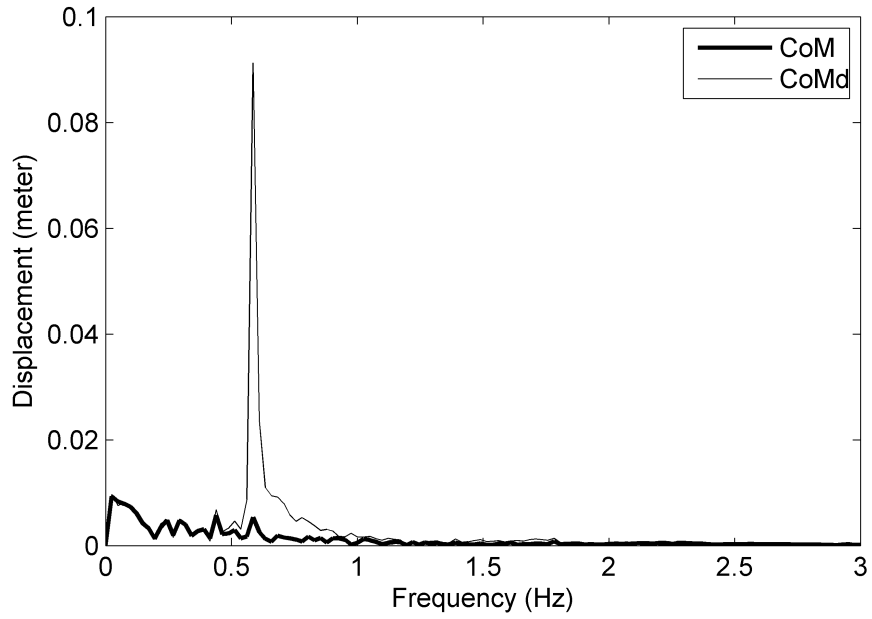
Figure 6.6 FFT of 5 degrees 0.59 Hz absolute CoM and relative CoM (See section 4.2.2 and Appendix B) go to Figure 6.14
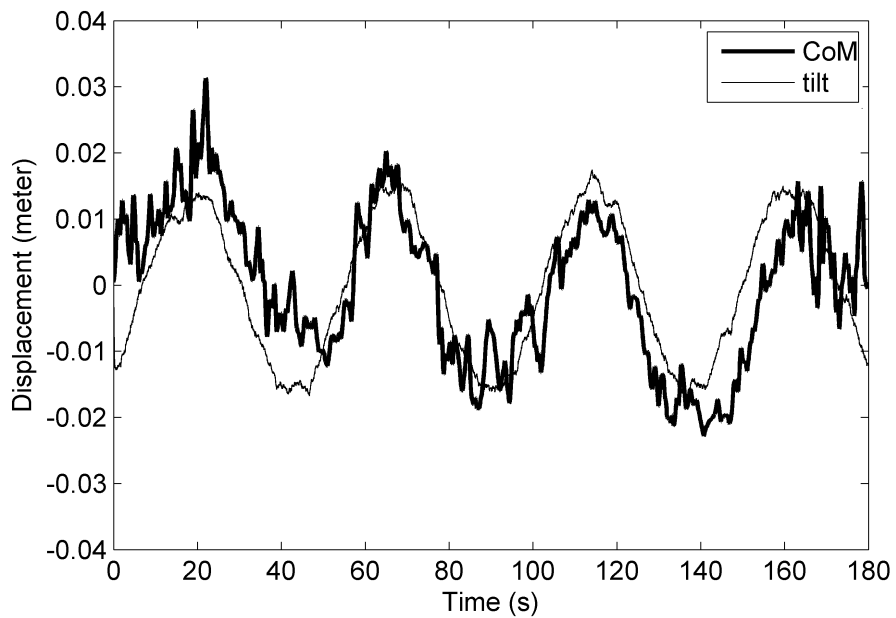
Figure 6.7 Center of mass excursion at 0.021 Hz 1 degree perturbation with respect to the gravity vertical
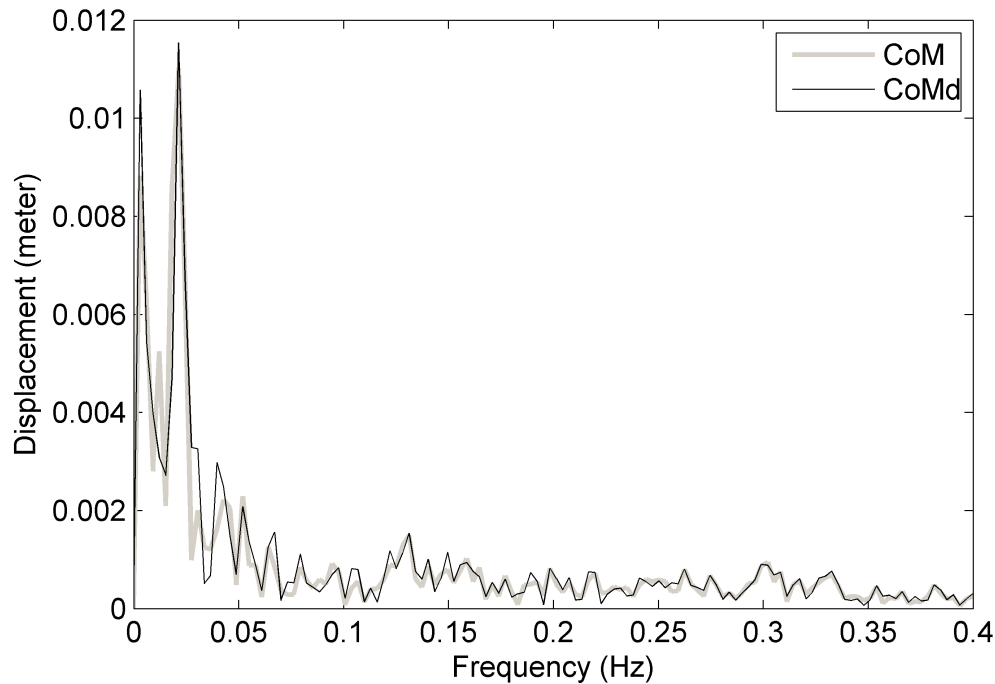
Figure 6.8 FFT of 1 degree 0.021 Hz absolute CoM and relative CoM. Go to Figure 6.15

In summary, the result of the overall control strategy applied by the subjects for 0.59 Hz, 5 degrees perturbation versus 0.021 Hz, 1 degree perturbation, one can notice that CoM excursion (absolute, see Figures 6.5 and 6.7) has been limited to almost 1 degree. Subjects decrease the CoM motion with an out-of-phase relation with respect to the stimulation with a significantly high coherence in high frequency case (Go to Figure 6.14), while moving (in-phase) with the platform with a low coherence in the low frequency case (Go to Figure 6.15). See Figures 6.6 and 6.8. Figure 6.6 (FFT plot) shows that amplitude of relative CoM excursion is almost ten times larger than absolute COM excursion at high frequency stimulation. However, they have almost the same amplitude for the low frequency case.

In order to understand the control strategies used by the subjects better, one has to look at the relative angular displacements of the ankle and hip joints as well. See Chapter 4 section 4.2.2 and Figure 4.3 equations 4.6 . Figure 6.9 shows the relative angular displacement of ankle and hip joints.
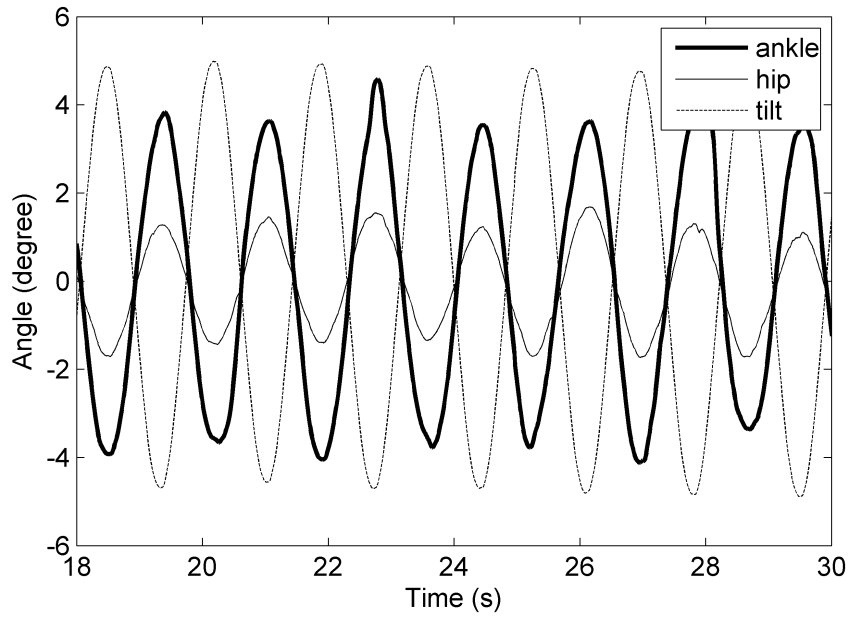
Figure 6.9 Relative angular displacement of the shank with repsect to the foot (ankle joint motion), and trunk with respect to shank (hip joint motion) at 0.59 Hz and 5 degrees of amplitude
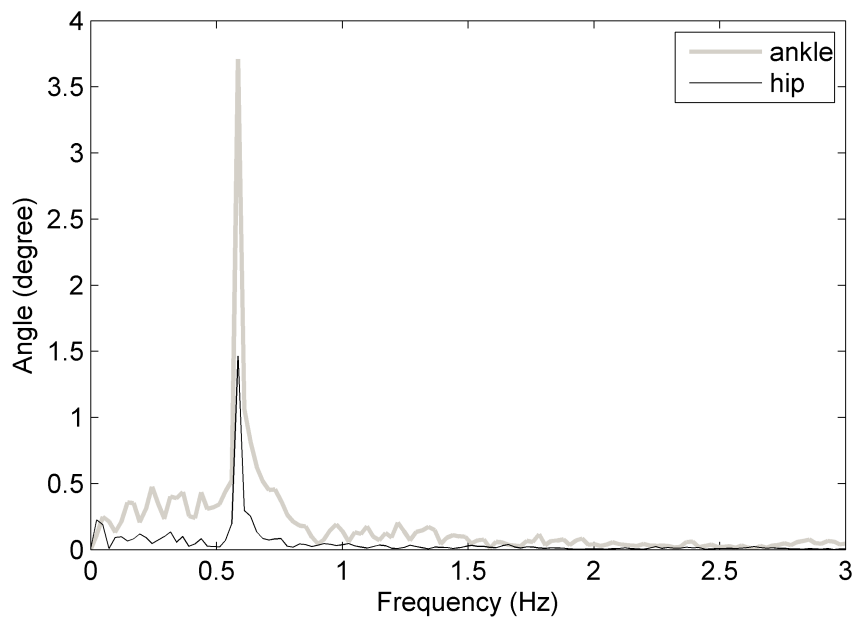
Figure 6.10 FFT of ankle and hip joint movement at 0.59 Hz and 5 degrees of amplitude

It can be noticed in Figure 6.9 that both ankle and hip joint's motions are out of phase with respect to the foot for 0.59 Hz and 5 degrees of amplitude platform disturbance. It seems that there exists a small amplitude compensation of the ankle joint movement by the hip joint motion (Table 6.3). Coherence values of relative angular displacements in-between platform disturbance and the ankle and hip joint's motion has been found to be 0.99 ± 0.01 and 0.99 ± 0.004, respectively (As it can be recalled that the absolute angular displacement of the trunk has not been that cohere with the perturbation, while absolute shank motion has been cohere with the platform motion. Discrepancy between coherence values of trunk's absolute and relative angular displacements may be interesting to estimate the noise on the vestibular versus proprioceptive base control for trunk). Furthermore, angular displacement of the hip joint is smaller than the angular displacement of the ankle joint. RMS values of angular motions for ankle and hip joints are 2.79 ± 0.37 and 1.07 ± 0.09 degrees (p<0.0000), respectively. Furthermore, cross spectral density function estimates between the platform perturbation and ankle and hip joint's angular motion are presented in Table 6.3.

Table 6.3 Magnitude and angle values of the Cross spectral density function estimates between platform perturbation (P) and relative angular displacement of trunk (T) (hip joint motion) and shank (S) (ankle joint motion), respectively

	f=0.59 Hz	f=0.59 Hz	f=0.021 Hz	f=0.021 Hz
	Magnitude	Angle	Magnitude	Angle
$G_{PH}(f)$	0.27 ± 0.02	176.1 ± 2.43	Not Cohere	Not Cohere
$G_{PA}(f)$	0.76 ± 0.11	174.85 ± 2.38	0.43 ± 0.211	158.73 ± 16.05
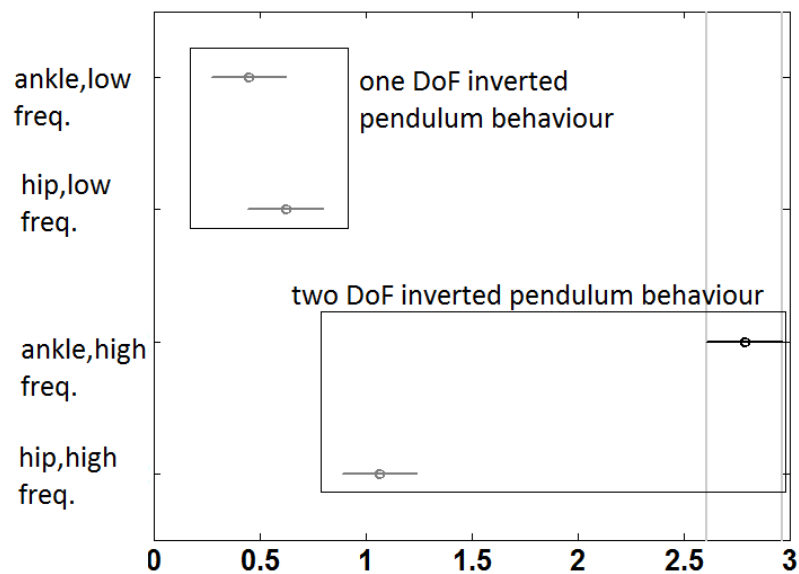
Figure 6.11 2D ANOVA for RMS values of ankle and hip angular displacements distrubuted over perturbation frequencies

On the contrary to high frequency stimulation, platform perturbation at 0.021 Hz and 1 degree of amplitude causes responses (see Figure 6.12) which are significantly low in coherence to platform perturbation; i.e., 0.64 ± 0.23 and 0.33 ± 0.15 for ankle and hip joint's movements, respectively (See against 0.99 ± 0.01 and 0.99 ± 0.004 ankle and hip, respectively). On the other hand, RMS values for relative angular motion of the limbs are 0.45 ± 0.25 and 0.62 ± 0.42 degrees for ankle and hip joints' angular motion, respectively (at lower frequency). When the variation in the RMS values of the relative motion of ankle and hip joints are distributed with respect to frequencies, the relative motion of ankle joint at high frequency perturbation is found to be significantly larger than relative motion of the hip joint (Go to Figure 6.11).
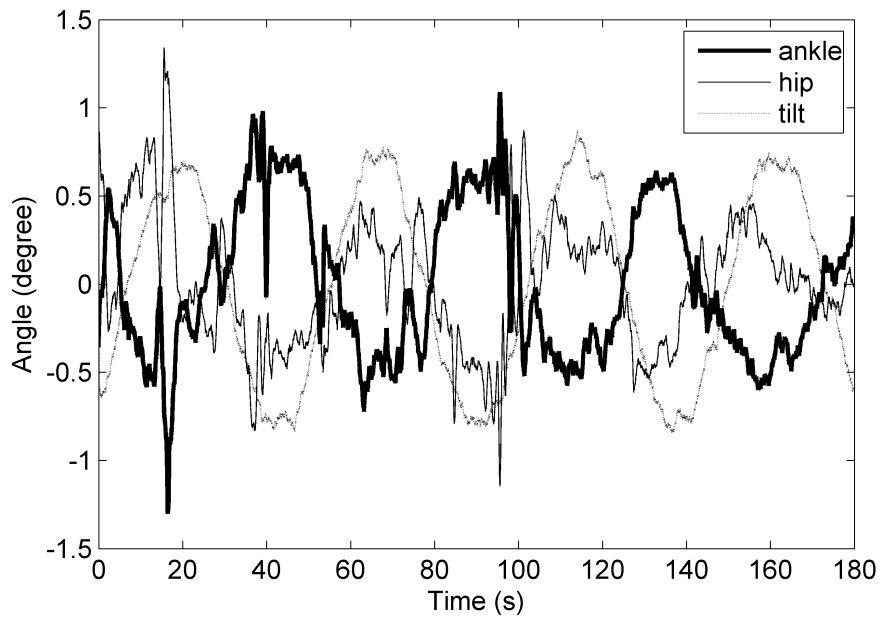
Figure 6.12 Relative angular displacement of the shank with respect to the foot (ankle joint motion), and trunk with respect to shank (hip joint motion) at 0.021 Hz and 1 degrees of amplitude
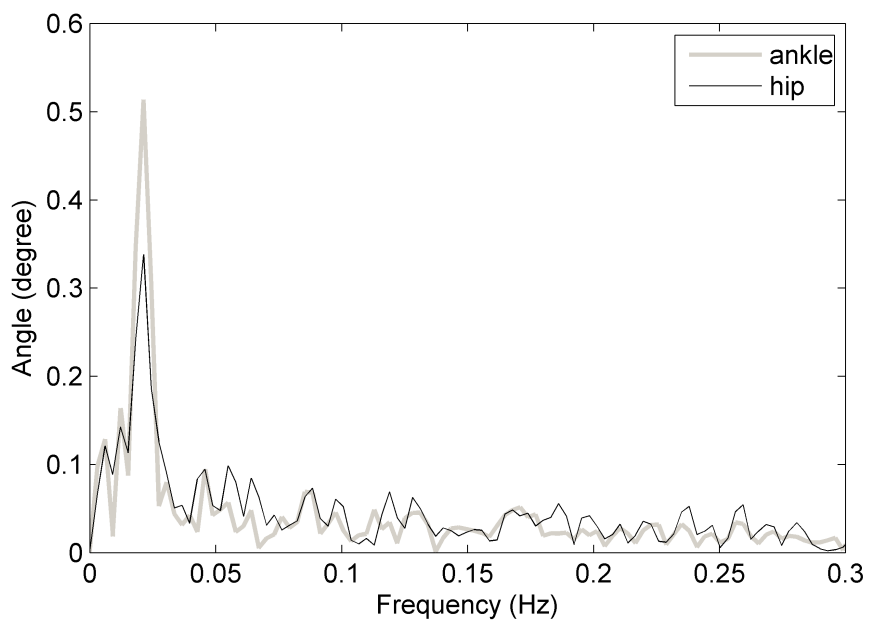
Figure 6.13 FFT of ankle and hip joint movement at 0.021 Hz and 1 degree of amplitude

In summary for the results presented at Tables 6.1 and 6.2, one can observe from the absolute kinematic signals of shank and trunk that at 0.59 Hz, 5 degrees platform stimulation that although shank followed the platform with a considerably small magnitude (See magnitude for shank at Table 6.1) trunk tries to resist the movement (see the same table, also Table 6.2), when relative kinematics data are searched hip joint's angular displacement is low compared to ankle joint suggesting that the body control strategy has been selected as a double DOF inverted pendulum, see Figure 6.11 (Considerable linear behavior where ankle and trunk dynamics are coupled). On the contrary, both trunk and the shank are in phase motion with the platform for the low frequency platform perturbation (See Table 6.1) but when Table 6.3 data for relative motion of trunk with respect to shank (hip joint angular motion) and shank with respect to the foot (ankle joint angular displacement) are looked at although ankle's motion is out of phase with the platform with a coherence value of 0.64 (medium size), hip joint angular displacement is not found to be cohere to the platform stimulation (0.33, very low); pointing to an uncoupled trunk dynamics (in contrast to the previous stimulation). Furthermore, when Figure 6.11 is looked at, RMS value of relative ankle joint is almost similar to relative hip joint motion at low frequency, which points to a single DOF-like inverted pendulum behavior (See Figure 6.11). However, when Table 6.1 is looked at it is seen that magnitude of absolute trunk compared to magnitude of absolute shank excursion is significantly different at low frequency perturbation, p<0.0002 (see Chapter 7 for this contradiction). This result may be interpreted behalf of quiet-stance like dynamics appeared as a result of adaptation of the subjects to the very low –below the vestibular threshold- frequency platform stimulation. It is important to note that high frequency results are much more stereotypic for relative link displacements but the low frequency results showed that limb's kinematics are much more involved with different dynamical sources other than platform perturbation.

Additionally relative motion of CoM ($CoM_{m/fp}$, see Chapter 4 equation 4.5) with respect to the platform can also be studied for verification of the results that have already been revealed, although these results will be dependent to the results of center of mass motion with respect to gravity vertical.

First of all, our expectation for 0.59 Hz 5 degrees stimulation to the subjects is

to cause a higher amplitude motion of the center of mass with a high coherence compared to the 0.021 Hz 1 degree perturbation. Thus, coherence values for relative motion of CoM with respect to the platform are found to be 0.998 ± 0.001 and 0.360 ± 0.144 whereas, RMS values for relative motion of CoM are 0.076 ± 0.003 and 0.015 ± 0.003 for high and low frequency stimulus, respectively. As expected, relative COM response to high frequency perturbation is cohere and manifests with large amplitude correction, while response to low frequency is not cohere with the platform perturbation. Figures 6.14 and 6.15 show relative COM displacements with respect to the platform where their FFT plots are presented at Figures 6.6 and 6.8.
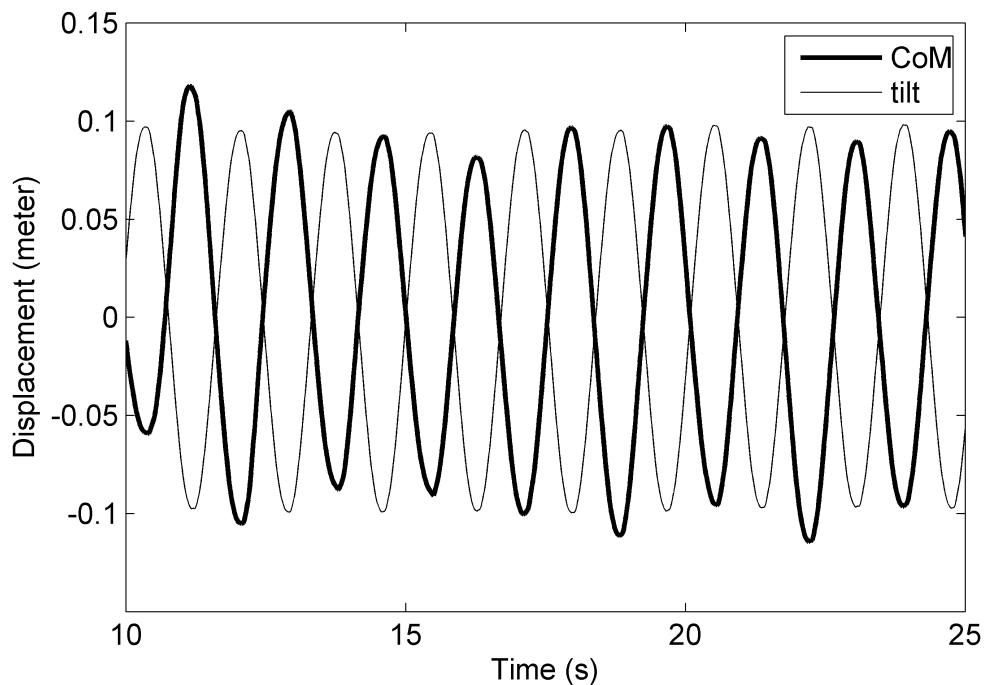
Figure 6.14 Relative COM linear motion with respect to the force plate or (the platform) at 0.59 Hz 5 degrees stimulation, go to Chapter 4 section 4.2.2, equation 4.5 and Appendix B
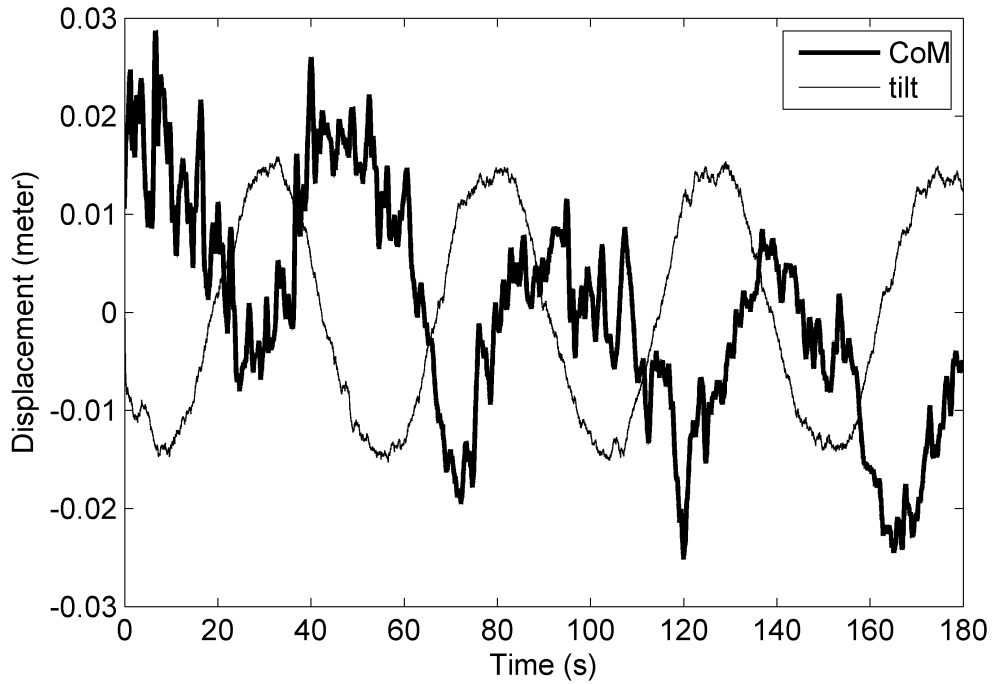
Figure 6.15 Relative CoM linear motion with respect to the force plate or (the platform) at 0.021 Hz 1 degree stimulation

Table 6.4 Cross spectral density function magnitude and angle estimations in-between the platform perturbation versus relative CoM motion at each frequency

	f=0.59 Hz	f=0.59 Hz	f=0.021 Hz	f=0.021 Hz
	Magnitude	Angle	Magnitude	Angle
$G_{PCM}(f)$	0.021 ± 0.001	177.84 ± 0.96	Not Cohere	Not Cohere

As both from Figure 6.15 and Table 6.4 can be seen that decomposed CoM trajectories are not cohere with the platform perturbation (0.360 ± 0.144). Low coherence estimate for CoM trajectory at low frequency stimulus and the power spectral density estimates for CoM motion seems like postural sway in quiet stance. Thus, Figure 6.16 shows decomposed CoP trajectories at sagittal plane (in antero-posterior direction) and its power spectral density estimates compared to the quiet stance CoP trajectories and with its power spectrum for the same subject (See Appendix B for a detailed explanation of CoM vs CoP relation).

83
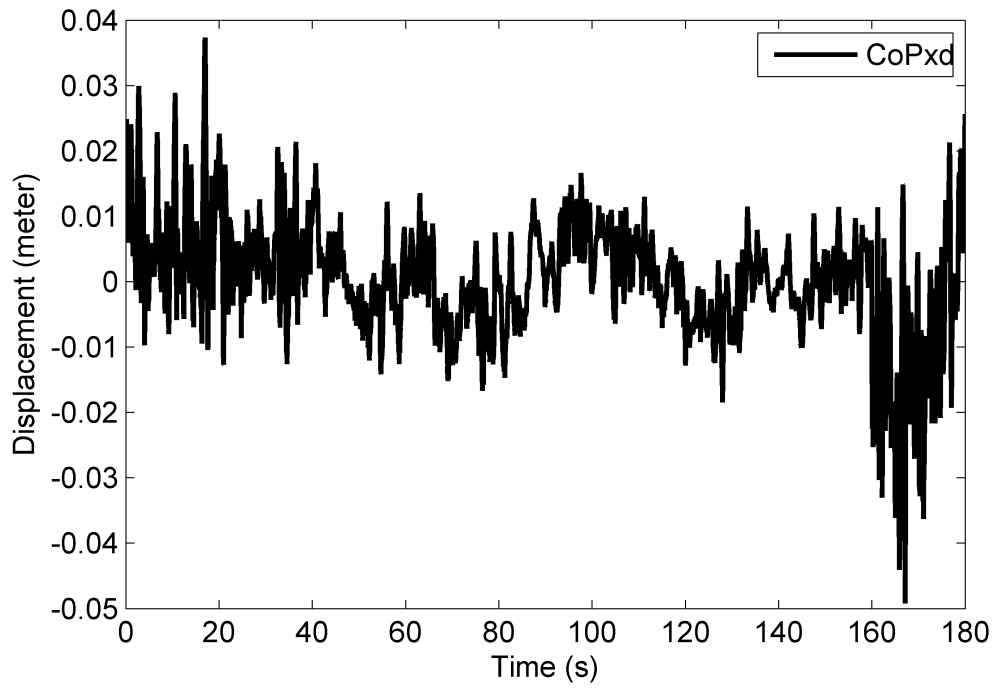
Figure 6.16 CoP decomposed trajectories at 0.021 Hz 1 degree platform perturbation to be compared to quiet stance
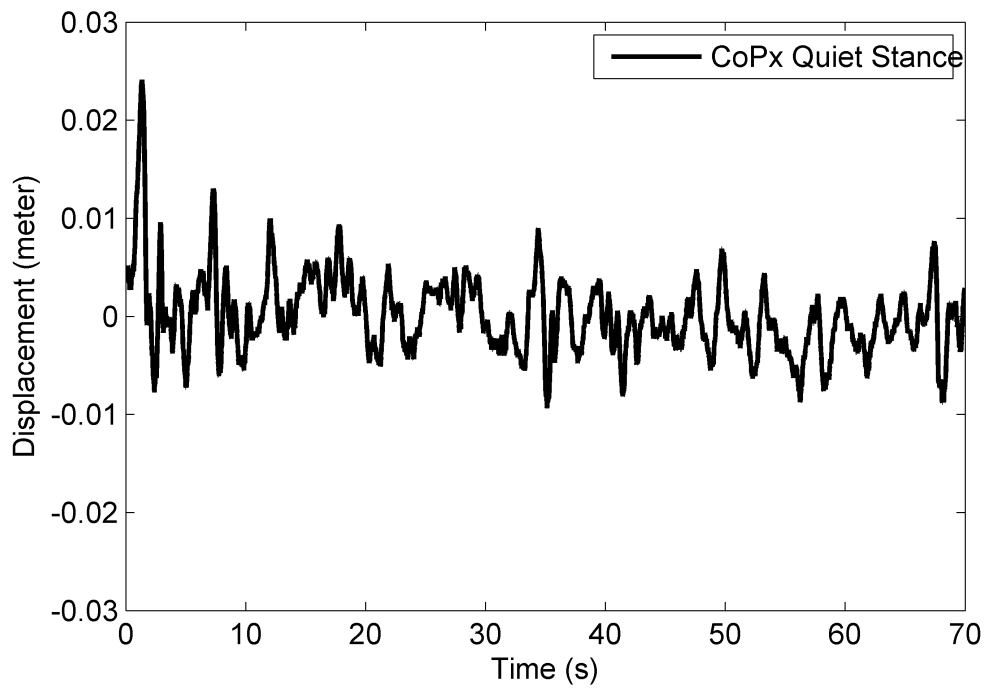
Figure 6.17 CoP trajectories for quiet stance
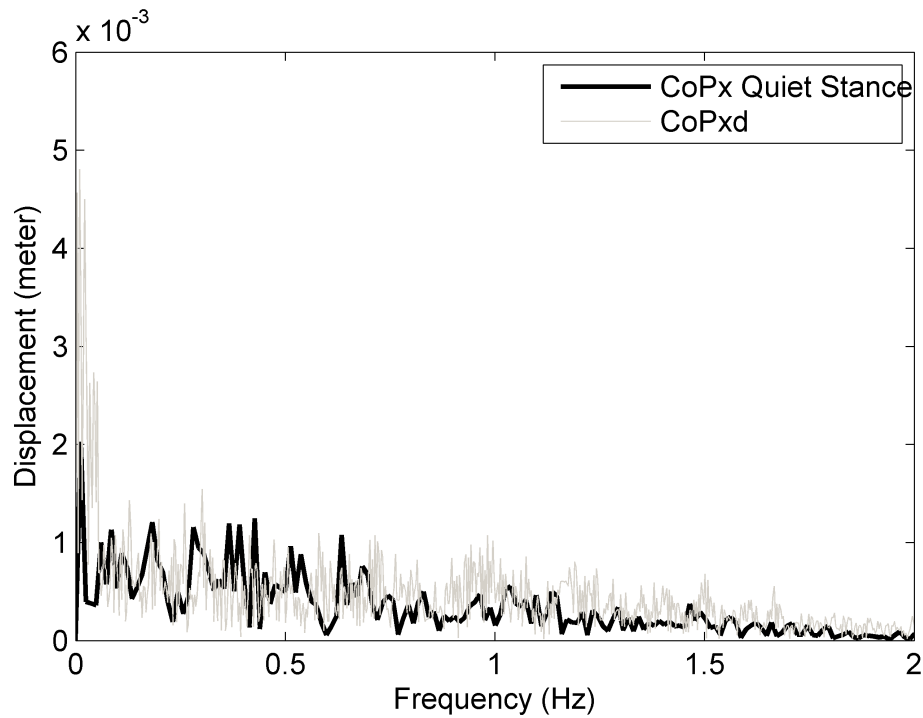
Figure 6.18 FFT of CoPx for quiet stance and CoPxd for 0.021 Hz and 1 degree of amplitude

Additionally, areas under the FFT of absolute and relative CoM excursions are computed (Go to Chapter 4 Equation 4.15 for the definition of area ratio). Area ratios related to absolute and relative CoM excursions have been presented in Table 6.5. Absolute CoM excursions are not significantly different with respect to frequency stimulations. However, area ratio related to decomposed CoM excursion at high frequency is found to be significantly larger than at low frequency stimulation and area ratios related to absolute CoM excursion (p<0.0000). See Table 6.5 and Figures 6.6 and 6.8.

Table 6.5 Area ratio of FFT of absoulute and relative CoM excursions for high and low frequencies

	f=0.59 Hz	f=0.59 Hz	f=0.021 Hz	f=0.021 Hz
	Absolute (Measured)	Relative (De-composed)	Absolute (Measured)	Relative (De-composed)
Area Ratio	0.104 ± 0.022	0.299 ± 0.017	0.119 ± 0.019	0.134 ± 0.035

6.2 Simulated Data Analysis Results

The simulation results are given for high frequency and low frequency inputs.

6.2.1 Results for High Frequency and Amplitude Input

Figure 6.19 shows the relative shank angle with respect to the foot. This is called ankle angle. Thus, the ankle angle and tilt input angle have out of phase relation. In addition, the amplitude of the ankle angle is closed to tilt input (see Figure 6.19). Therefore, the subject aligns the shank to the gravity vertical during the experiment of 5 degree and 0.59 Hz tilt input. On the other hand, the mathematical model simulation for the shank almost follows the ankle angle. Figure 6.19 shows the error values during the experiment. The reference command for joint torques (ankle, hip, head) at the mathematical model was computed with respect to gravity vertical (see Figure 5.6). Therefore, one can conclude that the subject's shank uses the gravity vertical reference frame for the postural control.

Figure 6.19 High Frequency Ankle Angle for subject 9 and trial 1
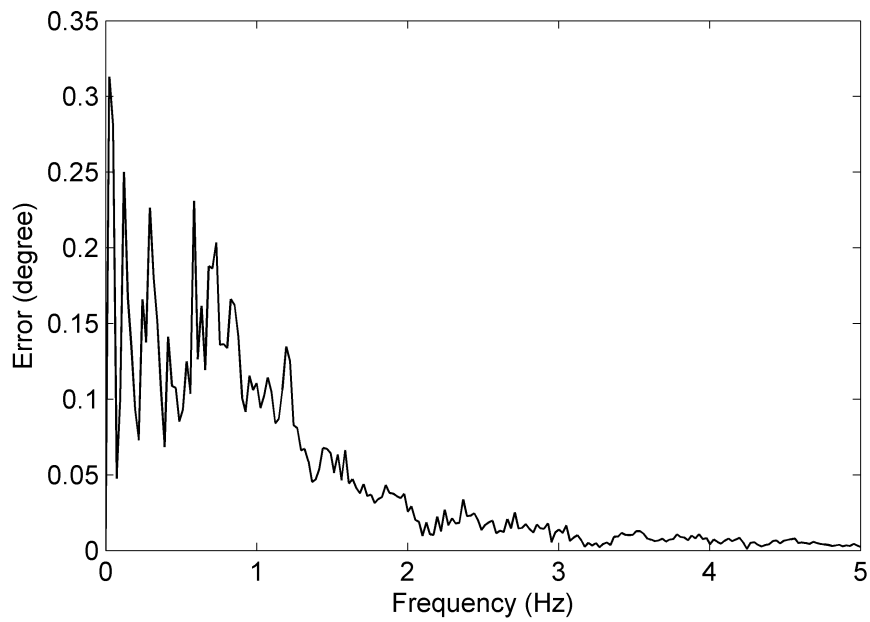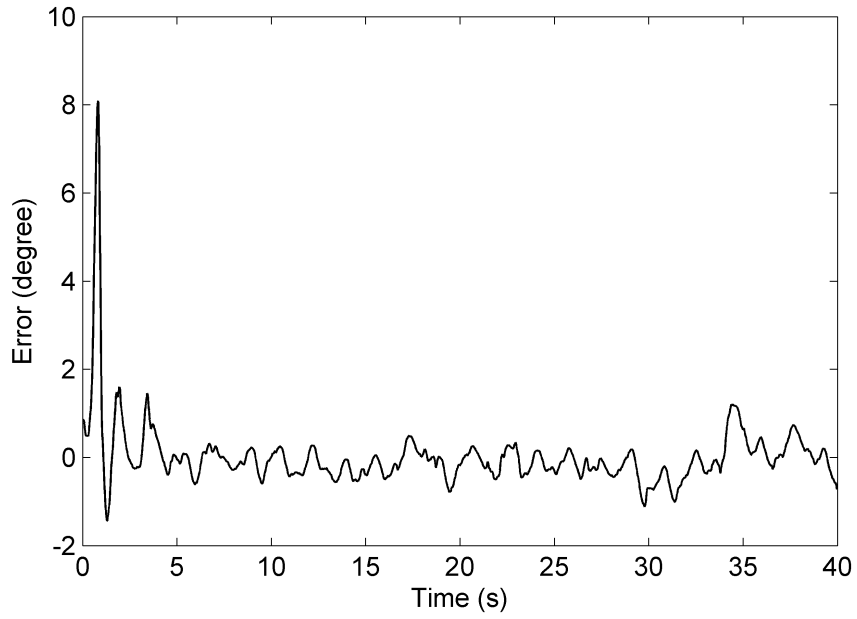
Figure 6.20 Error and FFT of error for subject 9 and trial 1

Figure 6.21 shows the absolute trunk angle with respect to the gravity vertical. One can see from Figure 6.21 that compared to the tilt input the amplitude of the trunk angle is so small. It is below the 1 degree. Therefore, the subject's trunk aligns itself to the gravity vertical. The reference command for joint torques (ankle, hip, head)

at the mathematical model was computed with respect to gravity vertical (see Figure 5.6). In conclusion, the subject's trunk uses the gravity vertical as a reference frame for the postural control. Figure 6.22 shows the error values during the experiment.
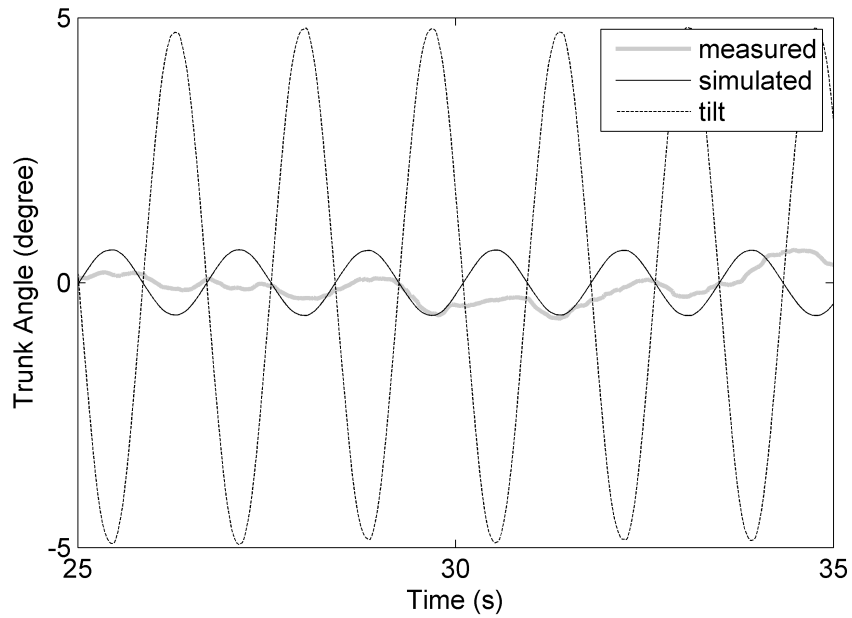
Figure 6.21 High Frequency Trunk Angle for subject 9 and trial 1
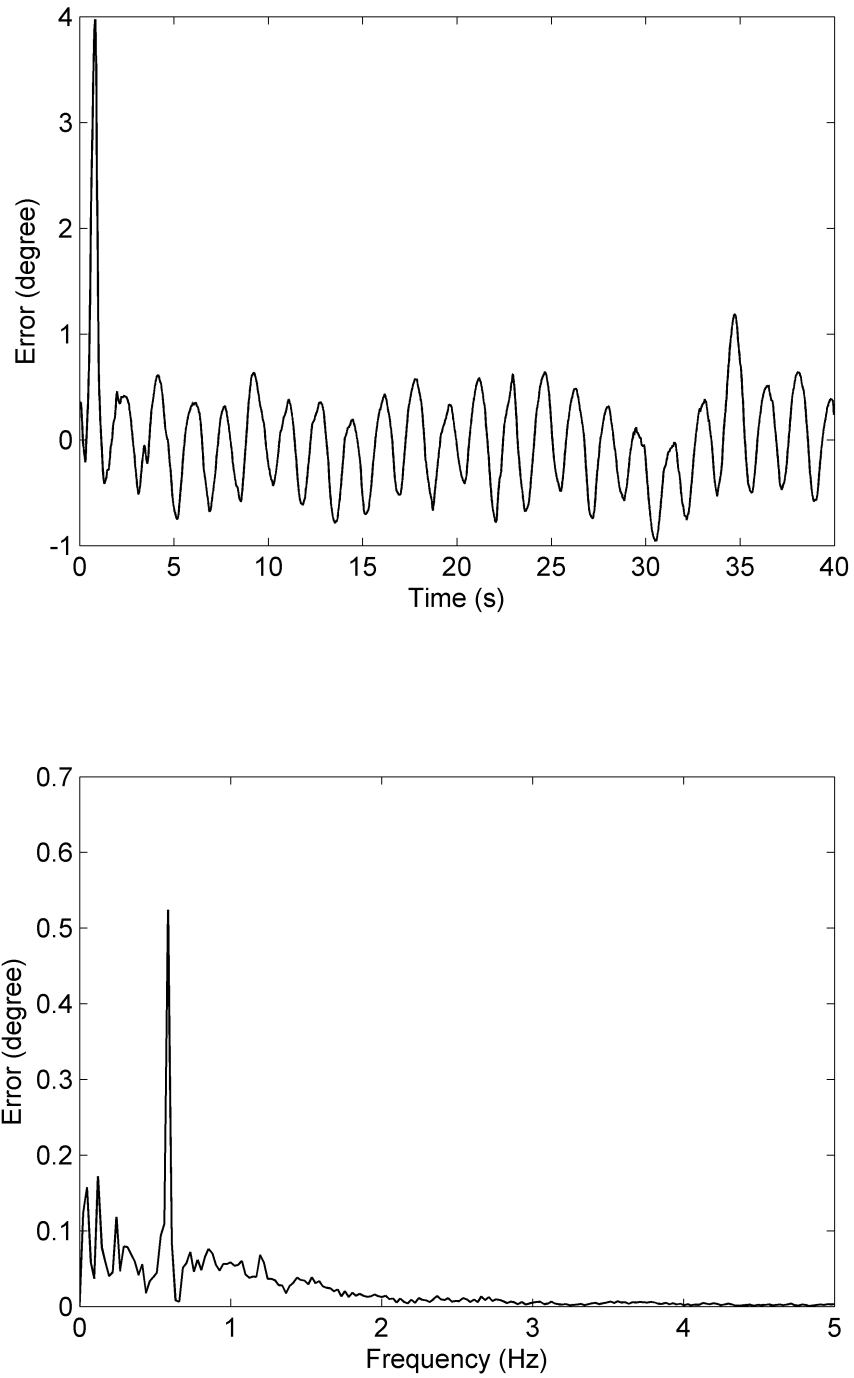
Figure 6.22 Error and FFT of error for subject 9 and trial 1

Figure 6.23 shows the absolute head angle with respect to the gravity vertical. Similar to the trunk and shank, the subject's head uses the gravity vertical as a reference frame. In addition, the reference command for the head of the mathematical model is zero with respect to the gravity vertical. On the other hand, the error values are

higher than the trunk and shank errors. The possible causes for this error can be the head's inertia is small compared to the trunk and shank for the human. Therefore, the subject could be more tolerant than trunk and shank. In addition to that, the voluntary movements could have effected head in larger amounts compared to the trunk and shank.
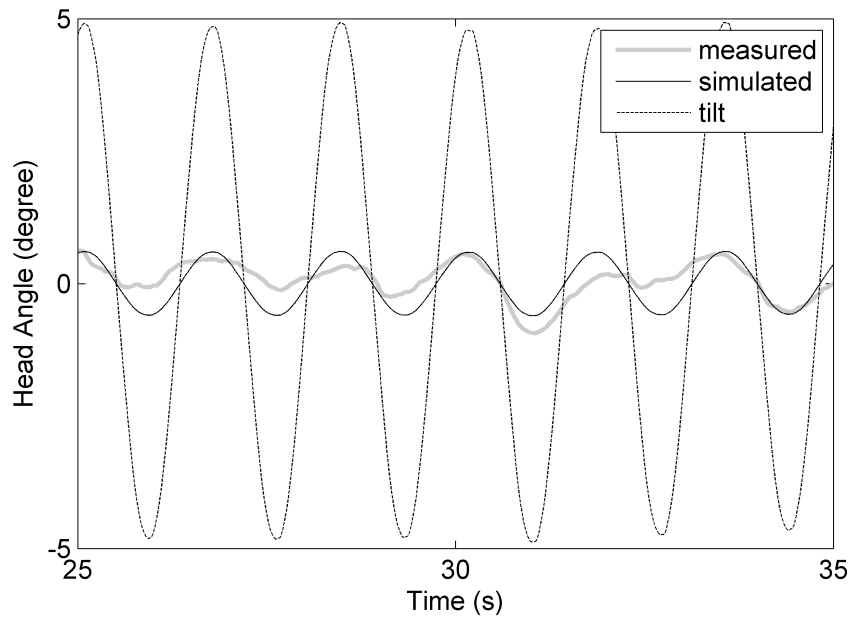
Figure 6.23 High Frequency Head Angle for subject 9 and trial 1
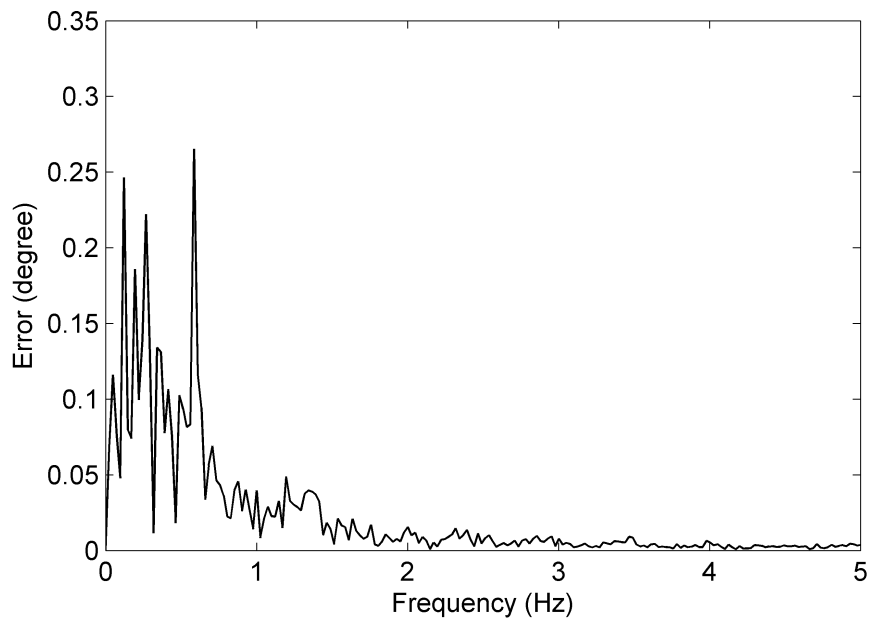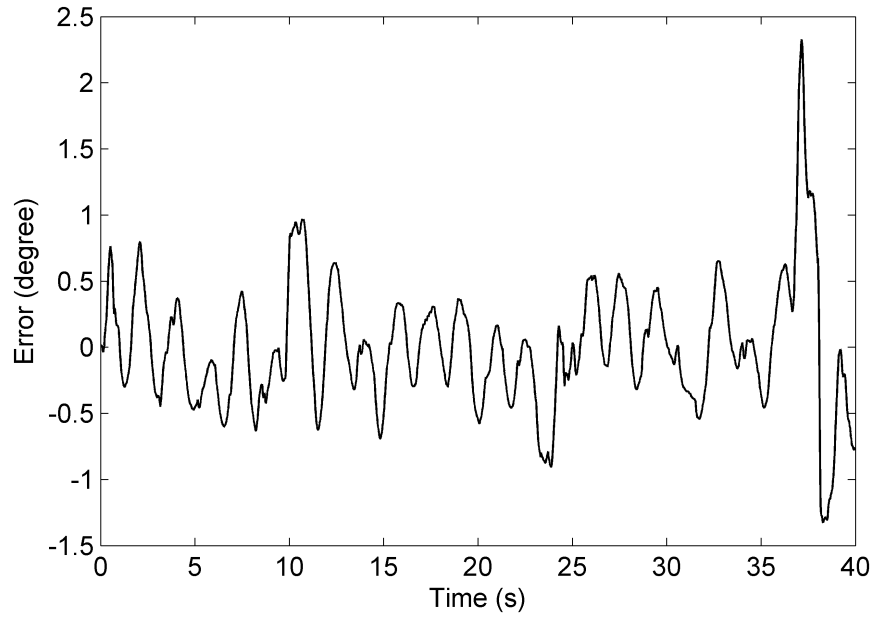
Figure 6.24 Error and FFT of error for subject 9 and trial 1

6.2.2 Results for Low Frequency and Amplitude Input

Figure 6.25 shows the absolute shank angle with respect to the gravity vertical. Thus, the shank angle and tilt input angle have in phase relation (see Figure 1.2). In addition,

the amplitude of the shank angle is closed to the tilt input. Therefore, the subject aligns the shank to the normal of the platform during the experiment of 1 degree and 0.021 Hz tilt input. On the other hand, the mathematical model simulation for the shank almost follows the tilt angle. Figure 6.20 shows the error values between the measured shank angle and simulated shank angle during the experiment. On the contrary to the previous case, the reference command for joint torques of the mathematical model is zero with respect to the platform normal for the 1 degree and 0.021 Hz tilt input (see Figure 5.6). Therefore, one can conclude that the subject's shank uses the platform normal as a reference frame for the postural control.
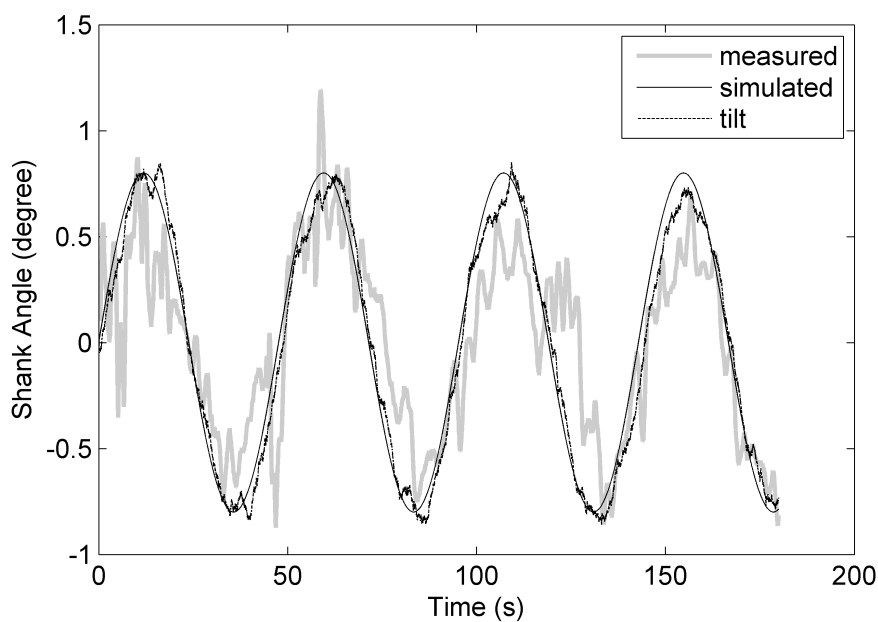
Figure 6.25 Low Frequency Shank Angle for subject 9 and trial 1
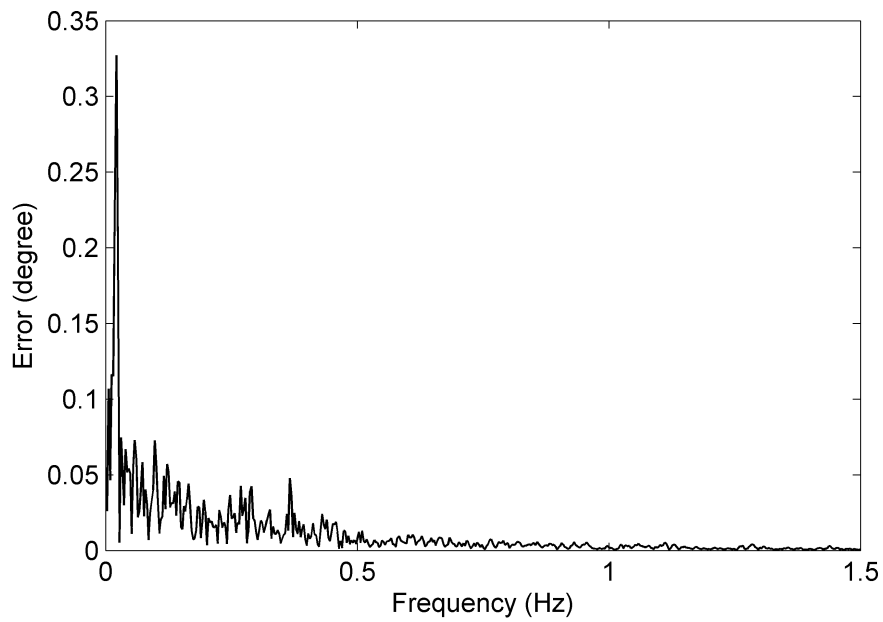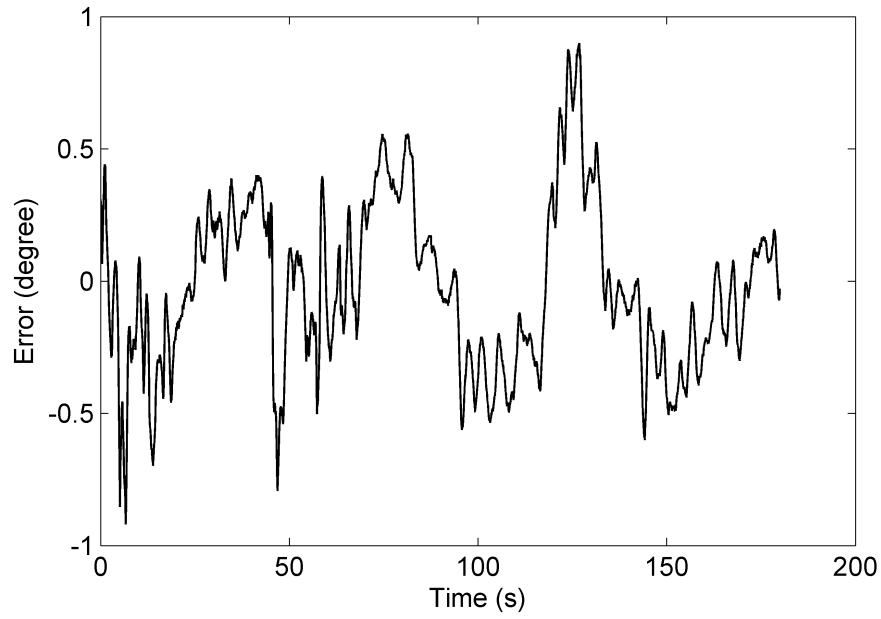
Figure 6.26 Error and FFT of error for subject 9 and trial 1

Figure 6.27 shows the absolute trunk angle with respect to the gravity vertical (see figure 1.2). One can see from figure 6.27 that the trunk almost follows the tilt input. Therefore, the subject's trunk sways with the platform normal. On the other hand, the reference command for trunk of the mathematical model is zero with respect to the

platform normal for the 1 degree and 0.021 Hz tilt input similar to the ankle angle. In conclusion, the subject's trunk uses the platform normal as a reference frame for the postural control. Figure 6.28 shows the error values during the experiment.
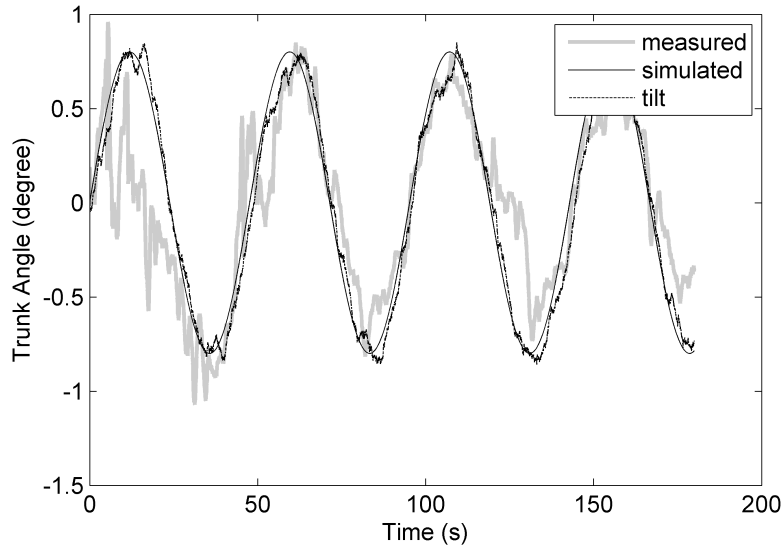
Figure 6.27 Low Frequency Trunk Angle for subject 9 and trial 1
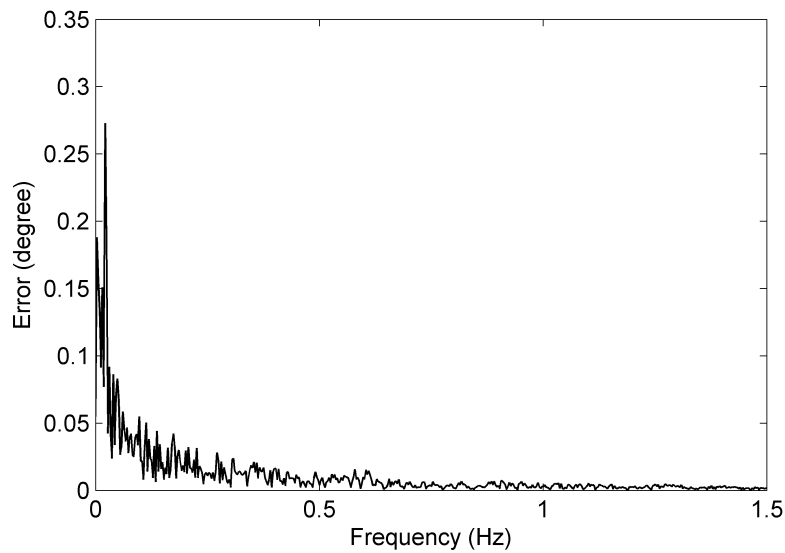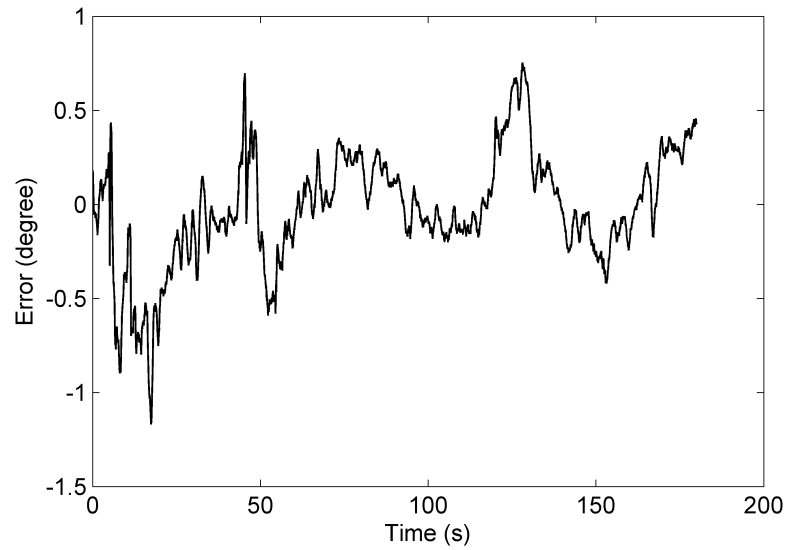
Figure 6.28 Error and FFT of error for subject 9 and trial 1

The head performance of the simulation was not good as hip or ankle joint because of the voluntary movements of head. One can find the questionnaire for the subject in Appendix A and all subject felt only one tilt movement. Therefore, the small tilt movement seems to be felt as quiet stance by the subject. In addition, the head's inertia is small compared to the trunk and legs. The voluntary movements were dominant for the small tilt input. There are some publications about modeling the voluntary movements [15]. There should be a task for the voluntary movements'

modeling. On the other hand, there was no task in this work. Thus, the voluntary movement could not be modeled for small tilt input and the performance of the head was not good enough like hip and ankle joints.
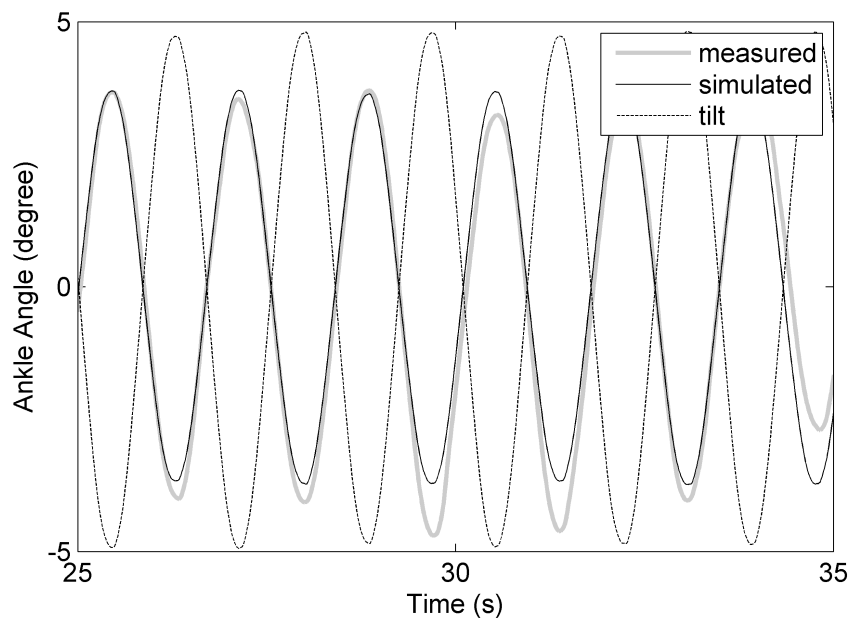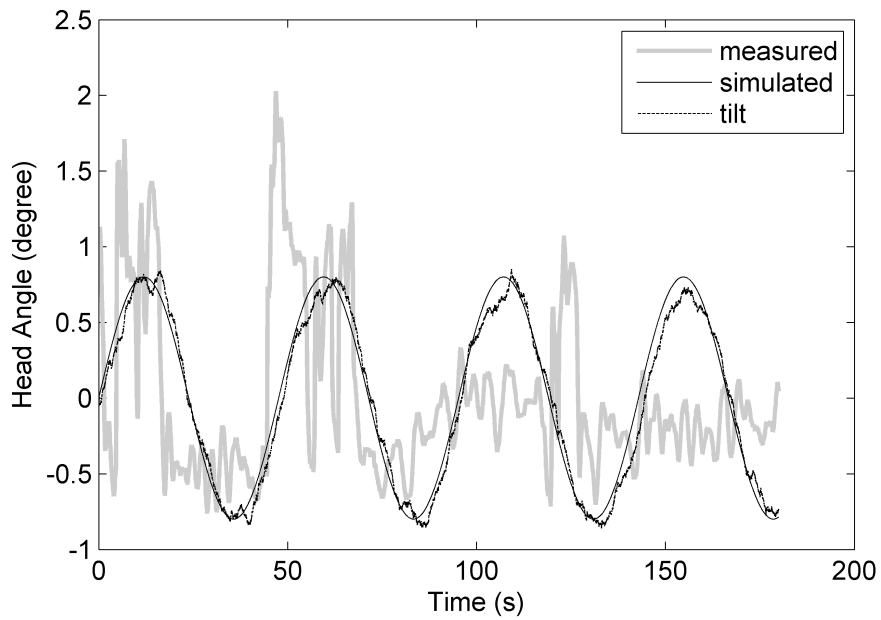

Figure 6.29 Low Frequency Head Angle for subject 9 and trial 1
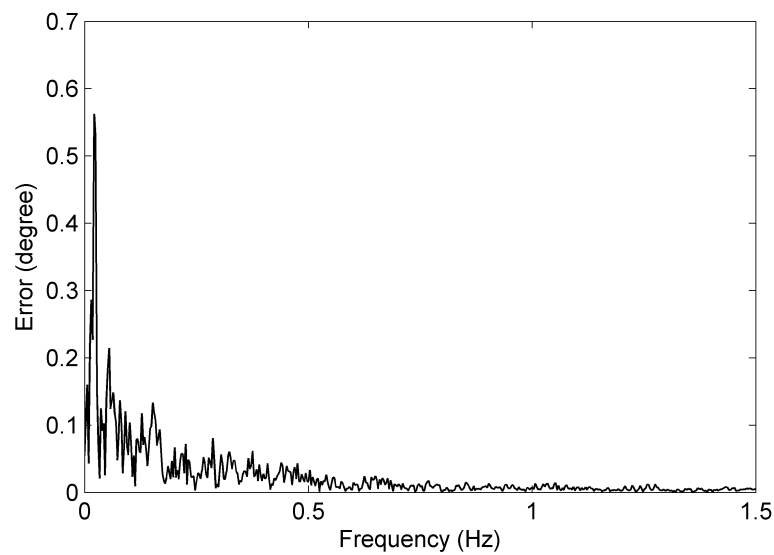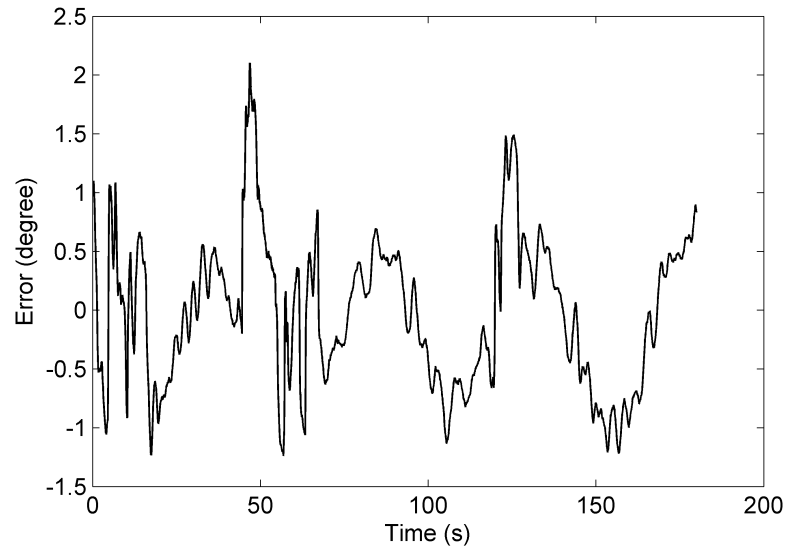
Figure 6.30 Error and FFT of error for subject 9 and trial 1

6.3 Summary for Simulation Results

The simulation results prove that the subjects change the reference frame. For movements above the vestibular sensor threshold, the gravity vertical reference frame is selected. On the other hand, for the movements below the vestibular threshold, the platform base reference frame is selected. In addition, if the error value is almost

periodic and also FFT of the error signal has a peak on the input frequency then, there could be an unmodeled part of the system. As a contrary, if the error value is not periodic and also FFT of the error has not a peak on the input frequency then, there could be a indeterministic part of the system. The head angle for low frequency is aperiodic and FFT of the error signal has a peak on the input frequency (Figure 6.30). Therefore, there could be an unmodeled part for the head. This could be the voluntary movement of the head. On the other hand, ankle for low frequency is well modeled because there is no periodic behavior for error (Figure 6.26). The error has a power up to 1 Hz. Thus, this could be related to the nonlinear dynamics of the system. The other subjects' data can be found in Appendix D.

CHAPTER 7

CONCLUSIONS

This chapter gives a brief summary of the findings and contributions of this thesis work and presents general conclusions and recommendations for future works.

7.1 General Conclusions and Discussion

The human postural control system was not well understood. Researchers can not divide the postural system into different pieces (subsystems) like a machine's components. Therefore, the collected data from the humans have been too complex for identification of postural control mechanisms. Thus, the measured data (i.e. kinematics data of the limb and force under the feet) was only the summary dynamics of the overall postural control system.

In this thesis work, the postural control system is analyzed using dynamic posture approach. In the first part of the work, the hydraulic tilt platform is designed, identified, modeled, simulated and manufactured. The platform has two DoF and can follow a predetermined command for the angular displacement. The second part of the work is related to the design of an experimental protocol for understanding the hypothesis, which is discussed in the Chapter 1. Briefly, the hypothesis of this work is a behavioral vestibular model being the subject trying to align himself with respect to the gravity vertical during the experiment. Alternatively, a behavioral somatosensory model can be defined when the subject allows himself to get tilted by the platform. Following, data is collected to prove the hypothesis. The kinematics data, CoP data and the pressure distribution under the feet of the subjects are acquired. Then, the

collected data is analyzed in time and frequency domain. In addition to that, a mathematical model is developed for human postural control system. The simulation of human behavior at two different frequencies has been performed through the developed model.

The first result from the data analyses is that the shank's absolute motion at the platform stimulation of 5 degrees 0.59 Hz sine wave has been found to be more cohere and in larger amplitude of motion compared to trunk's absolute angular motion with respect to gravity vertical. It is important to recall that the subjects have been informed not to move their feet from the platform. Thus, their feet have always been in contact with the platform. When trunk's relative motion with respect to shank has been searched it has been observed that trunk's motion is out of phase with shank's motion, which points to active hip joint control. Furthermore, it has been showed that (by looking at RMS values of relative joint kinematics) at higher perturbation the body behaves like a double DoF inverted pendulum (recall that the area ratios related to the decomposed CoM have revealed that the power at the perturbation frequency have been shown to be significantly larger compared to low frequency stimulation). This result shows that the subjects align themselves to the gravity vertical for high perturbation (i.e. 5 degrees 0.59 Hz sine wave). Indeed, the control strategy used for postural control (at the joints) has been selected to depend on generating compensated torque with respect to gravity vertical (see Chapter 5 Figure 5.6). The cited studies showed that the vestibular system is active above the vestibular velocity threshold [73]. The angular velocity at high perturbation, which is applied in this thesis' experiments, is higher than the vestibular velocity threshold. Thus, it can be claimed that the vestibular system is active for this perturbation and the reference frame for the postural control system is the gravity vertical.

In the literature, the gravity vertical has always been the reference system for the postural control models for quiet stance or static posture and also for the dynamic posture approaches. Thus, the results for the high frequency perturbation in this thesis justify that the selected reference frame is the gravity vertical similar to the studies in the literature. On the other hand, the results for the low perturbation (i.e. 1 degree 0.021 Hz sine wave) revealed that both the trunk and the shank follow the platform's motion. It is important to recall that RMS values of relative kinematics shank and trunk's mo-

tion are not significantly different (See Figure 6.11). However, relative shank's and trunk's motion have not been found to be cohere with the platform's motion, further the power carried in the signals for low frequency perturbation seems to be related to other dynamical sources other than the stimulation (This peculiar behavior of posture seems to be nonlinear in dynamical characteristics such that changing input and/or system parameters will end up with qualitatively different kinds of dynamics; from periodic motion to chaotic oscillations through bifurcations; i.e., in Figure 6.1 it is observed that shank absolute motion is periodic in character at high frequency however, Figure 6.3 presents shank's absolute motion at low frequency which seems not to be cohere with the perturbation. On the contrary, Figure 6.19 and Figure 6.26 demonstrate shank's simulated absolute motion at high and low frequency where the two responses are not qualitatively different in dynamical sense rather have been scaled with respect to the perturbation frequency and amplitude, which is characteristic in the linear system behavior). Indeed, area ratios computed at the decomposed CoM for low frequency perturbation have been shown to be significantly smaller than the high frequency perturbation. Furthermore, absolute shank and trunk's motion were found to be cohere with the platform perturbation while trunk's motion was found to be significantly larger than shank's motion (p<0.0002). By looking at this results, we conclude that there exists no active hip joint control for trunk (trunk sways passively with the platform depending on its mass), where as there seems a stretch reflex stiffness control at the ankle joint [52, 25]. Therefore, it can now be proposed that the subjects adapt to the platform for the low frequency perturbation and might have been using the platform normal as their kinematic frame of reference. As the low frequency perturbation is below the vestibular threshold, it is possible to claim that the postural control system is now using the somatosensory originated information for the stability of the balance, because there is no signal available coming from the visual and vestibular system. The somatosensory system is now the only sensor relaid on to maintain the balance for the subjects. For this reason, in the simulation of human behavior at low frequency perturbation, the control strategy selected partially depends on generating compensating joint torque with respect to initial ankle and hip angles (maintaining constant joints angle, partition 1; see equations 5.29, and 5.30 in Chapter 5); i.e., keeping the initial postural configuration on the platform stationary. Additionally, in this case it is also needed to monitor the projection of CoM on the

101

base of support continuously (to supply a safety margin for balancing the subject) in order to generate a joint torque (partition 2, see Chapter 5 equations 5.29, and 5.31) to compensate for deviation from CoP. There should also muscle stretch reflexes (proprioception) working against the perturbation [25], however, the perturbation is so small that the subjects did not feel the motion (see questionnaires in Appendix C). Indeed, it is possible to show that for the low frequency simulation (depending on simulation results), the stretch reflexes in this case can only help the subjects to align themselves to the platform normal. However, although the subjects can not feel the perturbation or motion of the platform, there should be a torque at the ankle joint and the hip joint of the subjects for compensating the gravitational forces effect acting to the center of mass of the subjects (partition 2 torque, see previous paragraph) in order to maintain a safety margin for CoP. Therefore, the somatosensory system is the crucial for producing this counter torque to keep the balance of the posture.

In summary, the somatosensory system is the contact force sensor, which is used for selecting the reference frame that is normal to the feet. While simulating the human behavior at high frequency versus low frequency cases weighted postural control strategy have been used in order to generate joint control torques (See section 5.6). Thus, for the simulation of the high frequency perturbation case, the stretch reflexes are inhibited (proprioceptive gain is decreased, and the somatosensory system's gain is decreased unlike the vestibular system, whose gain is higher than the somatosensory system. In other words, human postural control for high frequency perturbation mainly depends on compensated joint torque generated with respect to gravity vertical through vestibular senses. In contrary, the somatosensory system is the only sensor for the low perturbation case (proprioception has been suggested to be intact in this study). Therefore, the somatosensory and proprioceptive feedback are the main signal for generating joint torques which compensate for relative hip and ankle joint angles (partition 1, proprioceptive) and for deviation from CoP (partition 2, somatosensory). The joint control torque generated at partition 1 is mainly proprioceptive origin (stretch reflexes are behalf of postural control in this case, proprioceptive gain is inherently increased). On the other hand, the joint control torque generated at partition 2 is mainly somatosensory origin which might be determining the selection of the kinematic frame of reference as being the platform normal for the

reference frame of the postural control system. The mathematical model also reveals that the reference frames are changing for the subjects for high and low perturbation. The reference command (explicit, see previous paragraph) of the mathematical model for the high perturbation is the zero degree with respect to the gravity vertical. On the other hand, zero degree with respect to the platform normal is the reference command (implicit) for the low perturbation, which is realized by increasing the gain of the proprioceptive control.

The error value between simulated and measured data of the limbs came out to be small except the head angle. The error can be high for the head angle compared to the other limbs due to the voluntary movements of the head. The postural control system can be divided into three cascade hierarchical control systems. The fundamental control for this hierarchical control systems is the reflex control. The second is the autonomous (adaptive control through modulating stretch reflexes [74]) part of the postural control system. In this control, the sensors (i.e., vestibular, proprioceptive and somatosensory) and the sensory fusion play an important role. The last one is the voluntary control, which supplies the human with a predictive power (perception) in controlling the action [38] through internal representations [25, 20] of "*environment*" and posture, ("*self awareness*") . These parts of the control are difficult to study. The experimental protocol should be well defined to identify this part of the postural control. In this thesis work, only autonomous (adaptive) part and sensor fusion are studied.

It has been shown that the reference frame for the postural control system is not the gravity vertical (may be the platform normal) for low frequency perturbation. It is important to note that trunk's relative motion at low frequency perturbation has not been found to be cohere (0.33) with platform's perturbation but sways passively on the platform in a frequency range similar to quiet stance (see Figure 6.18, Figure 6.15). Thus, the movements of the subjects with respect to the platform normal are similar to quiet stance oscillations [25]. These results reveal that the subjects adapt to platform motion and start using platform's coordinate system as their reference frame for low frequency perturbation, which is below the vestibular threshold. Moreover, quiet stance dynamics is complex and the reasons for this complex behavior have not been revealed, yet. Thus, it may happen that although a physiological adap-

tion occurs at low frequency perturbation the subject might have been presenting a quiet stance like dynamics (complex dynamics) provoked by a low frequency low amplitude stimulation at the limits of thresholds causing bifurcations [36]. There is no ground perturbation as a deterministic signal for quiet stance. Thus, the complex structure of quiet stance may be troublesome to imitate [75, 76]. On the other hand, it becomes difficult to reveal which coordinate system (an inertial versus ground base kinematic reference system) is used by the subject during quiet stance (thus, the reference frame for the somatosensory and the vestibular system become identical for the quiet stance that is the gravity vertical which may cause ambiguous responses), which further needs to perform nonlinear dynamical analysis [77, 36].

As a conclusion, the adaptation for selecting the reference frame is crucial to understand the strategies, which are used by the postural control system. The dynamic posturography is the method to separate the strategies that are used by the subject given that the perturbation velocities should be designed (properly selected) for identifying contribution of different senses in the overall postural control depending on their thresholds.

7.2 Future Works

The proper electro physiological measurement (muscle dynamics) can be added to the data collection (simulation) to identify the first level of control which is the reflex loop of the postural control system. In addition to that, there can be well designed experimental protocol to model the third level control (predictive through cognition), which is the voluntary movements of the posture (especially for the head control). The somatosensory threshold value for the low frequency perturbation can be found, which is the first frequency to stimulate the somatosensory system to keep vestibular patients in balance. Thus, the vestibular lost patients could be the subjects for the same experimental protocol used in this thesis (Indeed, a study at Gülhane Military Medical Collage, Otorhinolaryngology department has been started for investigating vestibular lost subjects with almost a similar protocol). We expect that it will be possible to show a similar postural behavior by using higher frequencies than the vestibular threshold in vestibular lost subjects (a somatosensory triggered postural adaptive be-

havior at vestibular lost subjects). On the other hand, the physiological mechanisms for adaptation to tilt platform, especially for the low frequency perturbation, can be tested by blocking the somatosensory system.

REFERENCES

[1] "Three planes of motion for the human body." \url{http://biology.stackexchange.com/questions/13610/for-the-human-head-which-direction-is-anterior-and-which-direction-is-ventral}.

[2] G. C. Y. Peng, *Dynamics and Control of Head, Neck and Eye Stabilization: Neuromechanical and Experimental Models*. Northwestern University, 1996.

[3] F. B. Horak, "Clinical measurement of postural control in adults.," *Physical therapy*, vol. 67, pp. 1881–5, dec 1987.

[4] J. E. Deffeyes, *Nonlinear Dynamics of Infant Sitting Postural Control*. PhD thesis, 2009.

[5] J. M. Haddad, S. Rietdyk, L. J. Claxton, and J. E. Huber, "Task-dependent postural control throughout the lifespan.," *Exercise and Sport Sciences Reviews*, vol. 41, no. 2, pp. 123–32, 2013.

[6] F. E. Z. A D Kuo, "A biomechanical analysis of muscle strength as a limiting factor in standing posture," 1993.

[7] Y. C. Pai and J. Patton, "Center of mass velocity-position predictions for balance control," *Journal of Biomechanics*, vol. 30, no. 4, pp. 347–354, 1997.

[8] L. M. Nashner, "Vestibular postural control model.," *Kybernetik*, vol. 10, pp. 106–10, feb 1972.

[9] H. van der Kooij, R. Jacobs, B. Koopman, and H. Grootenboer, "A multisensory integration model of human stance control.," *Biological cybernetics*, vol. 80, pp. 299–308, may 1999.

[10] R. J. Peterka, "Sensorimotor Integration in Human Postural Control," *Journal of Neurophysiology*, vol. 88, pp. 1097–1118, 2002.

[11] J. Massion, "Postural control system.," *Current opinion in neurobiology*, vol. 4, no. 6, pp. 877–887, 1994.

[12] R. J. Peterka and P. J. Loughlin, "Dynamic regulation of sensorimotor integration in human postural control.," *Journal of neurophysiology*, vol. 91, no. 1, pp. 410–423, 2004.

[13] R. J. Peterka, P. Kowalczyk, P. Glendinning, M. Brown, G. Medrano-cerda, and H. Dallali, "Sensorimotor Integration in Human Postural Control Sensorimotor Integration in Human Postural Control," *Journal of Neurophysiology*, pp. 1097–1118, 2011.

[14] R. J. Peterka, "Postural control model interpretation of stabilogram diffusion analysis.," *Biological cybernetics*, vol. 82, pp. 335–43, apr 2000.

[15] T. Mergner, "A neurological view on reactive human stance control," *Annual Reviews in Control*, vol. 34, pp. 177–198, dec 2010.

[16] H. van der Kooij, S. Donker, M. de Vrijer, and F. van der Helm, "Identification of human balance control in standing," *2004 IEEE International Conference on Systems, Man and Cybernetics (IEEE Cat. No.04CH37583)*, vol. 3, pp. 2535–2541, 2004.

[17] H. van der Kooij, R. Jacobs, B. Koopman, and F. van der Helm, "An adaptive model of sensory integration in a dynamic environment applied to human stance control.," *Biological cybernetics*, vol. 84, pp. 103–15, feb 2001.

[18] P. F. Meyer, L. I. E. Oddsson, and C. J. De Luca, "The role of plantar cutaneous sensation in unperturbed stance.," *Experimental brain research. Experimentelle Hirnforschung. Expérimentation cérébrale*, vol. 156, pp. 505–12, jun 2004.

[19] J. Massion, "Postural control systems in developmental perspective.," *Neuroscience and biobehavioral reviews*, vol. 22, no. 4, pp. 465–472, 1998.

[20] J. Massion, "Postural control system," *Current Opinion in Neurobiology*, vol. 4, no. 6, pp. 877–887, 1994.

[21] G. M. Shepherd, *Neurobiology*. Oxford University Press, 1994.

[22] V. J. Wilson, *Mammalian Vestibular Physiology*. Springer US, 2013.

[23] D. A. Winter, *Biomechanics and motor control of human movement*. John Wiley & Sons, 2009.

[24] E. R. Kandel, J. H. Schwartz, T. M. Jessell, and Others, *Principles of neural science*, vol. 4. McGraw-Hill New York, 2000.

[25] V. S. Gurfinkel, Y. P. Ivanenko, Y. S. Levik, and I. A. Babakova, "Kinesthetic reference for human orthograde posture," *Neuroscience*, vol. 68, no. 1, pp. 229–243, 1995.

[26] V. S. Gurfinkel, Y. S. Levik, K. E. Popov, B. N. Smetanin, and V. Y. Shlikov, "Body scheme in the control of postural activity," in *Stance and motion*, pp. 185–193, Springer, 1988.

[27] R. Fitzpatrick, D. Burke, and S. C. Gandevia, "Task-dependent reflex responses and movement illusions evoked by galvanic vestibular stimulation in standing humans.," *The Journal of physiology*, vol. 478, no. 2, pp. 363–372, 1994.

[28] J. Dichgans, R. Held, L. R. Young, and T. Brandt, "Moving visual scenes influence the apparent direction of gravity," *Science*, vol. 178, no. 4066, pp. 1217–1219, 1972.

[29] G. Calvert, C. Spence, and B. E. Stein, *The handbook of multisensory processes*. MIT press, 2004.

[30] G. Clement, V. S. Gurfinkel, F. Lestienne, M. I. Lipshits, and K. E. Popov, "Adaptation of postural control to weightlessness," *Experimental Brain Research*, vol. 57, no. 1, pp. 61–72, 1984.

[31] R. B. Stein and C. Capaday, "The modulation of human reflexes during functional motor tasks," *Trends in neurosciences*, vol. 11, no. 7, pp. 328–332, 1988.

[32] J. J. Collins and C. J. De Luca, "Open-loop and closed-loop control of posture: a random-walk analysis of center-of-pressure trajectories," *Experimental brain research*, vol. 95, no. 2, pp. 308–318, 1993.

[33] J. J. Collins and C. J. De Luca, "Random walking during quiet standing," *Physical review letters*, vol. 73, no. 5, p. 764, 1994.

[34] M. Duarte and V. M. Zatsiorsky, "Long-range correlations in human standing," *Physics Letters A*, vol. 283, no. 1, pp. 124–128, 2001.

[35] M. Duarte and V. M. Zatsiorsky, "On the fractal properties of natural human standing," *Neuroscience letters*, vol. 283, no. 3, pp. 173–176, 2000.

[36] S. Gurses and H. Celik, "Correlation dimension estimates of human postural sway.," *Human movement science*, vol. 32, pp. 48–64, feb 2013.

[37] H. Haken, "lntroduction to Synergetics," *Cooperative Phenomena in Multi-Component Systems*, p. 9, 1973.

[38] A. Berthoz, *The brain's sense of movement*. Harvard University Press, 2002.

[39] S. Gurses, Y. Dhaher, T. C. Hain, and E. A. Keshner, "Perturbation parameters associated with nonlinear responses of the head at small amplitudes," *Chaos: An Interdisciplinary Journal of Nonlinear Science*, vol. 15, no. 2, p. 23905, 2005.

[40] V. M. Zatsiorsky and M. Duarte, "Rambling and trembling in quiet standing," *MOTOR CONTROL-CHAMPAIGN-*, vol. 4, no. 2, pp. 185–200, 2000.

[41] S. Gurses, B. E. Platin, S. T. Tumer, and N. Akkas, "Characteristic phase plane pattern of human postural sway," in *Modeling and Control in Biomedical Systems*, vol. 6, pp. 225–230, 2006.

[42] B. Isableu, T. Ohlmann, J. Crémieux, and B. Amblard, "Selection of spatial frame of reference and postural control variability," *Experimental Brain Research*, vol. 114, no. 3, pp. 584–589, 1997.

[43] A. Alexandrov, A. Frolov, and J. Massion, "Axial synergies during human upper trunk bending.," *Experimental brain research. Experimentelle Hirnforschung. Expérimentation cérébrale*, vol. 118, pp. 210–20, jan 1998.

[44] a. V. Alexandrov, a. a. Frolov, and J. Massion, "Biomechanical analysis of movement strategies in human forward trunk bending. I. Modeling.," *Biological cybernetics*, vol. 84, pp. 425–34, jun 2001.

[45] A. V. Alexandrov, A. A. Frolov, F. B. Horak, P. Carlson-Kuhta, and S. Park, "Feedback equilibrium control during human standing.," *Biological cybernetics*, vol. 93, pp. 309–22, nov 2005.

[46] A. V. Alexandrov and A. A. Frolov, "Closed-loop and open-loop control of posture and movement during human trunk bending.," *Biological cybernetics*, vol. 104, pp. 425–38, jun 2011.

[47] K. Barin, "Evaluation of a generalized model of human postural dynamics and control in the sagittal plane," *Biological cybernetics*, vol. 50, no. 1919, 1989.

[48] V. Bonnet, S. Ramdani, P. Fraisse, N. Ramdani, J. Lagarde, and B. G. Bardy, "A structurally optimal control model for predicting and analyzing human postural coordination," *Journal of Biomechanics*, vol. 44, no. 11, pp. 2123–2128, 2011.

[49] J. BORAH, L. R. YOUNG, and R. E. CURRY, "Optimal Estimator Model for Human Spatial Orientation," *Annals of the New York Academy of Sciences*, vol. 545, pp. 51–73, dec 1988.

[50] E. J. Cheng, I. E. Brown, and G. E. Loeb, "Virtual muscle: a computational approach to understanding the effects of muscle properties on motor control.," *Journal of neuroscience methods*, vol. 101, pp. 117–30, sep 2000.

[51] M. Ferrarin and E. D'Acquisto, "An experimental PID controller for knee movement restoration with closed loop FES system," *... in Medicine and ...*, pp. 453–454, 1996.

[52] L. Nashner, "Adapting reflexes controlling the human posture," *Experimental Brain Research*, vol. 26, pp. 59–72, aug 1976.

[53] L. M. Nashner and G. McCollum, "The organization of human postural movements: A formal basis and experimental synthesis," *Behavioral and Brain Sciences*, vol. 8, no. 01, pp. 135–150, 1985.

[54] F. B. Horak and L. M. Nashner, "Central programming of postural movements: adaptation to altered support-surface configurations.," *Journal of neurophysiology*, vol. 55, no. 6, pp. 1369–1381, 1986.

[55] C. F. Runge, C. L. Shupert, F. B. Horak, and F. E. Zajac, "Ankle and hip postural strategies defined by joint torques," *Gait & posture*, vol. 10, no. 2, pp. 161–170, 1999.

[56] P. Gatev, S. Thomas, T. Kepple, and M. Hallett, "Feedforward ankle strategy of balance during quiet stance in adults," *The Journal of physiology*, vol. 514, no. 3, pp. 915–928, 1999.

[57] K. Masani, M. R. Popovic, K. Nakazawa, M. Kouzaki, and D. Nozaki, "Importance of body sway velocity information in controlling ankle extensor activities during quiet stance," *Journal of Neurophysiology*, vol. 90, no. 6, pp. 3774–3782, 2003.

[58] J. Jeka, T. Kiemel, R. Creath, F. Horak, and R. Peterka, "Controlling human upright posture: velocity information is more accurate than position or acceleration," *Journal of neurophysiology*, vol. 92, no. 4, pp. 2368–2379, 2004.

[59] H. van der Kooij, B. Koopman, R. Jacobs, T. Mergner, and H. Grootenboer, "Quantification of sensory information in human balance control," *Proceedings of the 20th Annual International Conference of the IEEE Engineering in Medicine and Biology Society. Vol.20 Biomedical Engineering Towards the Year 2000 and Beyond (Cat. No.98CH36286)*, vol. 5, no. 5, pp. 2393–2396, 1998.

[60] T. Mergner, G. Schweigart, and L. Fennell, "Vestibular humanoid postural control," *Journal of Physiology-Paris*, vol. 103, no. 3, pp. 178–194, 2009.

[61] G. Schweigart and T. Mergner, "Human stance control beyond steady state response and inverted pendulum simplification," *Experimental brain research*, vol. 185, no. 4, pp. 635–653, 2008.

[62] C. Maurer, T. Mergner, B. Bolha, and F. Hlavacka, "Vestibular, visual, and somatosensory contributions to human control of upright stance," *Neuroscience letters*, vol. 281, no. 2, pp. 99–102, 2000.

[63] T. Mergner, C. Maurer, and R. J. Peterka, "A multisensory posture control model of human upright stance," *Progress in brain research*, vol. 142, pp. 189–201, 2003.

[64] C. Cnyrim, T. Mergner, and C. Maurer, "Potential roles of force cues in human stance control," *Experimental brain research*, vol. 194, no. 3, pp. 419–433, 2009.

[65] G. Schweigart, T. Mergner, I. Evdokimidis, S. Morand, and W. Becker, "Gaze stabilization by optokinetic reflex (OKR) and vestibulo-ocular reflex (VOR) during active head rotation in man," *Vision research*, vol. 37, no. 12, pp. 1643–1652, 1997.

[66] G. Schweigart, T. Mergner, and W. Becker, "Eye stabilization by vestibulo-ocular reflex (VOR) and optokinetic reflex (OKR) in macaque monkey: which helps which?," *Acta oto-laryngologica*, vol. 115, no. 1, pp. 19–25, 1995.

[67] T. Mergner, W. Becker, and L. Deecke, "Canal-neck interaction in vestibular neurons of the cat's cerebral cortex," *Experimental brain research*, vol. 61, no. 1, pp. 94–108, 1985.

[68] T. Mergner, W. Huber, and W. Becker, "Vestibular-neck interaction and transformation of sensory coordinates," *Journal of Vestibular Research*, vol. 7, no. 4, p. 347, 1997.

[69] D. Anastasopoulos and T. Mergner, "Canal-neck interaction in vestibular nuclear neurons of the cat," *Experimental brain research*, vol. 46, no. 2, pp. 269–280, 1982.

[70] D. Anastasopoulos, C. Maurer, and T. Mergner, "Interactions between voluntary head control and neck proprioceptive reflexes in cervical dystonia," *Parkinsonism & related disorders*, vol. 20, no. 11, pp. 1165–1170, 2014.

[71] F. Hlavačka, T. Mergner, and G. Schweigart, "Interaction of vestibular and proprioceptive inputs for human self-motion perception," *Neuroscience letters*, vol. 138, no. 1, pp. 161–164, 1992.

[72] *AUTOMATIC CONTROL SYSTEMS, 8TH ED (With CD)*. Wiley India Pvt. Limited, 2007.

[73] T. Mergner and S. Glasauer, "A Simple Model of Vestibular Canal-Otolith Signal Fusion," *Annals of the New York Academy of Sciences*, vol. 871, no. 1, pp. 430–434, 1999.

[74] H. I. Cakar, M. Cidem, O. Sebik, G. Yilmaz, S. S. Karamehmetoglu, S. Kara, I. Karacan, and K. S. Türker, "Whole-body vibration-induced muscular reflex: Is it a stretch-induced reflex?," *Journal of physical therapy science*, vol. 27, no. 7, p. 2279, 2015.

[75] M. Keshner, "1/f noise," *Proceedings of the IEEE*, vol. 70, no. 3, pp. 212–218, 1982.

[76] E. Milotti, "1 / f noise : a pedagogical review .," *Scientific American*, 1921.

[77] H. Çelik, *LINEAR AND NONLINEAR ANALYSIS OF HUMAN POSTURAL SWAY*. PhD thesis, 2008.

[78] Y. Wang, V. M. Zatsiorsky, and M. L. Latash, "Muscle synergies involved in preparation to a step made under the self-paced and reaction time instructions," *Clinical Neurophysiology*, vol. 117, no. 1, pp. 41–56, 2006.

[79] H. S. Choi and Y. H. Kim, "The Relationship between the COP–COM Variable and the Horizontal Acceleration of the Body in Postural Sway, Falling and Walking," in *World Congress on Medical Physics and Biomedical Engineering, September 7-12, 2009, Munich, Germany*, pp. 281–283, Springer, 2010.

APPENDIX A

TABLES FOR THE SUBJECTS

0.021Hz shank RMS	Trial1	Trial2	Trial3	Trial4	Trial5
Subject1	0.64	1.05	1.21	1.56	1.39
Subject2	0.38	0.5	0.47	0.66	0.44
Subject3	0.27	0.29	0.36	0.38	0.45
Subject4	0.3	0.39	0.38	0.36	0.49
Subject5	0.88	1.03	0.55	0.46	0.87
Subject6	0.37	0.51	0.49	0.6	0.5
Subject7	0.4	0.39	0.48	0.43	0.41
Subject8	0.47	0.35	0.42	0.38	0.46
Subject9	0.43	0.39	0.42	0.41	0.39
Subject10	0.37	0.4	0.48	0.36	0.85
Subject11	0.51	0.43	0.5	0.51	0.52

0.021Hz trunk RMS	Trial1	Trial2	Trial3	Trial4	Trial5
Subject1	0.59	0.69	0.75	1.33	1.38
Subject2	0.46	0.46	0.49	0.52	0.51
Subject3	0.41	0.42	0.48	0.46	0.51
Subject4	0.57	0.67	0.56	0.58	0.75
Subject5	0.65	0.86	0.63	0.52	0.77
Subject6	0.64	1.13	0.82	1.13	2.07
Subject7	0.45	0.47	0.47	0.52	0.33
Subject8	0.4	0.4	0.39	0.4	0.4
Subject9	0.46	0.49	0.55	0.59	0.52
Subject10	0.57	0.48	0.72	0.45	0.8
Subject11	0.68	0.57	0.62	0.68	0.67

0.59Hz shank RMS	Trial1	Trial2	Trial3	Trial4	Trial5
Subject1	0.89	1.18	1.32	0.75	0.86
Subject2	0.99	0.96	1.03	0.63	0.46
Subject3	1.55	0.94	0.8	0.69	0.44
Subject4	1.46	1	1.16	1.11	1.12
Subject5	1.29	1.84	1.77	1.82	1.45
Subject6	0.85	0.57	0.47	0.57	0.45
Subject7	0.75	1.59	1.58	0.64	0.78
Subject8	1.64	1.10	2.07	1.32	1.36
Subject9	1.09	1.68	1.14	2.12	2.20
Subject10	1.45	1.2	1.39	1.82	1.57
Subject11	1.17	2.95	2.24	2.04	0.94

0.59Hz trunk RMS	Trial1	Trial2	Trial3	Trial4	Trial5
Subject1	0.81	0.8	0.86	0.68	0.78
Subject2	1.35	0.72	0.82	0.82	0.83
Subject3	1.59	0.59	0.51	0.93	0.78
Subject4	1.42	0.55	1.2	0.6	1.04
Subject5	0.79	1.36	1.26	1.73	1.17
Subject6	1.24	1.18	0.95	0.91	0.91
Subject7	0.93	0.76	0.67	0.68	0.61
Subject8	0.86	0.54	1.13	0.6	0.75
Subject9	0.71	0.94	0.66	1.19	1.36
Subject10	1.72	1.55	0.68	1.14	0.9
Subject11	1.31	2.23	1.84	1.88	1.07

0.021Hz ankle RMS	Trial1	Trial2	Trial3	Trial4	Trial5
Subject1	0.5	0.98	1.17	1.45	1.35
Subject2	0.28	0.4	0.26	0.5	0.33
Subject3	0.42	0.39	0.39	0.34	0.36
Subject4	0.4	0.5	0.4	0.41	0.6
Subject5	0.76	1.05	0.45	0.32	0.82
Subject6	0.38	0.47	0.46	0.57	0.34
Subject7	0.22	0.22	0.22	0.25	0.2
Subject8	0.24	0.32	0.26	0.3	0.25
Subject9	0.29	0.25	0.24	0.25	0.29
Subject10	0.3	0.27	0.42	0.33	0.79
Subject11	0.41	0.31	0.29	0.34	0.39

0.021Hz hip RMS	Trial1	Trial2	Trial3	Trial4	Trial5
Subject1	0.78	1.47	1.59	2.44	2.16
Subject2	0.37	0.39	0.37	0.51	0.35
Subject3	0.36	0.41	0.39	0.35	0.49
Subject4	0.55	0.76	0.57	0.61	0.91
Subject5	0.66	0.71	0.46	0.42	0.37
Subject6	0.47	0.93	0.73	1.18	2.01
Subject7	0.21	0.25	0.37	0.33	0.29
Subject8	0.22	0.36	0.28	0.25	0.25
Subject9	0.31	0.31	0.25	0.44	0.34
Subject10	0.33	0.46	0.47	0.41	1.12
Subject11	0.7	0.59	0.6	0.71	0.68

0.59Hz ankle RMS	Trial1	Trial2	Trial3	Trial4	Trial5
Subject1	2.94	2.67	2.7	2.95	2.9
Subject2	3.49	2.77	2.72	3.19	3.15
Subject3	3.13	2.68	2.71	3.2	3.13
Subject4	3.33	2.61	3.32	2.52	3.04
Subject5	2.75	2.87	2.68	2.96	2.7
Subject6	3.35	3.34	3.24	3.1	3.11
Subject7	3.1	2.07	2.04	2.89	2.9
Subject8	2.19	2.51	1.67	2.35	2.11
Subject9	2.77	2.28	2.63	1.43	1.4
Subject10	3.4	3.4	2.39	2.47	2.29
Subject11	3.19	3.38	2.65	3.49	3.06

0.59Hz hip RMS	Trial1	Trial2	Trial3	Trial4	Trial5
Subject1	1	1.15	1.11	0.98	1.04
Subject2	1.18	1.19	1.37	1.08	1.03
Subject3	1.13	1.2	1.11	0.79	0.94
Subject4	1.10	0.84	1.01	0.81	0.88
Subject5	1.10	1.13	1.18	1.09	0.86
Subject6	1.10	1.09	1.07	1.15	1.10
Subject7	0.95	1.05	1.12	0.83	0.96
Subject8	1.06	1	1.03	0.96	0.79
Subject9	0.94	1.12	1.10	1.04	1.12
Subject10	1.01	1.24	1.10	1.35	1.2
Subject11	1.35	1.29	1.21	1.01	1

0.021Hz shank Magnitude	Trial1	Trial2	Trial3	Trial4	Trial5
Subject1	0.86	0.9	0.71	1.5	0.81
Subject2	0.64	0.68	0.77	0.82	0.68
Subject3	0.36	0.43	0.47	0.56	0.62
Subject4	0.39	0.36	0.46	0.44	0.35
Subject5	0.88	0.83	0.7	0.72	0.67
Subject6	0.5	0.59	0.58	0.58	0.76
Subject7	0.68	0.69	0.8	0.73	0.73
Subject8	0.74	0.55	0.67	0.57	0.74
Subject9	0.66	0.64	0.69	0.66	0.62
Subject10	0.6	0.63	0.61	0.58	0.63
Subject11	0.68	0.64	0.78	0.76	0.67

0.021Hz trunk Magnitude	Trial1	Trial2	Trial3	Trial4	Trial5
Subject1	0.74	0.52	0.93	1.03	1.44
Subject2	0.76	0.7	0.78	0.77	0.88
Subject3	0.72	0.63	0.79	0.76	0.75
Subject4	0.93	0.93	0.85	0.8	0.86
Subject5	0.86	0.93	0.95	0.82	0.77
Subject6	0.74	0.91	0.81	0.45	2.11
Subject7	0.72	0.8	0.77	0.86	0.52
Subject8	0.65	0.54	0.59	0.63	0.64
Subject9	0.69	0.81	0.92	0.8	0.8
Subject10	0.83	0.71	1.01	0.6	0.66
Subject11	1.10	0.62	0.95	0.78	0.81

0.59Hz shank Magnitude	Trial1	Trial2	Trial3	Trial4	Trial5
Subject1	0.18	0.27	0.28	0.13	0.17
Subject2	0.18	0.25	0.26	0.11	0.11
Subject3	0.27	0.24	0.21	0.05	0.09
Subject4	0.23	0.26	0.1	0.28	0.17
Subject5	0.26	0.3	0.35	0.3	0.28
Subject6	0.1	0.09	0.09	0.14	0.11
Subject7	0.13	0.43	0.44	0.15	0.18
Subject8	0.44	0.29	0.56	0.35	0.38
Subject9	0.24	0.41	0.27	0.61	0.63
Subject10	0.19	0.22	0.36	0.37	0.4
Subject11	0.16	0.39	0.46	0.12	0.16

0.59Hz trunk Magnitude	Trial1	Trial2	Trial3	Trial4	Trial5
Subject1	0.11	0.08	0.07	0.15	0.17
Subject2	0.33	0.15	0.17	0.19	0.2
Subject3	0.22	0.1	0.11	0.19	0.17
Subject4	0.21	0.04	0.18	0.06	0.06
Subject5	0.09	0.06	0.1	0.12	0.07
Subject6	0.21	0.29	0.23	0.2	0.23
Subject7	0.17	0.13	0.13	0.16	0.13
Subject8	0.15	0.01	0.28	0.1	0.16
Subject9	0.05	0.13	0.05	0.32	0.34
Subject10	0.21	0.31	0.09	0.06	0.12
Subject11	0.24	0.11	0.22	0.13	0.16

0.021Hz ankle Magnitude	Trial1	Trial2	Trial3	Trial4	Trial5
Subject1	0.25	0.66	0.43	0.99	0.3
Subject2	0.36	0.32	0.23	0.27	0.34
Subject3	0.71	0.64	0.56	0.46	0.39
Subject4	0.62	0.66	0.55	0.59	0.72
Subject5	0.33	1.06	0.36	0.32	0.41
Subject6	0.55	0.48	0.43	0.49	0.28
Subject7	0.33	0.32	0.22	0.29	0.3
Subject8	0.26	0.45	0.33	0.43	0.31
Subject9	0.35	0.36	0.31	0.35	0.39
Subject10	0.42	0.37	0.4	0.49	0.38
Subject11	0.35	0.36	0.28	0.24	0.34

0.021Hz hip Magnitude	Trial1	Trial2	Trial3	Trial4	Trial5
Subject1	0.2	0.98	0.27	1.88	0.92
Subject2	0.2	0.18	0.31	0.36	0.24
Subject3	0.47	0.2	0.4	0.33	0.18
Subject4	0.58	0.61	0.43	0.47	0.68
Subject5	0.22	0.19	0.26	0.17	0.13
Subject6	0.45	0.47	0.49	0.29	1.57
Subject7	0.12	0.18	0.37	0.23	0.33
Subject8	0.09	0.08	0.08	0.07	0.16
Subject9	0.12	0.22	0.25	0.2	0.19
Subject10	0.28	0.08	0.41	0.29	0.31
Subject11	0.49	0.06	0.65	0.32	0.16

0.59Hz ankle Magnitude	Trial1	Trial2	Trial3	Trial4	Trial5
Subject1	0.82	0.74	0.73	0.87	0.84
Subject2	0.98	0.8	0.77	0.91	0.92
Subject3	0.81	0.76	0.79	0.96	0.91
Subject4	0.85	0.75	0.9	0.73	0.84
Subject5	0.77	0.71	0.69	0.74	0.72
Subject6	0.92	0.97	0.94	0.89	0.91
Subject7	0.89	0.58	0.57	0.89	0.84
Subject8	0.57	0.71	0.44	0.66	0.62
Subject9	0.77	0.59	0.74	0.39	0.37
Subject10	0.91	0.95	0.66	0.64	0.63
Subject11	0.87	0.62	0.6	0.89	0.88

0.59Hz hip Magnitude	Trial1	Trial2	Trial3	Trial4	Trial5
Subject1	0.28	0.33	0.32	0.28	0.29
Subject2	0.33	0.33	0.37	0.28	0.28
Subject3	0.32	0.34	0.32	0.23	0.26
Subject4	0.27	0.23	0.26	0.22	0.23
Subject5	0.28	0.3	0.33	0.27	0.23
Subject6	0.29	0.3	0.29	0.31	0.31
Subject7	0.27	0.31	0.31	0.26	0.28
Subject8	0.29	0.28	0.28	0.27	0.23
Subject9	0.27	0.28	0.28	0.29	0.29
Subject10	0.21	0.32	0.31	0.34	0.33
Subject11	0.36	0.3	0.28	0.24	0.25

0.021Hz shank Coherence	Trial1	Trial2	Trial3	Trial4	Trial5
Subject1	0.69	0.55	0.2	0.4	0.19
Subject2	0.86	0.65	0.92	0.82	0.9
Subject3	0.75	0.89	0.86	0.91	0.89
Subject4	0.66	0.56	0.83	0.88	0.63
Subject5	0.44	0.46	0.66	0.95	0.3
Subject6	0.78	0.62	0.73	0.74	0.9
Subject7	0.98	0.98	0.95	0.92	0.97
Subject8	0.93	0.94	0.91	0.92	0.98
Subject9	0.91	0.97	0.95	0.95	0.9
Subject10	0.94	0.91	0.87	0.97	0.74
Subject11	0.77	0.83	0.96	0.85	0.82

0.021Hz trunk Coherence	Trial1	Trial2	Trial3	Trial4	Trial5
Subject1	0.78	0.41	0.66	0.28	0.51
Subject2	0.86	0.87	0.9	0.84	0.94
Subject3	0.97	0.76	0.96	0.97	0.85
Subject4	0.9	0.92	0.92	0.9	0.9
Subject5	0.72	0.73	0.86	0.86	0.44
Subject6	0.58	0.24	0.57	0.12	0.56
Subject7	0.92	0.86	0.94	0.92	0.9
Subject8	0.96	0.88	0.89	0.93	0.98
Subject9	0.86	0.91	0.96	0.88	0.87
Subject10	0.81	0.83	0.92	0.68	0.75
Subject11	0.86	0.51	0.95	0.68	0.8

0.59Hz shank Coherence	Trial1	Trial2	Trial3	Trial4	Trial5
Subject1	0.95	0.83	0.88	0.82	0.95
Subject2	0.9	0.99	0.96	0.89	0.95
Subject3	0.86	0.98	0.98	0.45	0.95
Subject4	0.81	0.94	0.52	0.94	0.74
Subject5	0.95	0.92	0.93	0.83	0.96
Subject6	0.84	0.88	0.94	0.98	0.98
Subject7	0.92	0.98	0.99	0.93	0.94
Subject8	0.97	0.96	1	0.99	0.99
Subject9	0.99	0.98	0.97	1	0.99
Subject10	0.69	0.96	0.98	0.93	0.97
Subject11	0.78	0.85	0.86	0.5	0.87

0.59Hz trunk Coherence	Trial1	Trial2	Trial3	Trial4	Trial5
Subject1	0.95	0.45	0.59	0.88	0.95
Subject2	0.98	0.9	0.89	0.94	0.93
Subject3	0.8	0.9	0.94	0.89	0.96
Subject4	0.83	0.45	0.77	0.5	0.34
Subject5	0.78	0.37	0.43	0.12	0.61
Subject6	0.95	0.98	0.97	0.98	0.98
Subject7	0.95	0.82	0.91	0.95	0.85
Subject8	0.79	0.02	0.99	0.87	0.93
Subject9	0.84	0.87	0.56	0.98	0.97
Subject10	0.77	0.97	0.67	0.34	0.75
Subject11	0.87	0.39	0.56	0.44	0.79

0.021Hz ankle Coherence	Trial1	Trial2	Trial3	Trial4	Trial5
Subject1	0.26	0.25	0.04	0.25	0.02
Subject2	0.67	0.34	0.42	0.33	0.68
Subject3	0.93	0.94	0.88	0.86	0.79
Subject4	0.86	0.79	0.81	0.92	0.83
Subject5	0.12	0.39	0.44	0.78	0.16
Subject6	0.68	0.56	0.67	0.55	0.38
Subject7	0.93	0.89	0.57	0.68	0.83
Subject8	0.63	0.91	0.75	0.86	0.9
Subject9	0.76	0.94	0.83	0.84	0.74
Subject10	0.89	0.76	0.76	0.96	0.5
Subject11	0.4	0.56	0.8	0.46	0.59

0.021Hz hip Coherence	Trial1	Trial2	Trial3	Trial4	Trial5
Subject1	0.03	0.39	0	0.3	0.08
Subject2	0.11	0.14	0.44	0.43	0.23
Subject3	0.79	0.15	0.56	0.68	0.21
Subject4	0.57	0.64	0.48	0.75	0.69
Subject5	0.11	0.12	0.42	0.26	0.1
Subject6	0.41	0.17	0.54	0.04	0.31
Subject7	0.41	0.32	0.59	0.39	0.75
Subject8	0.07	0.03	0.05	0	0.55
Subject9	0.33	0.37	0.74	0.43	0.2
Subject10	0.45	0.05	0.6	0.37	0.11
Subject11	0.27	0.02	0.83	0.19	0.1

0.59Hz ankle Coherence	Trial1	Trial2	Trial3	Trial4	Trial5
Subject1	1	0.98	0.98	0.99	1
Subject2	1	1	1	1	1
Subject3	0.99	1	1	1	1
Subject4	0.99	0.99	0.99	0.99	0.99
Subject5	0.99	0.98	0.98	0.97	0.99
Subject6	1	1	1	1	1
Subject7	1	0.99	1	1	1
Subject8	0.98	0.99	0.99	1	1
Subject9	1	0.99	1	0.99	0.98
Subject10	0.98	1	0.99	0.97	0.99
Subject11	0.99	0.93	0.92	0.98	0.99

0.59Hz hip Coherence	Trial1	Trial2	Trial3	Trial4	Trial5
Subject1	1	0.99	0.99	0.99	1
Subject2	1	0.99	0.99	0.99	0.98
Subject3	0.99	1	1	1	0.99
Subject4	0.99	0.99	0.99	0.99	0.98
Subject5	0.98	0.99	0.99	0.99	0.97
Subject6	0.98	0.99	0.99	0.99	0.99
Subject7	1	1	1	1	1
Subject8	0.99	1	1	1	1
Subject9	1	0.99	1	1	0.99
Subject10	0.98	1	1	0.98	0.99
Subject11	1	0.99	0.98	0.98	0.99

0.021Hz shank Angle	Trial1	Trial2	Trial3	Trial4	Trial5
Subject1	16.61	31.54	17.96	45.36	7.02
Subject2	0.2	3.17	4.75	14.03	8.85
Subject3	28.27	31.2	14.13	11.98	6.91
Subject4	16.06	19.36	9.58	17.05	28.08
Subject5	22.99	44.61	17.85	7.55	27.22
Subject6	16.59	16.54	12.84	15.47	6.27
Subject7	8.04	7.28	6.39	9.58	6.62
Subject8	0.81	3.88	2.53	2.87	11.12
Subject9	8.69	3.42	2.02	0.08	5.15
Subject10	9.9	6.34	8.01	20.68	2.21
Subject11	11.29	4.33	12.66	3.87	4.98

0.021Hz trunk Angle	Trial1	Trial2	Trial3	Trial4	Trial5
Subject1	5.4	53.24	11.57	59.68	15.21
Subject2	8.6	19.45	28.16	11.36	18.27
Subject3	1.52	13.41	9.02	13.96	3.51
Subject4	12.03	4.87	13.86	14.42	20.14
Subject5	6.67	43.11	11.18	20.33	25.87
Subject6	16.3	18.72	27.19	26.49	19.48
Subject7	3.25	7.65	23.8	8.34	16.46
Subject8	1.47	2.12	2.61	1.85	2.33
Subject9	3.92	8.80	4.79	11.8	0.18
Subject10	1.49	3.17	4.41	15.57	15.22
Subject11	10.36	0.39	31.91	18.84	13.59

0.59Hz shank Angle	Trial1	Trial2	Trial3	Trial4	Trial5
Subject1	15.21	9.62	17.47	3.14	15.34
Subject2	79.37	33.80	26.37	36.95	38.01
Subject3	34.91	0.56	5.83	14.87	10.37
Subject4	51.32	3.07	23.67	9.09	8.32
Subject5	22.08	17.41	19.62	11.24	1.15
Subject6	33.05	62.92	47.62	30.88	34.20
Subject7	26.97	9.36	6.77	41.13	24.45
Subject8	5.82	0.38	4.23	10.59	7.07
Subject9	11.58	0.94	11.65	3.04	1.9
Subject10	57.12	70.31	14.55	12.25	14.15
Subject11	34.1	16.37	24.56	18.94	38.32

0.59Hz trunk Angle	Trial1	Trial2	Trial3	Trial4	Trial5
Subject1	166.65	153.86	133.93	172.52	159.70
Subject2	155.01	140.23	148.56	168.34	165.65
Subject3	132.1	179.35	170.43	171.3	177.58
Subject4	132.4	48.18	146.86	13.5	152.38
Subject5	114.44	86.83	86.15	70.22	39.25
Subject6	165.33	159.94	168.79	162.98	165.36
Subject7	166.09	20.18	16.11	157.12	151.70
Subject8	14.45	119.18	5.83	42.54	21.21
Subject9	146.80	1.02	112.78	3.83	2.4
Subject10	122.64	145.9	62.18	55.86	51.76
Subject11	158.85	46.2	52.68	167.43	141.92

0.021Hz ankle Angle	Trial1	Trial2	Trial3	Trial4	Trial5
Subject1	134.07	89.91	130	85.6	157.70
Subject2	179.66	173.93	160.33	131.72	161.42
Subject3	166.67	157.91	167.25	164.11	169.77
Subject4	170.86	168.75	169.79	166.52	164.15
Subject5	112.18	125.83	150.96	163	135.93
Subject6	158.61	161.24	165.31	156.14	155.23
Subject7	164.63	163.82	155.69	157.55	163.73
Subject8	177.75	175.33	175.24	175.95	151.14
Subject9	164.11	174.53	176.07	179.86	170.93
Subject10	166.59	168.58	168.38	156.5	176.29
Subject11	154.53	171.37	146.16	169.96	171.15

0.021Hz hip Angle	Trial1	Trial2	Trial3	Trial4	Trial5
Subject1	84.09	125.13	30.1	107.02	36.37
Subject2	42.15	98.8	103.72	110.83	52.41
Subject3	23.44	35.01	42.38	62.87	32.18
Subject4	27.91	18.94	45.05	40	45.77
Subject5	69.08	35.36	3.73	67.52	15.35
Subject6	62.35	69.84	79.43	171.48	43.42
Subject7	73.26	73.59	99.49	60.2	131.6
Subject8	173.54	84.33	129.04	75.11	128.17
Subject9	62.52	43.15	23.19	34.86	14.84
Subject10	23.91	78.87	20.10	88.42	63.78
Subject11	44.82	150.82	83.65	67.99	41.77

0.59Hz ankle Angle	Trial1	Trial2	Trial3	Trial4	Trial5
Subject1	177.29	176.8	173.97	179.48	177.14
Subject2	170.63	169.83	171.59	175.36	175.83
Subject3	171.09	179.83	178.46	179.17	179
Subject4	170.88	178.97	177.21	176.58	178.33
Subject5	172.59	172.37	170.01	175.68	179.57
Subject6	177.5	175.64	176.01	175.73	176.07
Subject7	176.83	172.92	174.88	174	174.67
Subject8	175.92	179.85	174.63	174.69	175.72
Subject9	176.79	179.36	175.74	175.37	176.79
Subject10	170.89	167.88	172.4	171.78	171.07
Subject11	173.82	169.73	162.18	177.09	172.92

0.59Hz hip Angle	Trial1	Trial2	Trial3	Trial4	Trial5
Subject1	177.85	179	176.93	177.91	178.02
Subject2	176.04	173.02	174.87	172.66	176.24
Subject3	176.34	179.42	179.48	176.69	178.12
Subject4	175.43	167.29	167.94	172.09	166.51
Subject5	175.86	176.04	174.6	178.25	171.03
Subject6	176.23	175.52	176.02	178.89	178.59
Subject7	178.61	175.23	176.99	172.79	175.71
Subject8	178.13	178.26	177.31	179.27	177.31
Subject9	177.01	179.1	178.45	177.85	178.69
Subject10	173.33	173.78	176.36	178.49	177.22
Subject11	178.8	175.33	176.2	175.73	176.69

APPENDIX B

RELATIONSHIP BETWEEN THE COM AND COP

In this Appendix, the graph of the CoPx and CoM are given for the relation of the CoPx and CoM [78]. One can see from the Figures B.1,B.2,B.3 and B.4 that CoPx has high oscillations than the CoM [79], where CoM excursion is almost the mean path traveled by CoP signal. CoPxd and CoMd signals, which are shown in Figures B.3 and B.4, are explained in Chapter 4 and section 4.2.2.
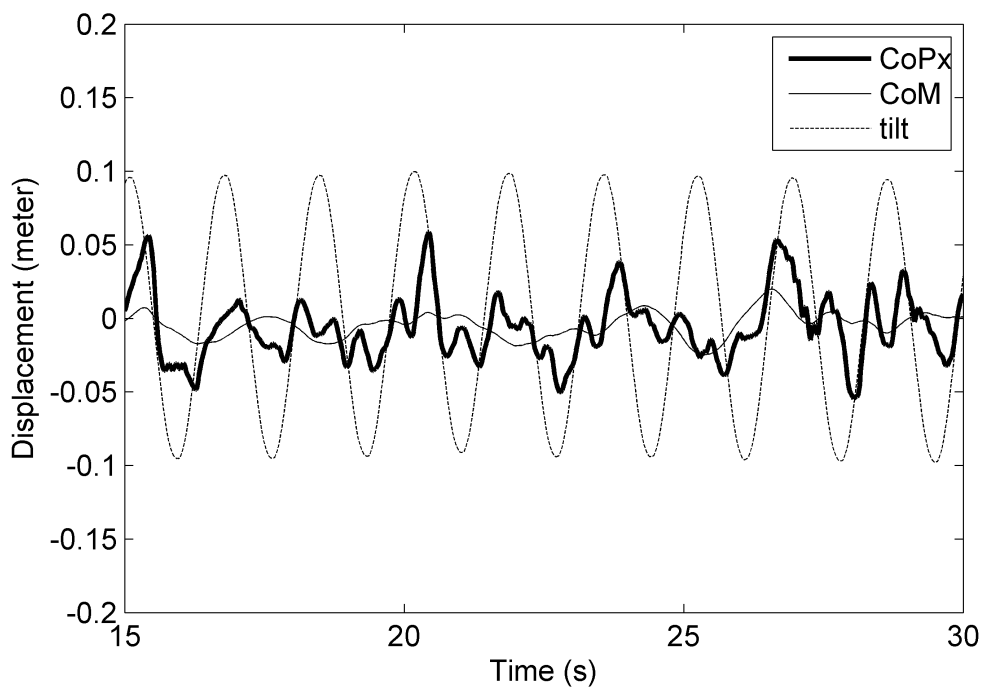
Figure B.1 CoPx vs CoM trajectories for 5 degrees, 0.59 Hz perturbation
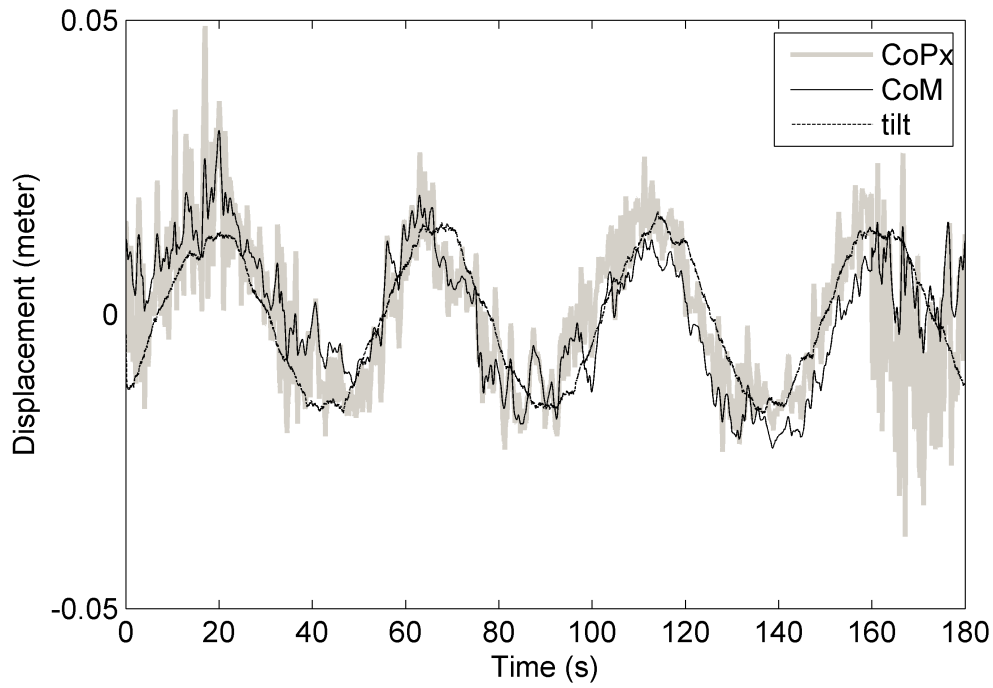
Figure B.2 CoPx vs CoM trajectories for 1 degree, 0.021 Hz perturbation
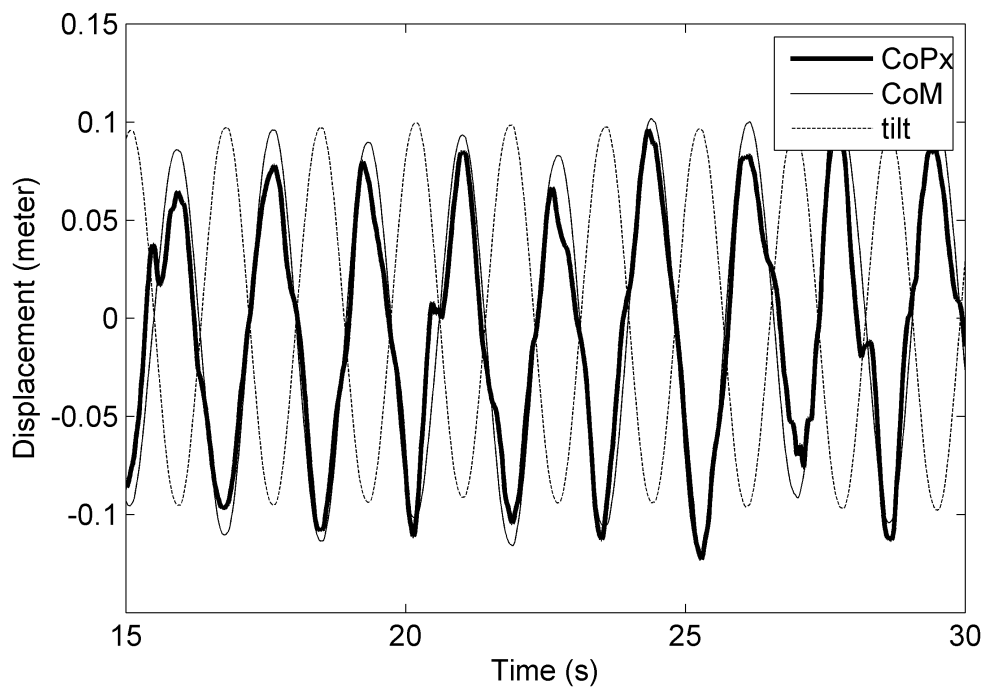
Figure B.3 CoPxd vs CoMd trajectories for 5 degrees, 0.59 Hz perturbation

134
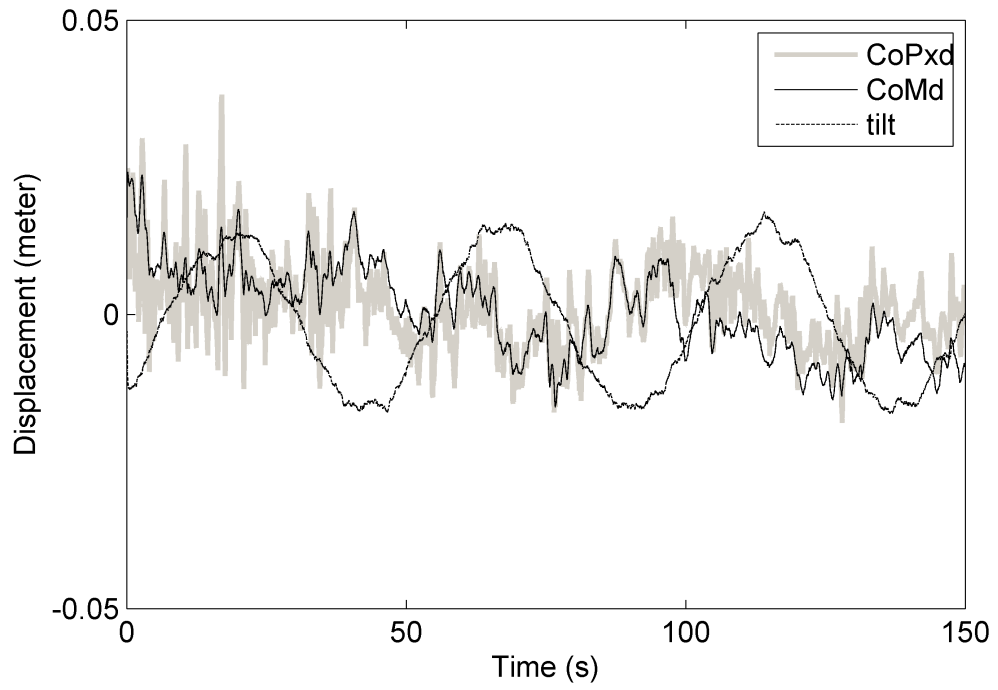
Figure B.4 CoPxd vs CoMd trajectories for 1 degree, 0.021 Hz perturbation

APPENDIX C

QUESTIONNAIRE FOR THE SUBJECTS

Number of the Subject: 01

Date of Birth: 13.04.1986

Height: 181 cm

Weight: 75 kg

Questions before the experiments.

Are there any surgery or illness related to the balance passed before?

No.

Are there any information about the experiments?

No.

Are you tired?

No.

Questions after the experiments.

Did you get bored during the experiments?

Yes. It was very enjoyable until about 5th or 6th experiment. Then, I thought about my exam tomorrow morning.

Have many different movements did you feel?

Only one and very long quite stance.

Did something caught the attention during the experiments?

No.

Number of the Subject: 02

Date of Birth: 02.06.1985

Height: 178 cm

Weight: 76 kg

Questions before the experiments.

Are there any surgery or illness related to the balance passed before?

No.

Are there any information about the experiments?

No.

Are you tired?

No.

Questions after the experiments.

Did you get bored during the experiments?

No.

Have many different movements did you feel?

One.

Did something caught the attention during the experiments?

No.

Number of the Subject: 03

Date of Birth: 01.08.1979

Height: 184 cm

Weight: 85 kg

Questions before the experiments.

Are there any surgery or illness related to the balance passed before?

No.

Are there any information about the experiments?

No.

Are you tired?

No.

Questions after the experiments.

Did you get bored during the experiments?

Yes.

Have many different movements did you feel?

Only one.

Did something caught the attention during the experiments?

No.

Number of the Subject: 04

Date of Birth: 15.12.1988

Height: 171 cm

Weight: 65 kg

Questions before the experiments.

Are there any surgery or illness related to the balance passed before?

No.

Are there any information about the experiments?

No.

Are you tired?

No.

Questions after the experiments.

Did you get bored during the experiments?

Yes. About 10 minutes later after starting the experiments.

Have many different movements did you feel?

One big perturbation.

Did something caught the attention during the experiments?

No.

Number of the Subject: 05

Date of Birth: 12.01.1990

Height: 178 cm

Weight: 78 kg

Questions before the experiments.

Are there any surgery or illness related to the balance passed before?

No.

Are there any information about the experiments?

No.

Are you tired?

No.

Questions after the experiments.

Did you get bored during the experiments?

No.

Have many different movements did you feel?

One perturbation.

Did something caught the attention during the experiments?

No.

Number of the Subject: 06

Date of Birth: 21.03.1980

Height: 175 cm

Weight: 86 kg

Questions before the experiments.

Are there any surgery or illness related to the balance passed before?

No.

Are there any information about the experiments?

No.

Are you tired?

No.

Questions after the experiments.

Did you get bored during the experiments?

No.

Have many different movements did you feel?

One.

Did something caught the attention during the experiments?

No.

Number of the Subject: 07

Date of Birth: 02.08.1982

Height: 173 cm

Weight: 77 kg

Questions before the experiments.

Are there any surgery or illness related to the balance passed before?

No.

Are there any information about the experiments?

No.

Are you tired?

No.

Questions after the experiments.

Did you get bored during the experiments?

No.

Have many different movements did you feel?

Only one.

Did something caught the attention during the experiments?

No.

Number of the Subject: 08

Date of Birth: 03.02.1978

Height: 169 cm

Weight: 78 kg

Questions before the experiments.

Are there any surgery or illness related to the balance passed before?

No.

Are there any information about the experiments?

No.

Are you tired?

No.

Questions after the experiments.

Did you get bored during the experiments?

Yes.

Have many different movements did you feel?

One.

Did something caught the attention during the experiments?

No.

Number of the Subject: 09

Date of Birth: 01.11.1984

Height: 172 cm

Weight: 80 kg

Questions before the experiments.

Are there any surgery or illness related to the balance passed before?

No.

Are there any information about the experiments?

No.

Are you tired?

No.

Questions after the experiments.

Did you get bored during the experiments?

Yes. A little.

Have many different movements did you feel?

One.

Did something caught the attention during the experiments?

No.

Number of the Subject: 10

Date of Birth: 04.12.1987

Height: 168 cm

Weight: 65 kg

Questions before the experiments.

Are there any surgery or illness related to the balance passed before?

No.

Are there any information about the experiments?

No.

Are you tired?

No.

Questions after the experiments.

Did you get bored during the experiments?

No.

Have many different movements did you feel?

Only one.

Did something caught the attention during the experiments?

No.

Number of the Subject: 11

Date of Birth: 14.05.1986

Height: 171 cm

Weight: 75 kg

Questions before the experiments.

Are there any surgery or illness related to the balance passed before?

No.

Are there any information about the experiments?

No.

Are you tired?

No.

Questions after the experiments.

Did you get bored during the experiments?

Yes.

Have many different movements did you feel?

One high perturbation.

Did something caught the attention during the experiments?

No.

APPENDIX D

FIGURES FOR THE REMAINING SUBJECTS

In this Appendix, the simulation and measurement data for 5 degrees, 0.59 Hz and 1 degree, 0.021 Hz perturbations. The subject 9 is given in Chapter 6. The remaining ten subjects are given in this appendix.
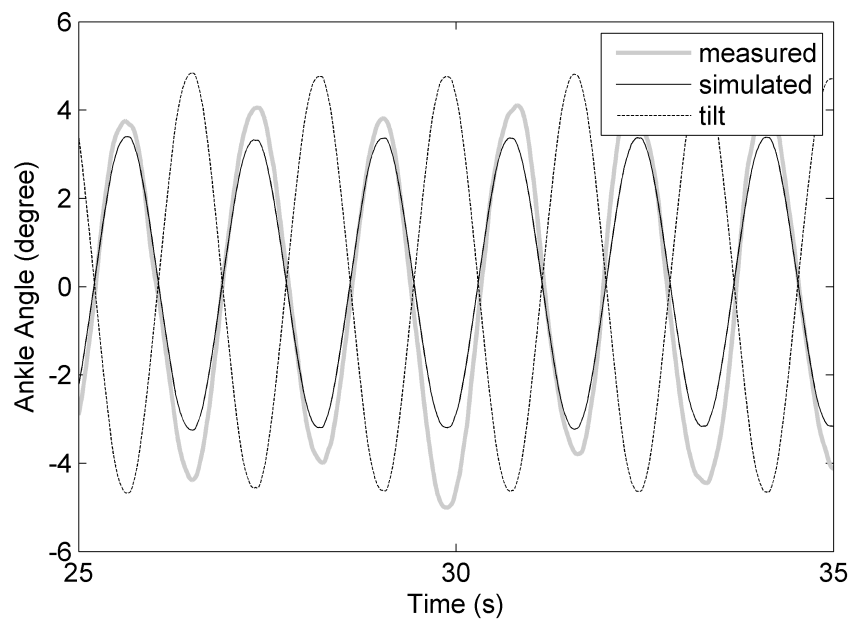
Figure D.1 Ankle angle for subject 1 and trial 1 for 5 degrees, 0.59 Hz perturbation
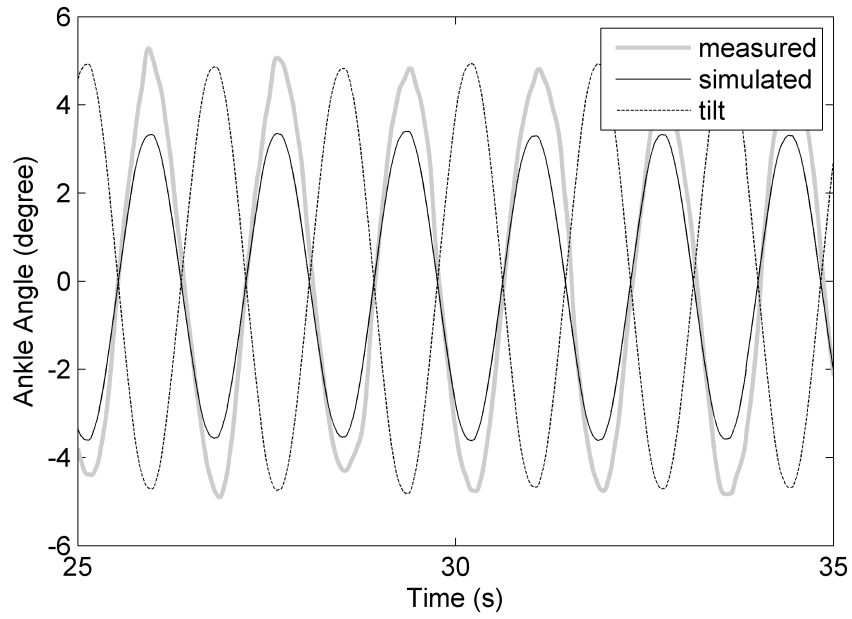
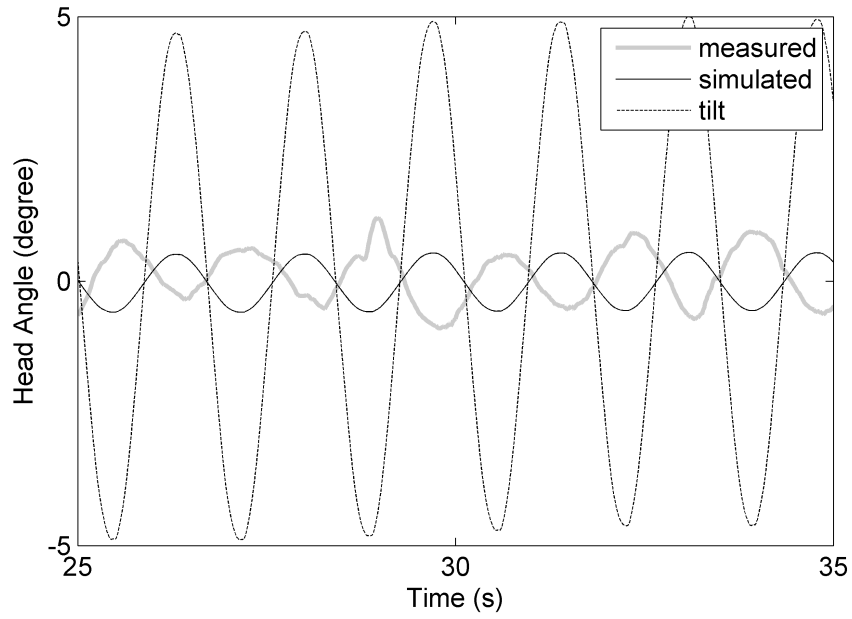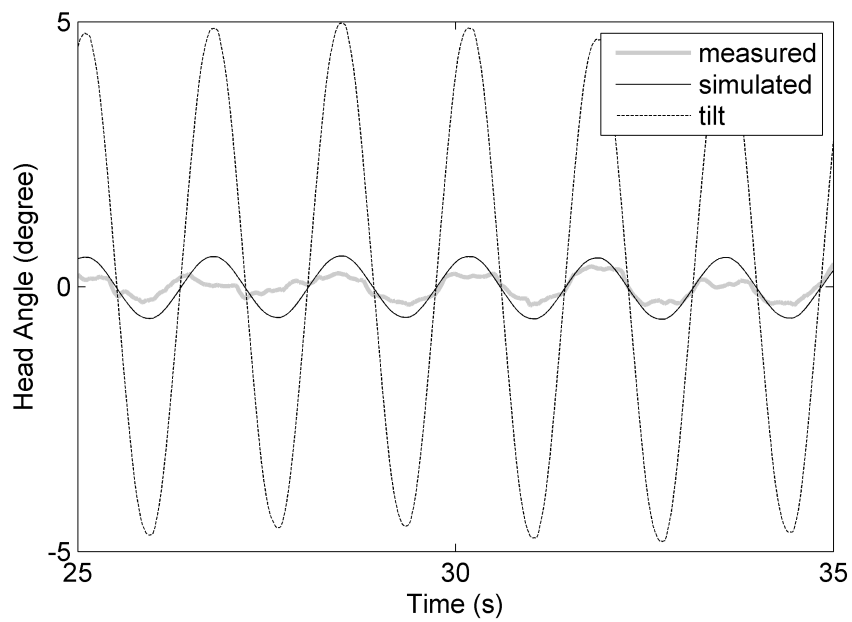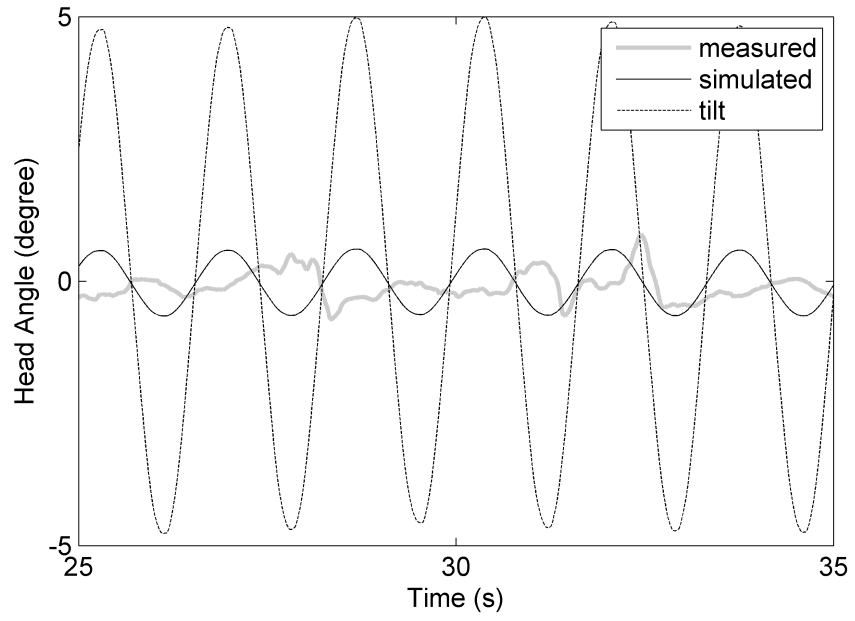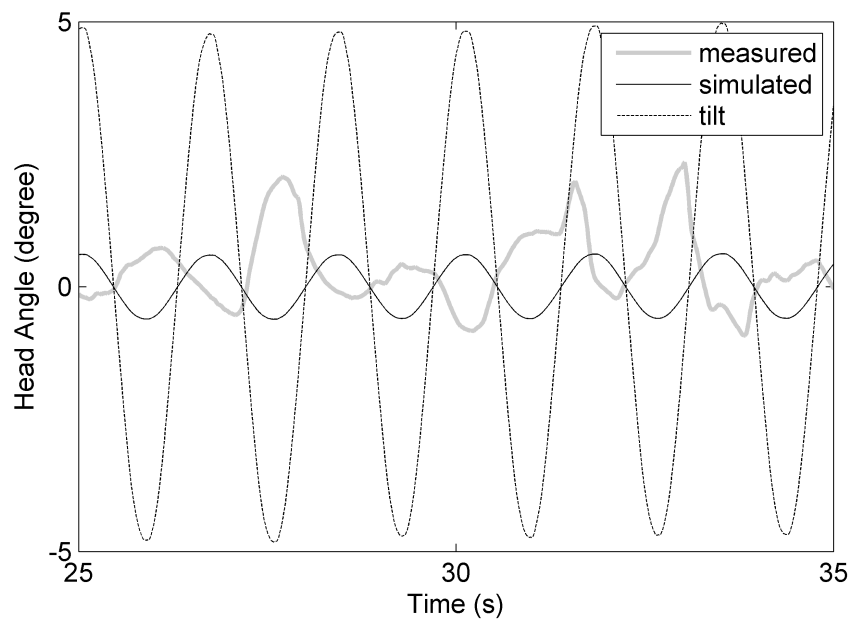Figure D.2 Ankle angle for subject 2 and trial 1 for 5 degrees, 0.59 Hz perturbation
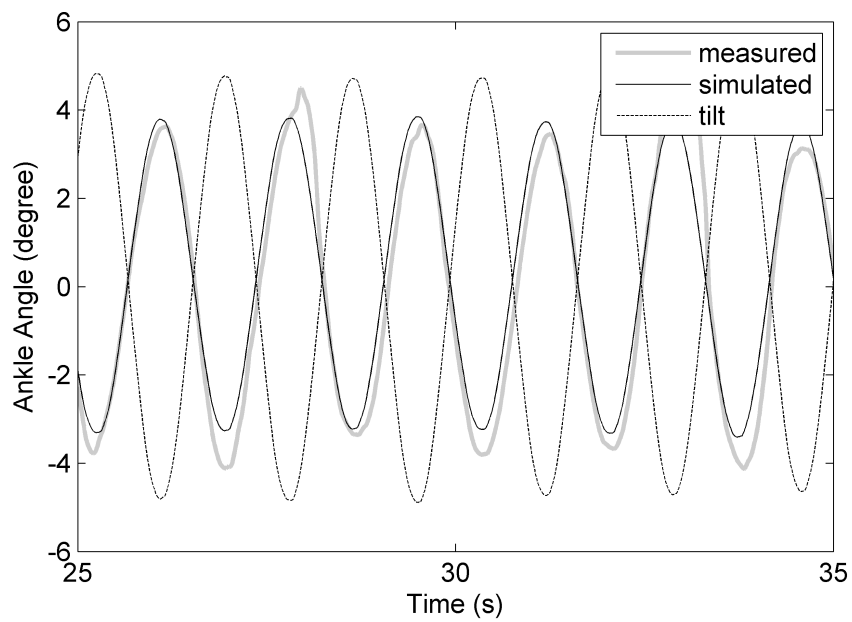
Figure D.3 Ankle angle for subject 3 and trial 1 for 5 degrees, 0.59 Hz perturbation
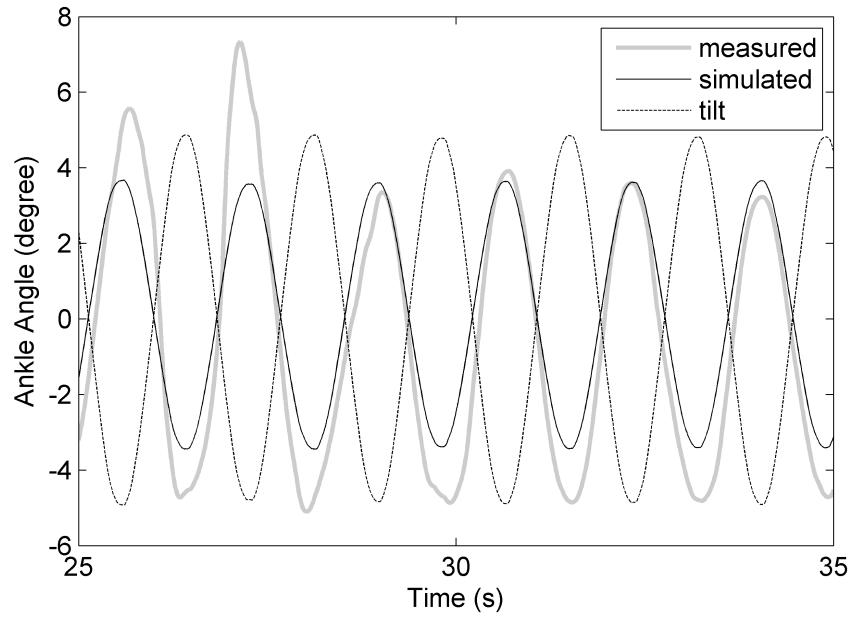
Figure D.4 Ankle angle for subject 4 and trial 1 for 5 degrees, 0.59 Hz perturbation
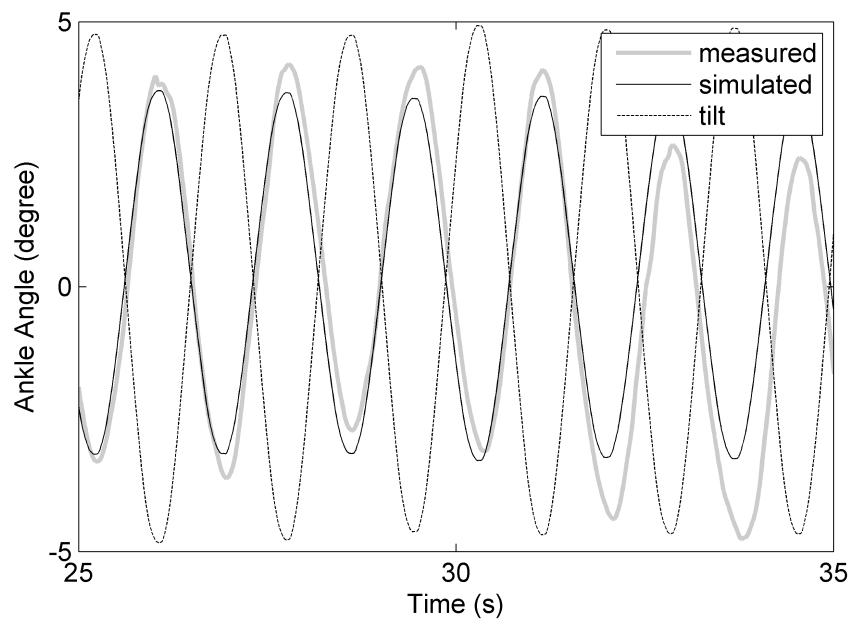
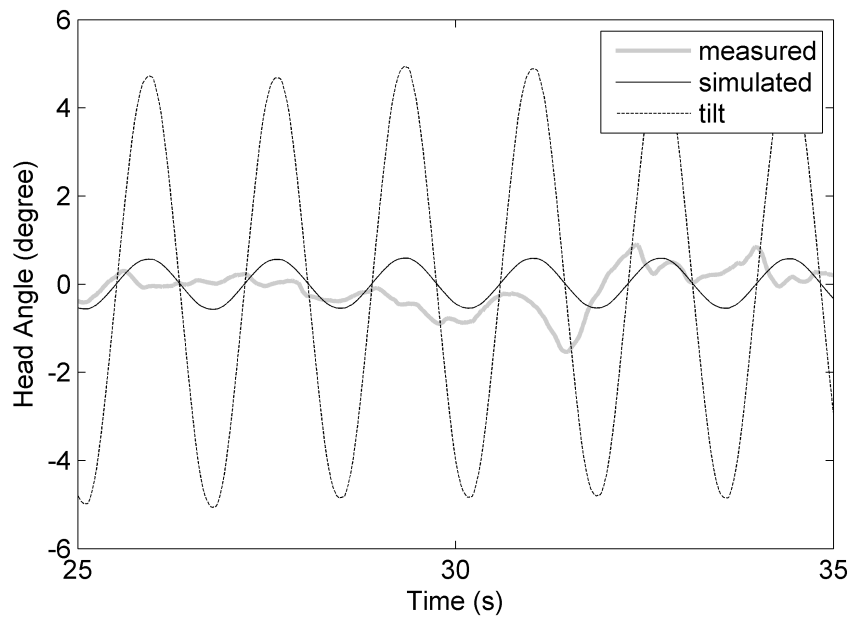Figure D.5 Ankle angle for subject 5 and trial 1 for 5 degrees, 0.59 Hz perturbation

151
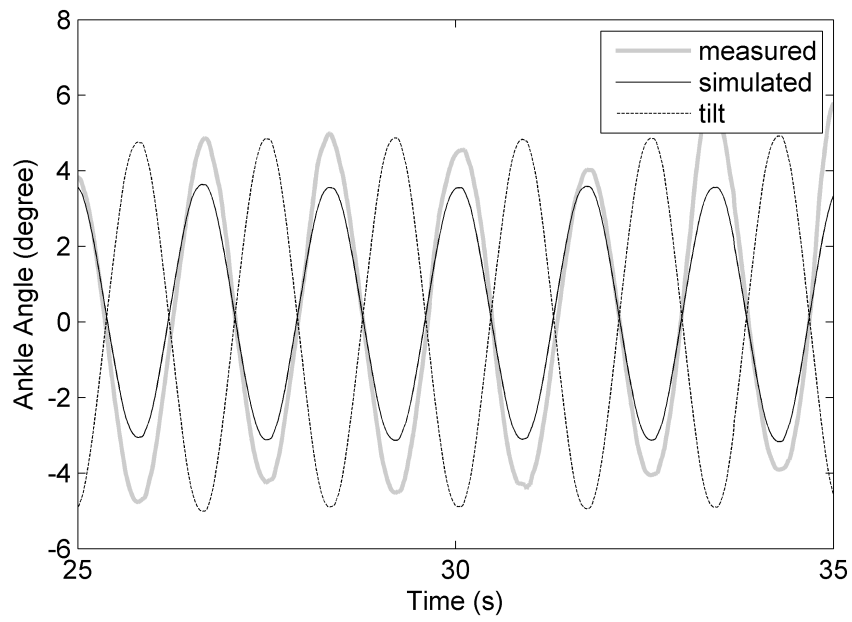
Figure D.6 Ankle angle for subject 6 and trial 1 for 5 degrees, 0.59 Hz perturbation
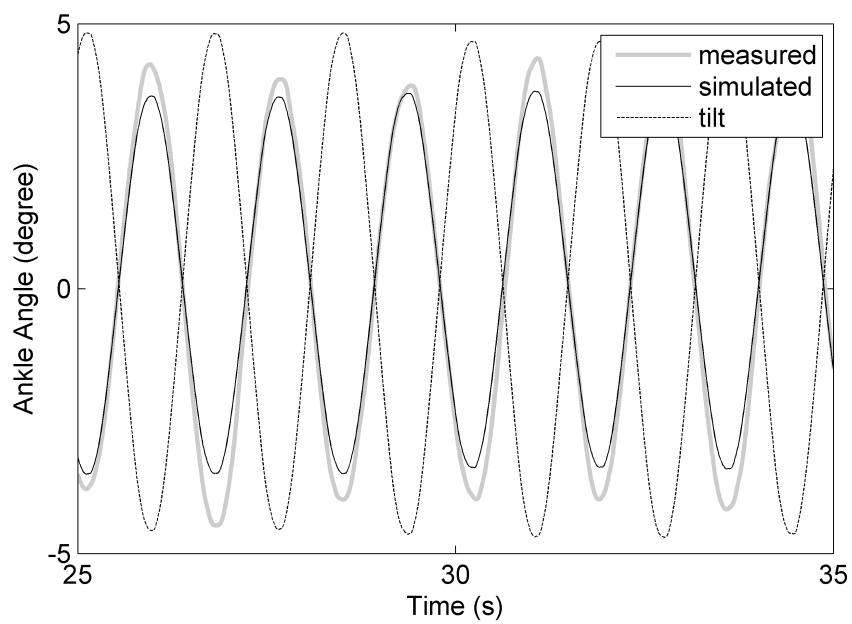
Figure D.7 Ankle angle for subject 7 and trial 1 for 5 degrees, 0.59 Hz perturbation
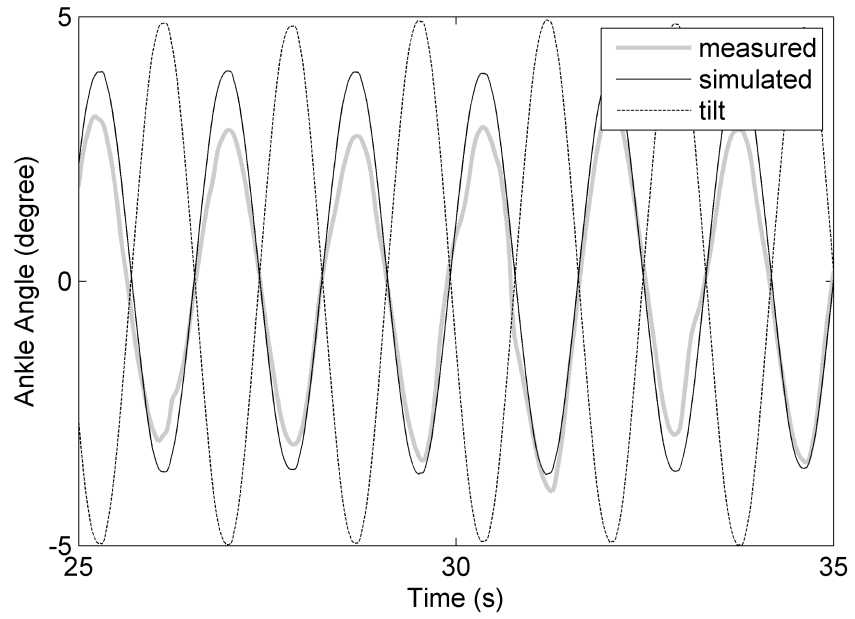
Figure D.8 Ankle angle for subject 8 and trial 1 for 5 degrees, 0.59 Hz perturbation
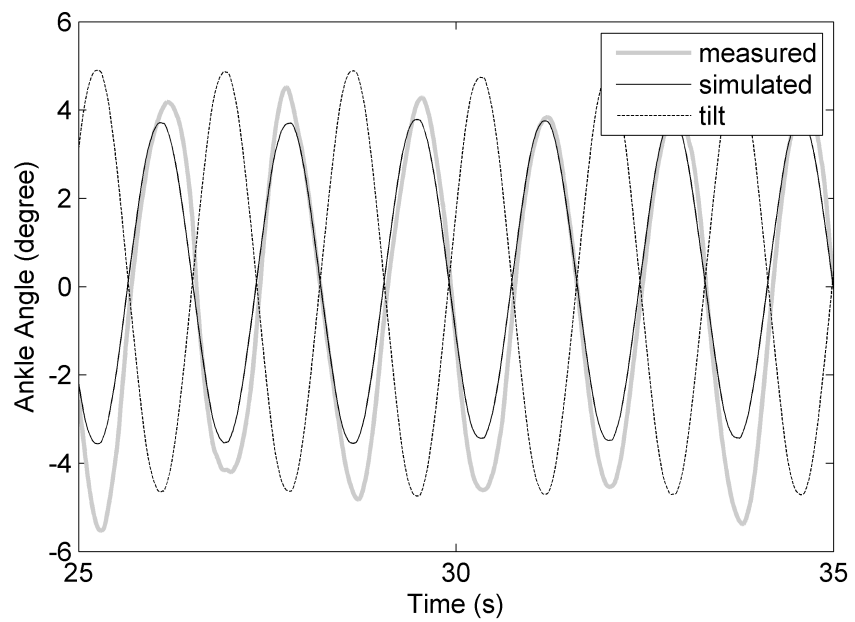
Figure D.9 Ankle angle for subject 10 and trial 1 for 5 degrees, 0.59 Hz perturbation
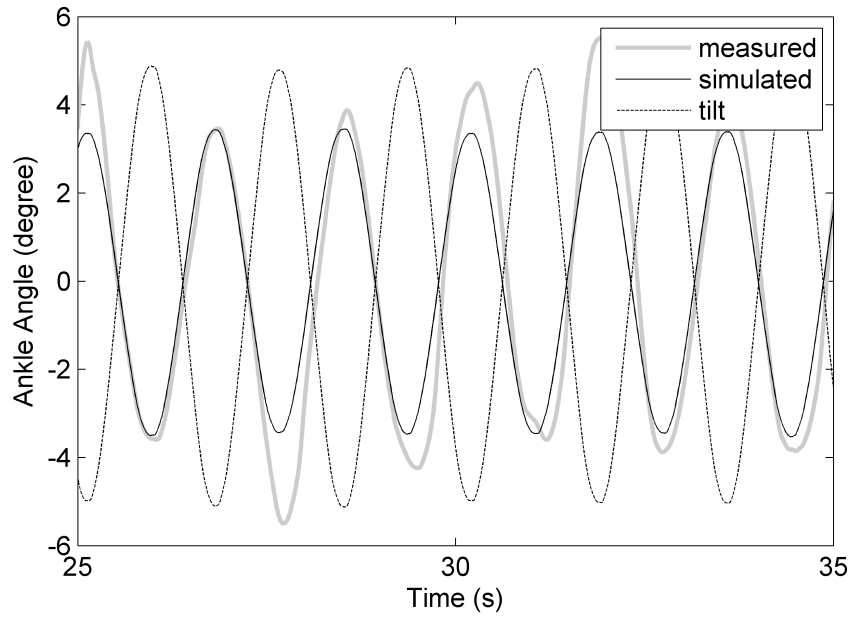
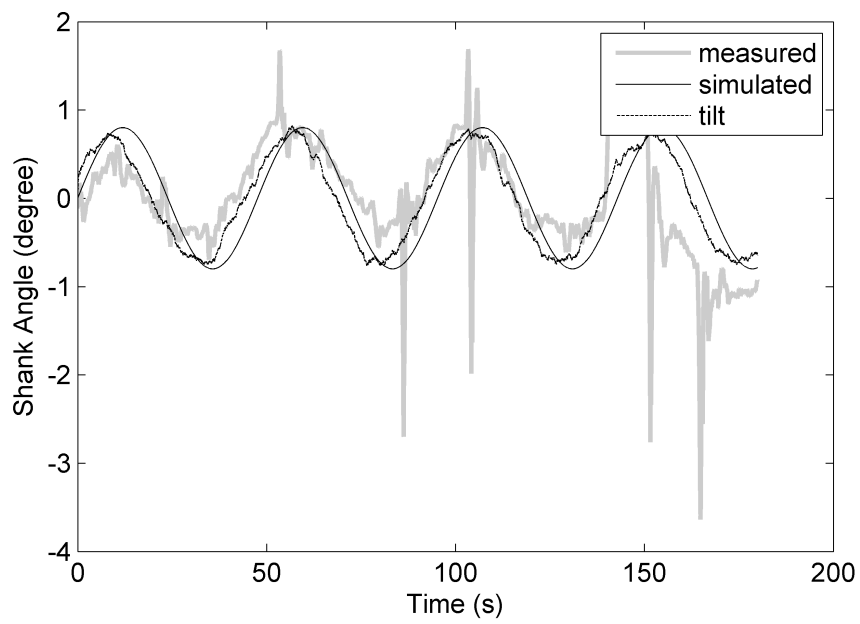Figure D.10 Ankle angle for subject 11 and trial 1 for 5 degrees, 0.59 Hz perturbation
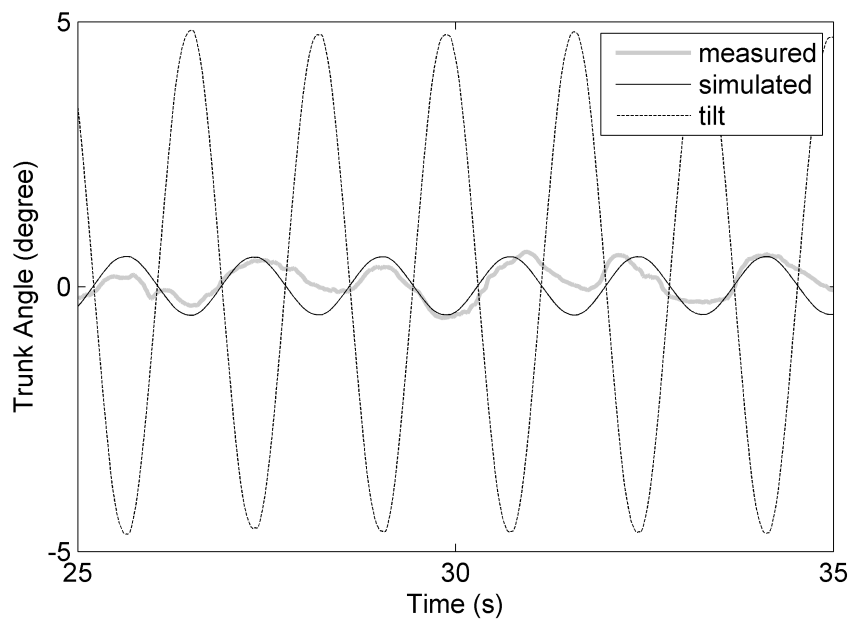
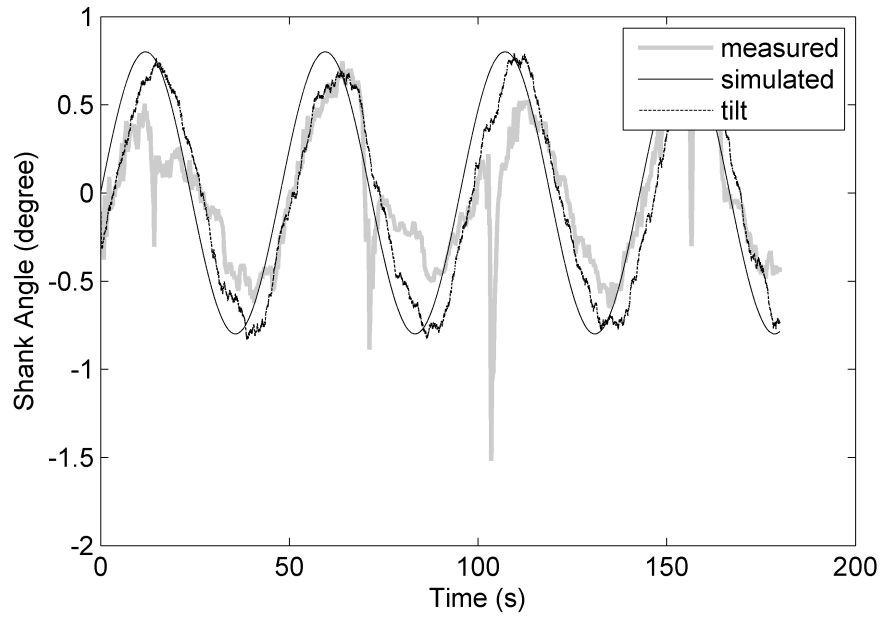Figure D.11 Trunk angle for subject 1 and trial 1 for 5 degrees, 0.59 Hz perturbation

154
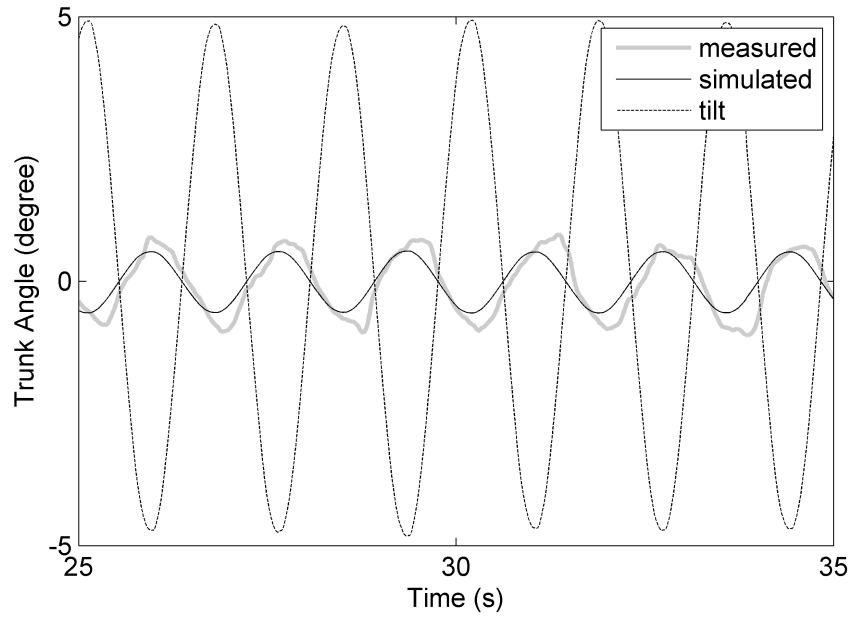
Figure D.12 Trunk angle for subject 2 and trial 1 for 5 degrees, 0.59 Hz perturbation
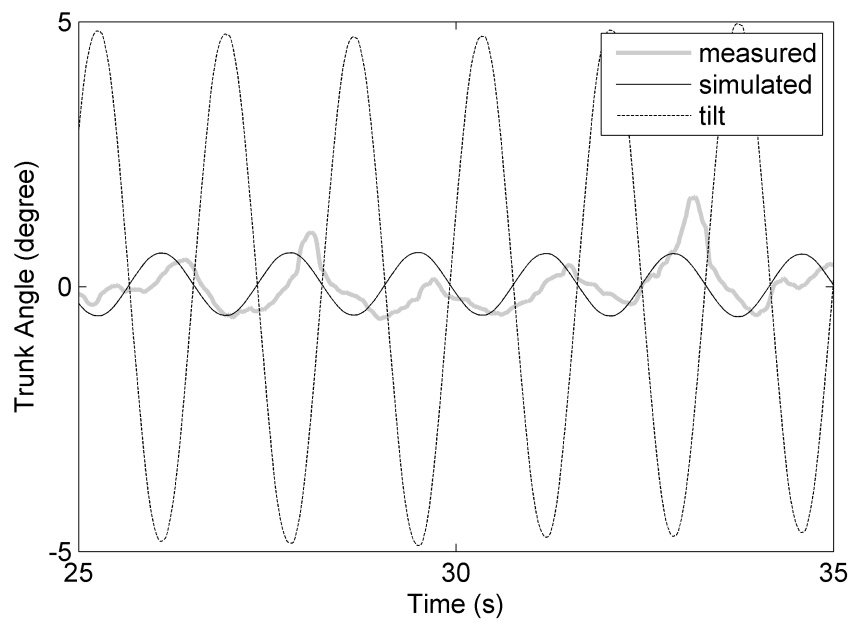
Figure D.13 Trunk angle for subject 3 and trial 1 for 5 degrees, 0.59 Hz perturbation
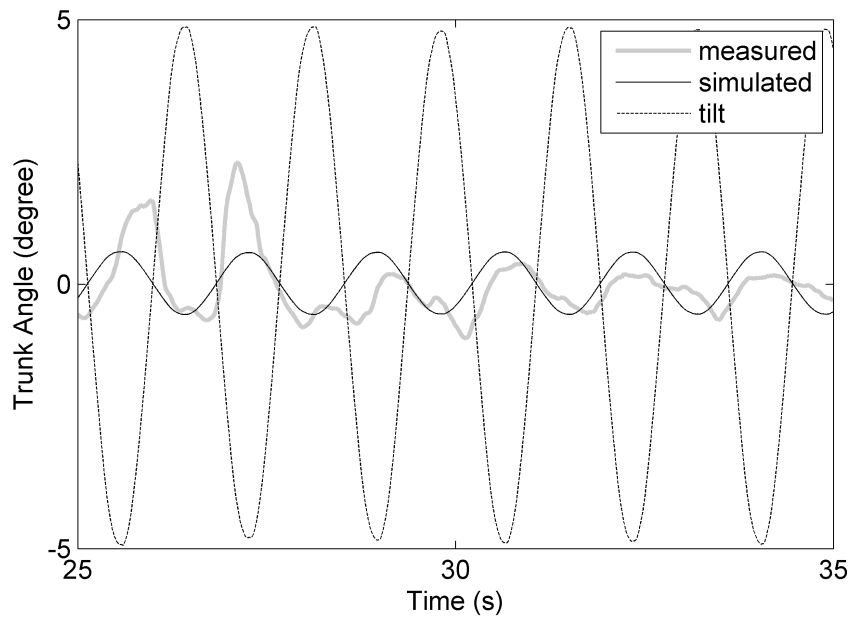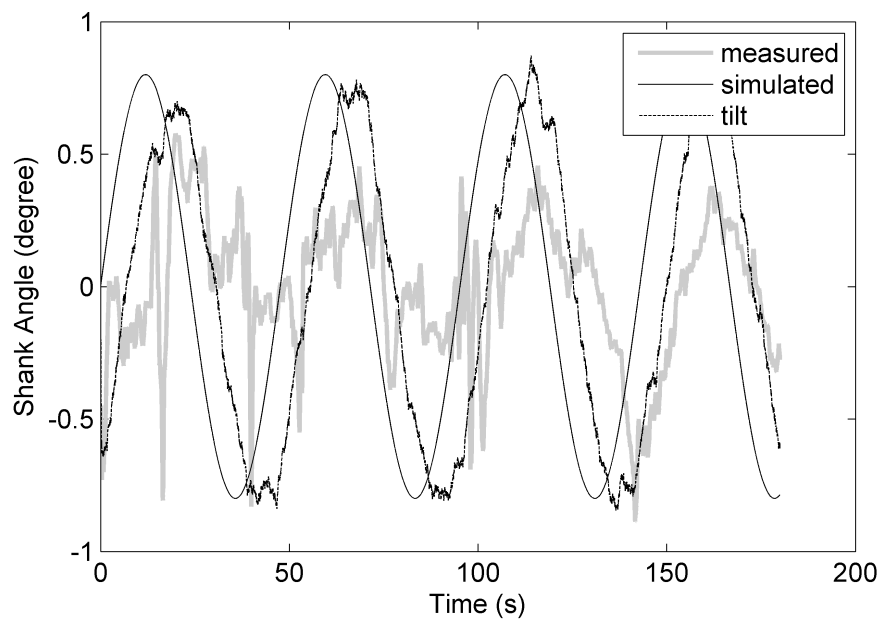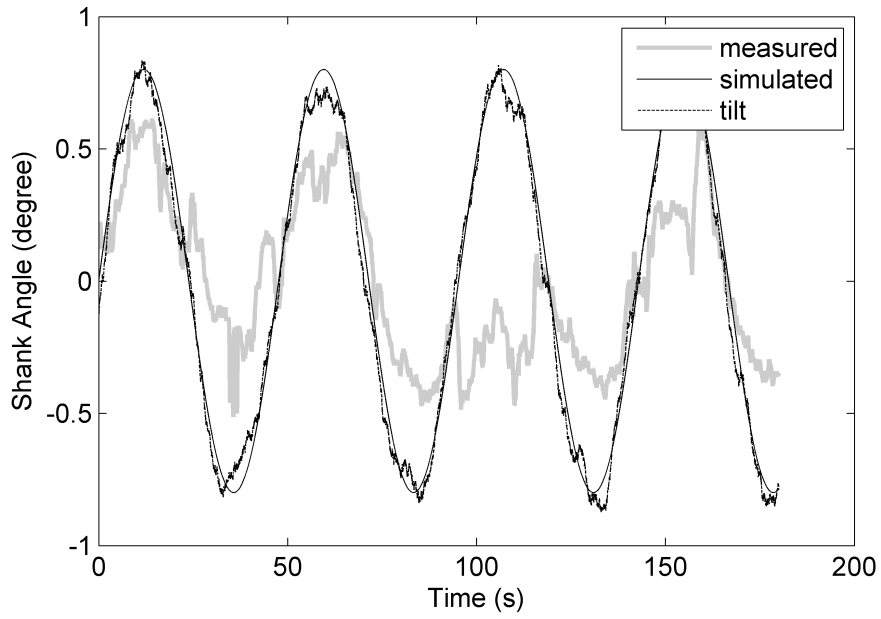
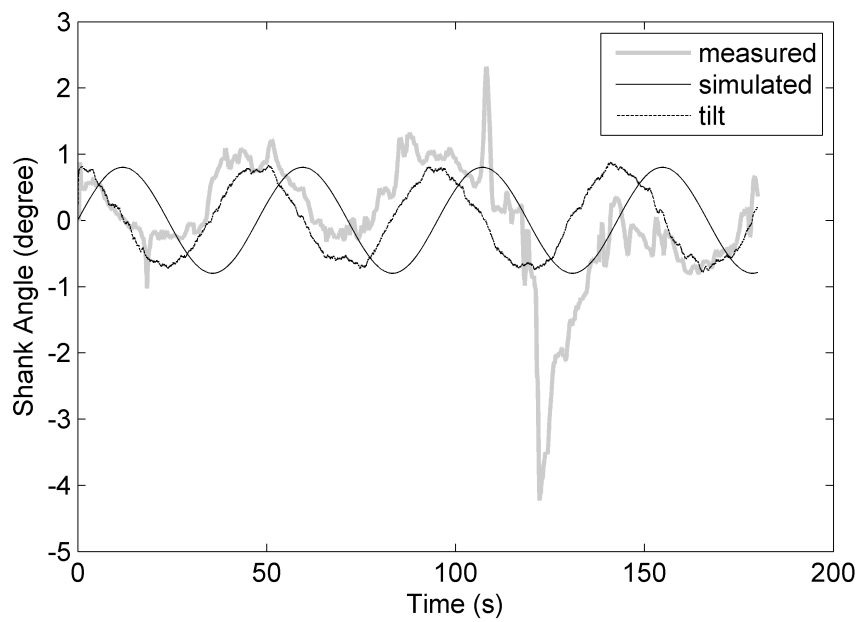Figure D.14 Trunk angle for subject 4 and trial 1 for 5 degrees, 0.59 Hz perturbation
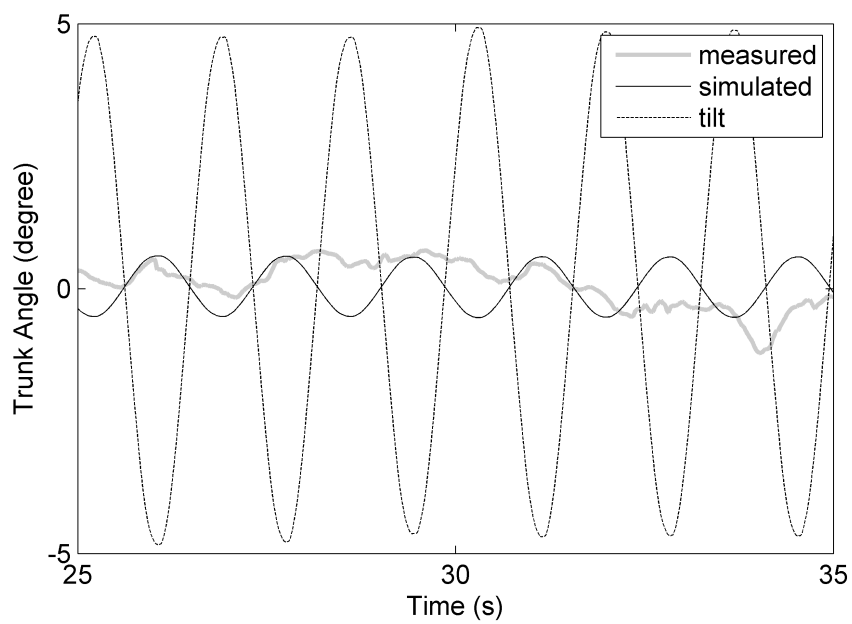
Figure D.15 Trunk angle for subject 5 and trial 1 for 5 degrees, 0.59 Hz perturbation
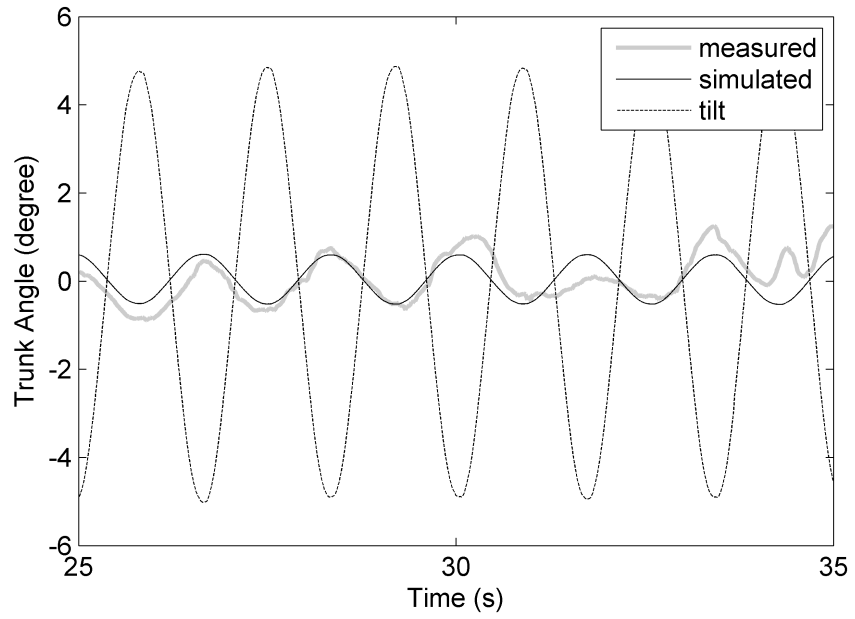
Figure D.16 Trunk angle for subject 6 and trial 1 for 5 degrees, 0.59 Hz perturbation
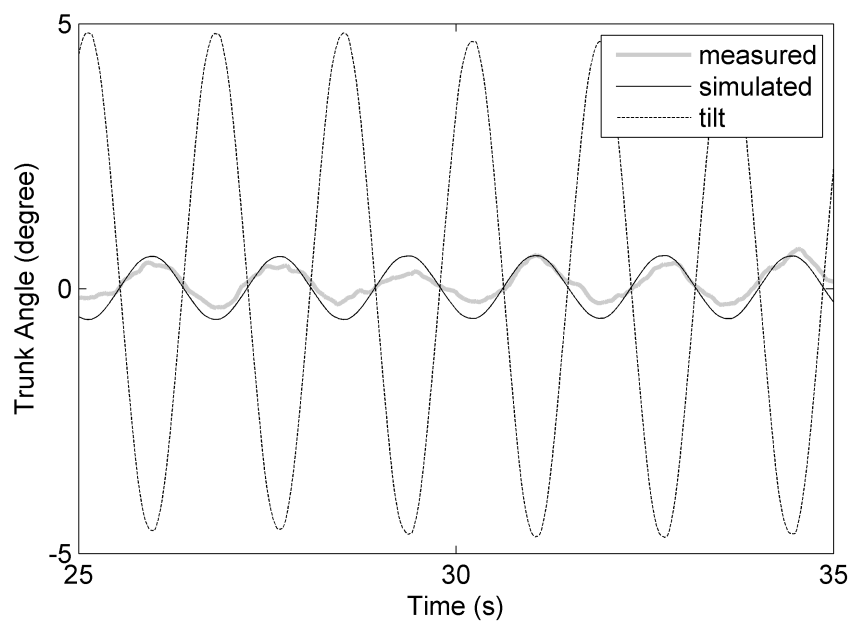
Figure D.17 Trunk angle for subject 7 and trial 1 for 5 degrees, 0.59 Hz perturbation
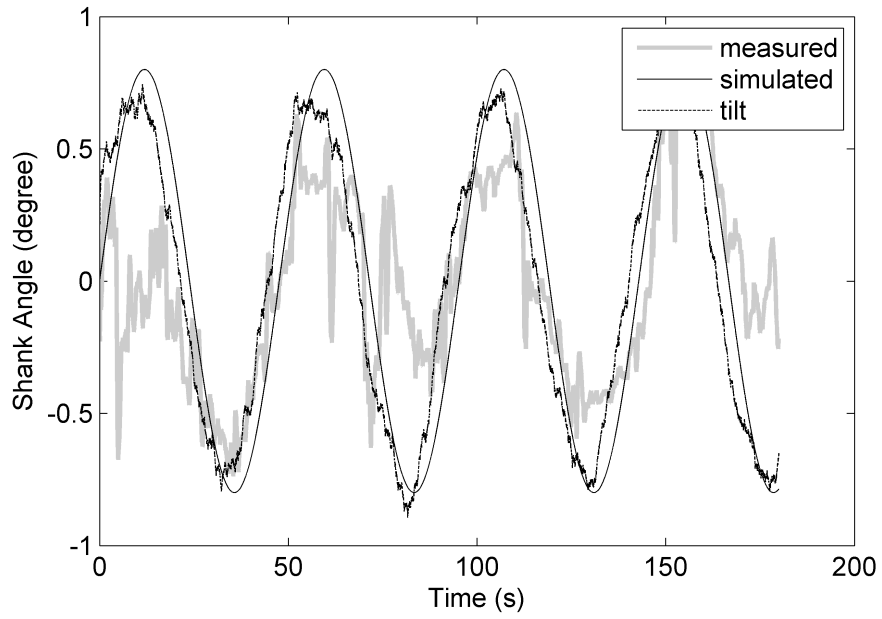
157
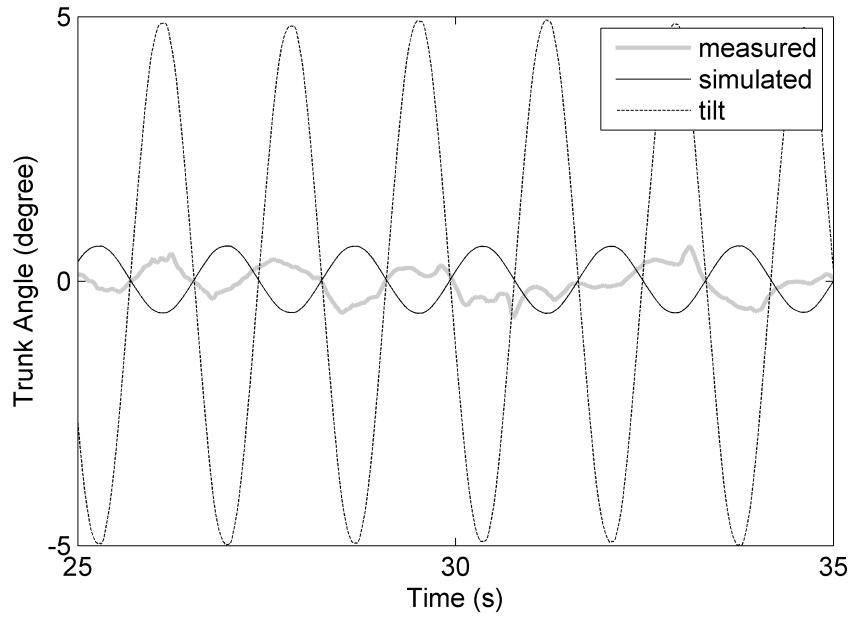
Figure D.18 Trunk angle for subject 8 and trial 1 for 5 degrees, 0.59 Hz perturbation
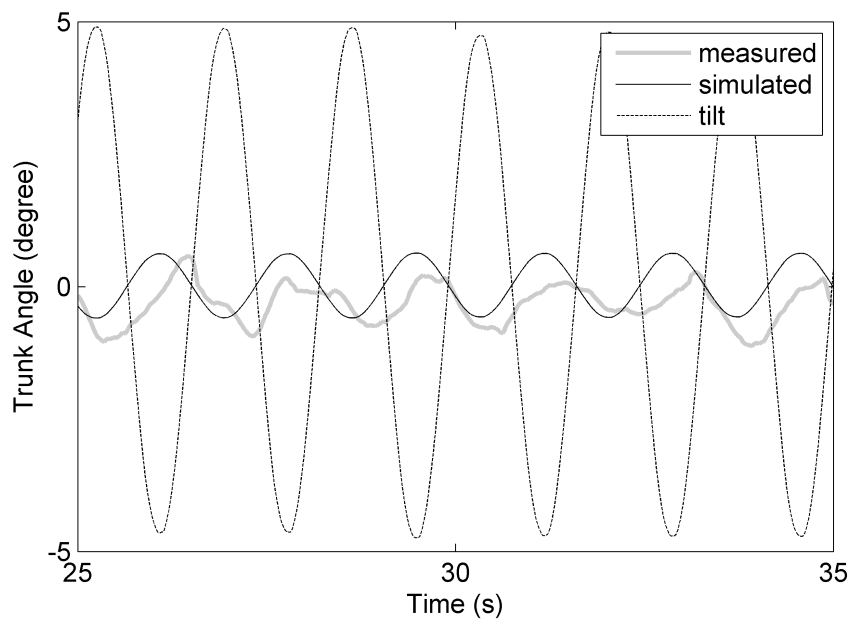
Figure D.19 Trunk angle for subject 10 and trial 1 for 5 degrees, 0.59 Hz perturbation
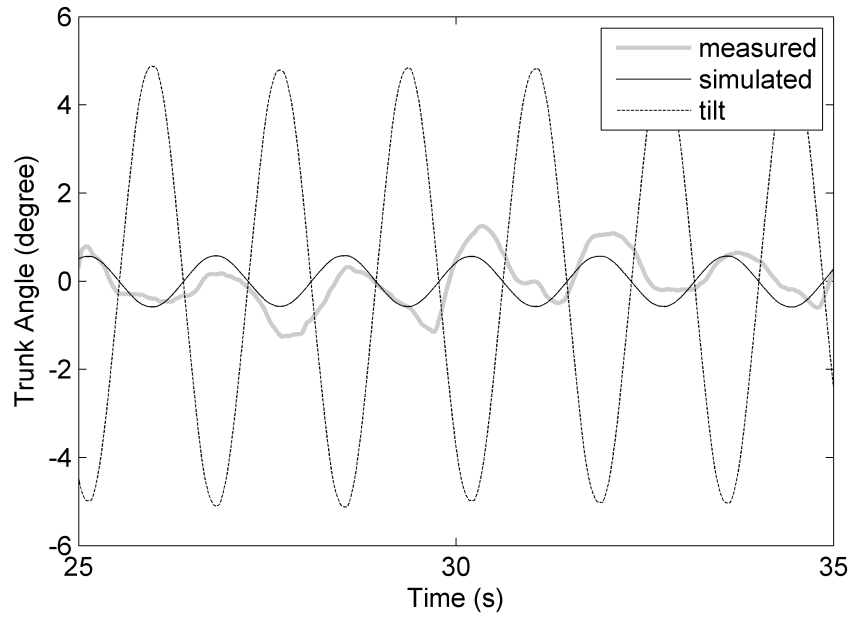
Figure D.20 Trunk angle for subject 11 and trial 1 for 5 degrees, 0.59 Hz perturbation
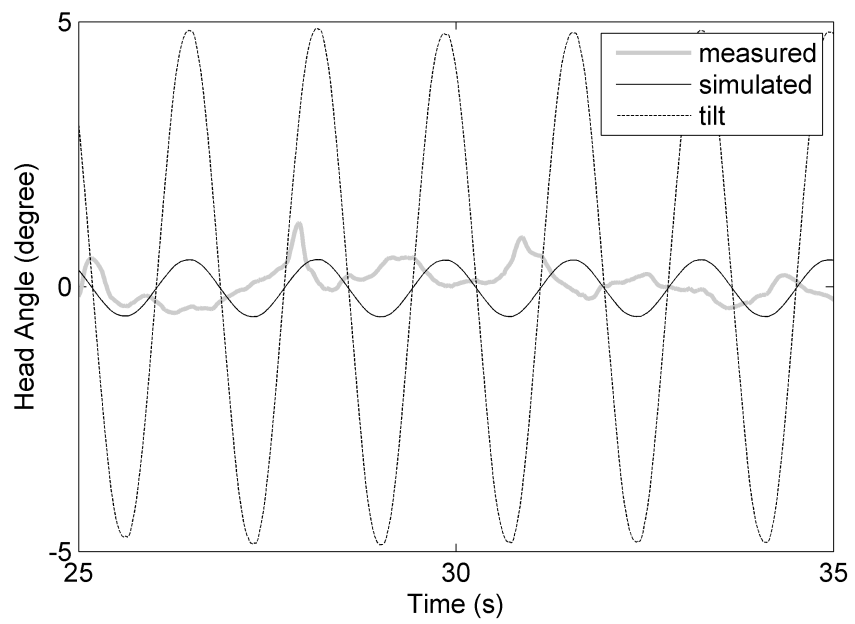
Figure D.21 Head angle for subject 1 and trial 1 for 5 degrees, 0.59 Hz perturbation
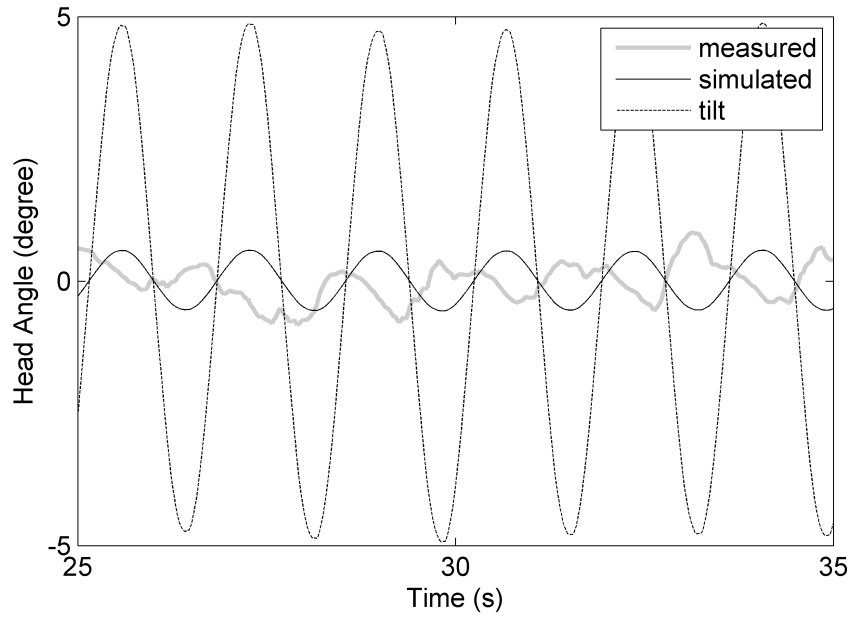
Figure D.22 Head angle for subject 2 and trial 1 for 5 degrees, 0.59 Hz perturbation
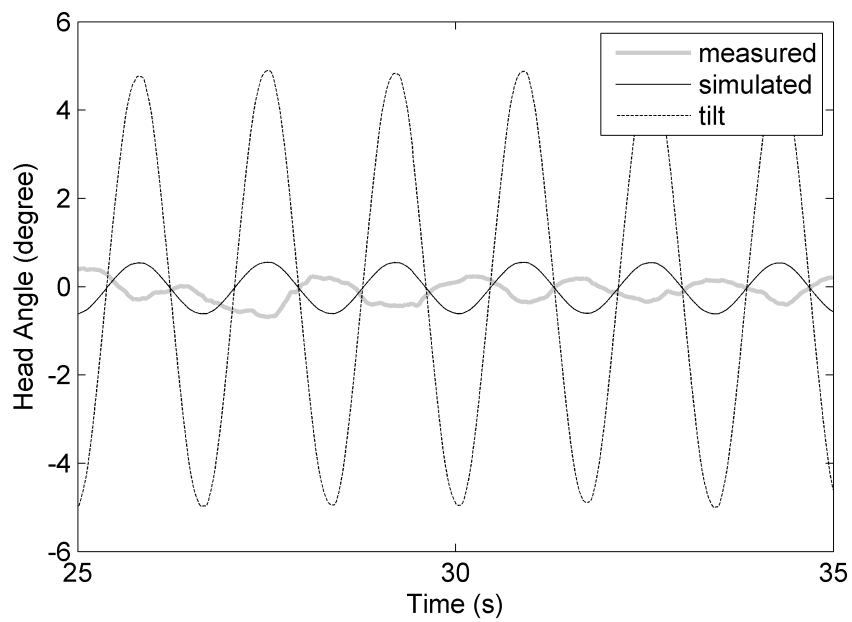
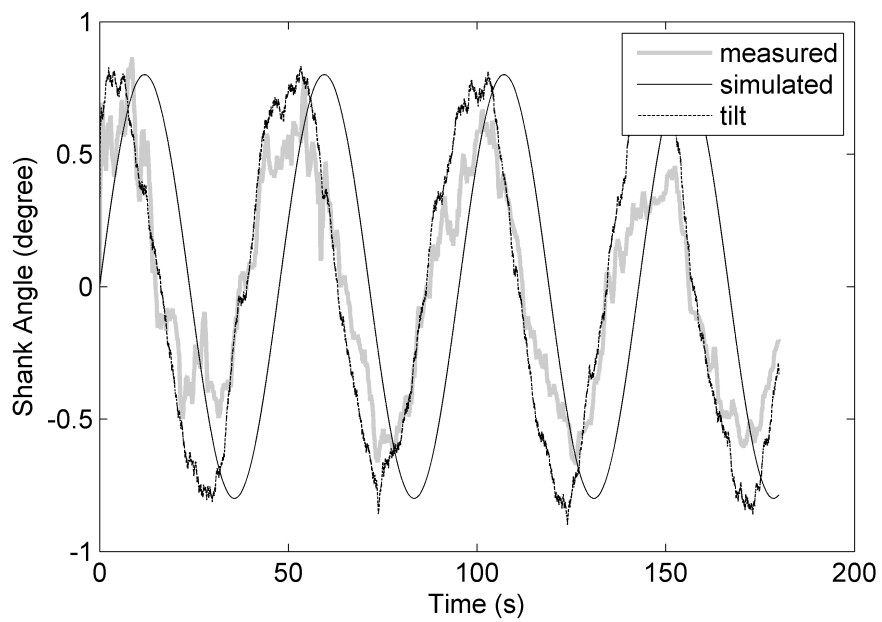Figure D.23 Head angle for subject 3 and trial 1 for 5 degrees, 0.59 Hz perturbation
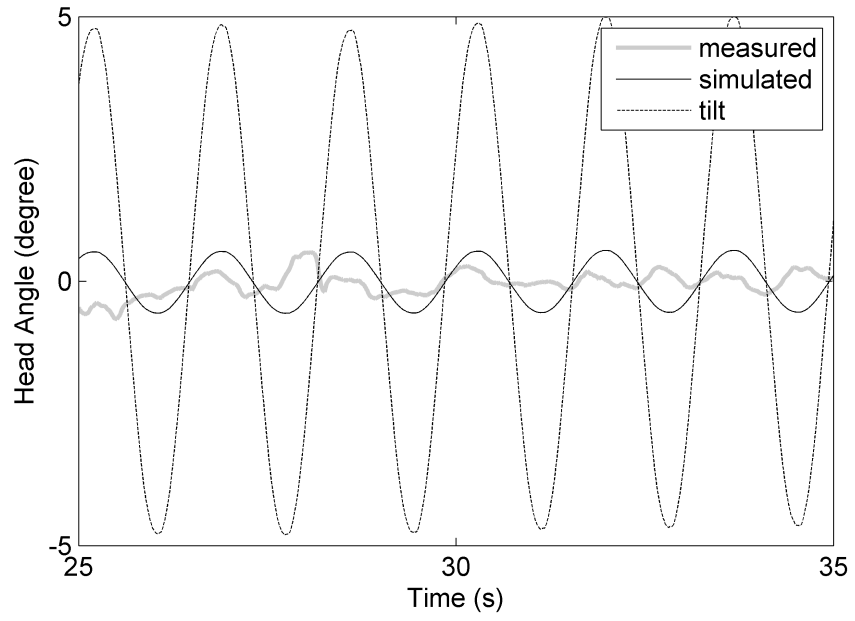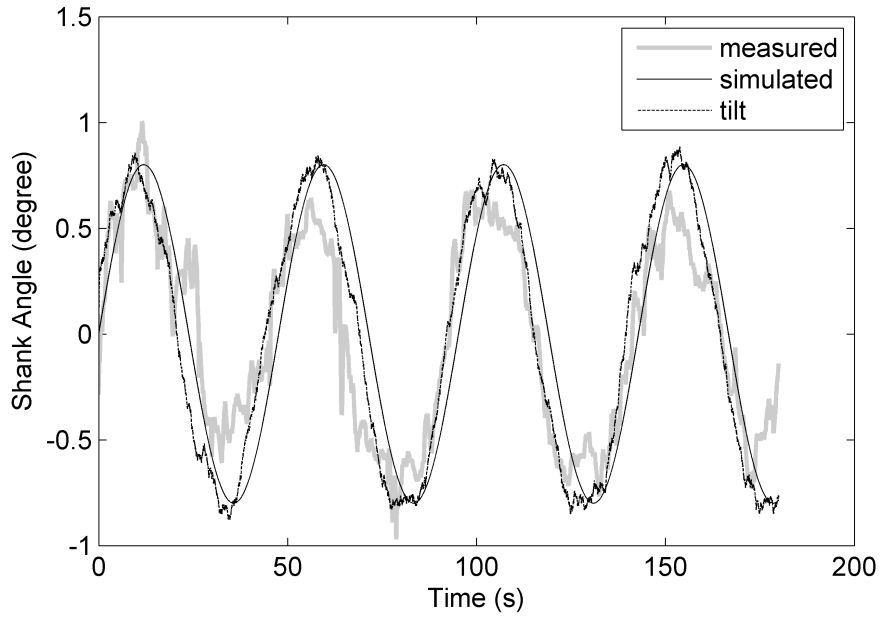
Figure D.24 Head angle for subject 4 and trial 1 for 5 degrees, 0.59 Hz perturbation
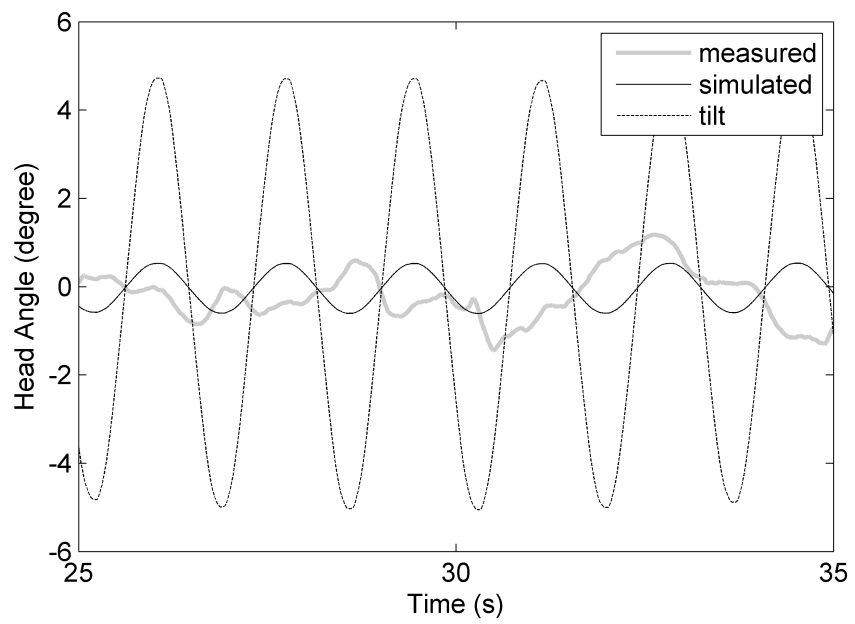
Figure D.25 Head angle for subject 5 and trial 1 for 5 degrees, 0.59 Hz perturbation
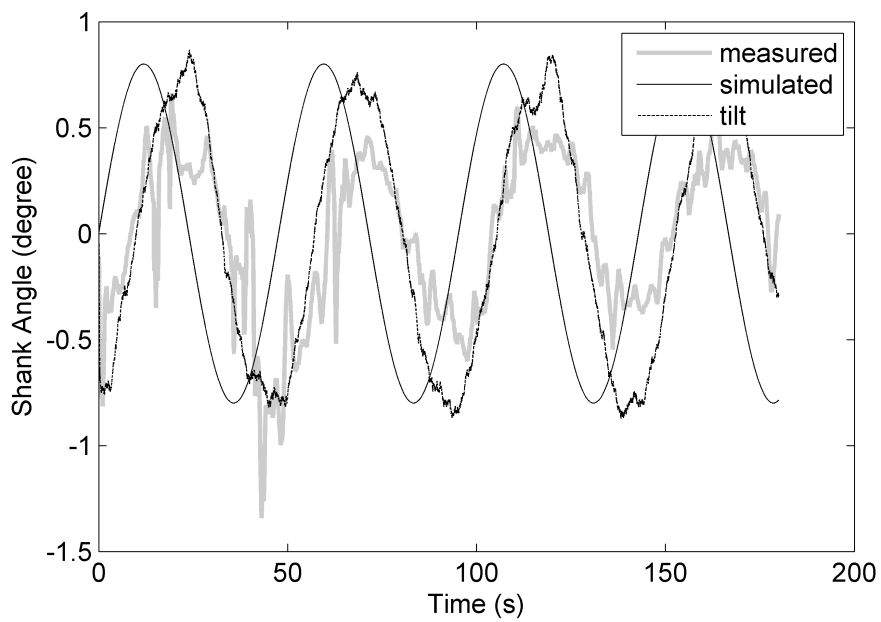
Figure D.26 Head angle for subject 6 and trial 1 for 5 degrees, 0.59 Hz perturbation

Figure D.27 Head angle for subject 7 and trial 1 for 5 degrees, 0.59 Hz perturbation

Figure D.28 Head angle for subject 8 and trial 1 for 5 degrees, 0.59 Hz perturbation

Figure D.29 Head angle for subject 10 and trial 1 for 5 degrees, 0.59 Hz perturbation

163

Figure D.30 Head angle for subject 11 and trial 1 for 5 degrees, 0.59 Hz perturbation

Figure D.31 Shank angle for subject 1 and trial 1 for 1 degree, 0.021 Hz perturbation

Figure D.32 Shank angle for subject 2 and trial 1 for 1 degree, 0.021 Hz perturbation

Figure D.33 Shank angle for subject 3 and trial 1 for 1 degree, 0.021 Hz perturbation
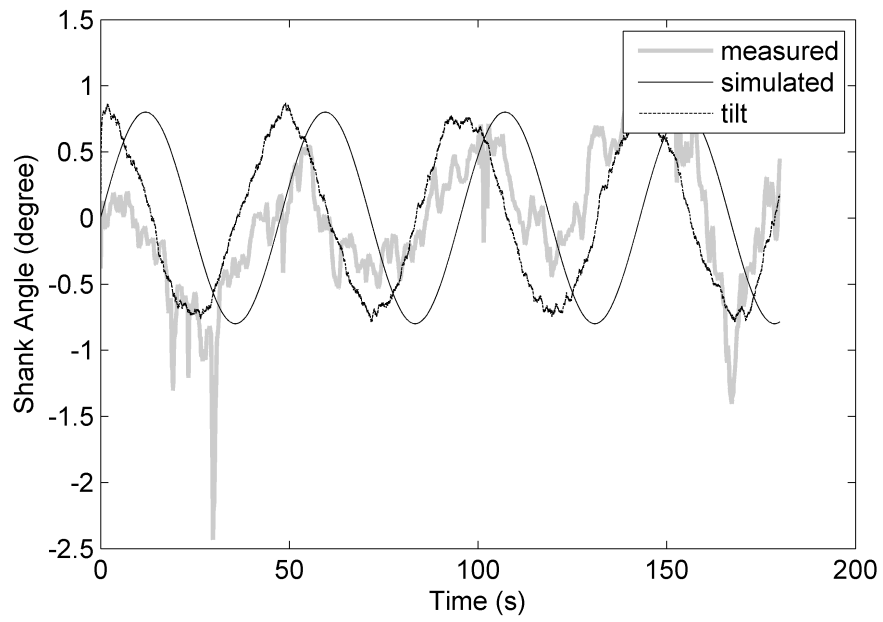
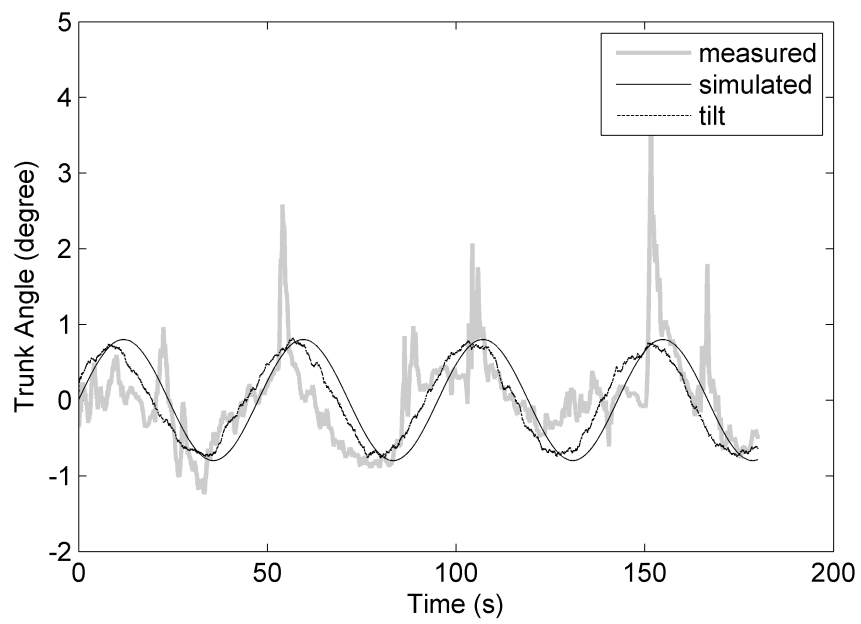Figure D.34 Shank angle for subject 4 and trial 1 for 1 degree, 0.021 Hz perturbation
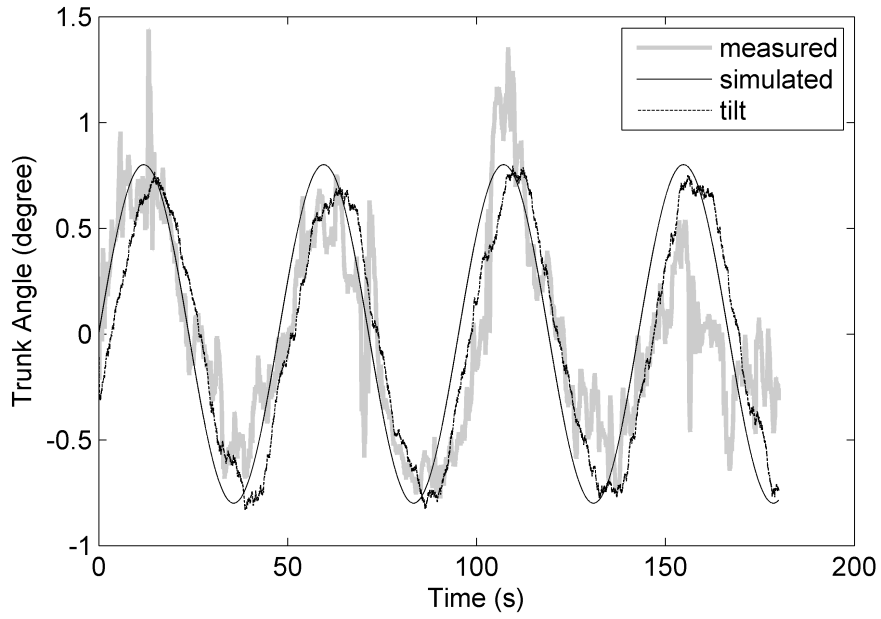

Figure D.35 Shank angle for subject 5 and trial 1 for 1 degree, 0.021 Hz perturbation

Figure D.36 Shank angle for subject 6 and trial 1 for 1 degree, 0.021 Hz perturbation

Figure D.37 Shank angle for subject 7 and trial 1 for 1 degree, 0.021 Hz perturbation
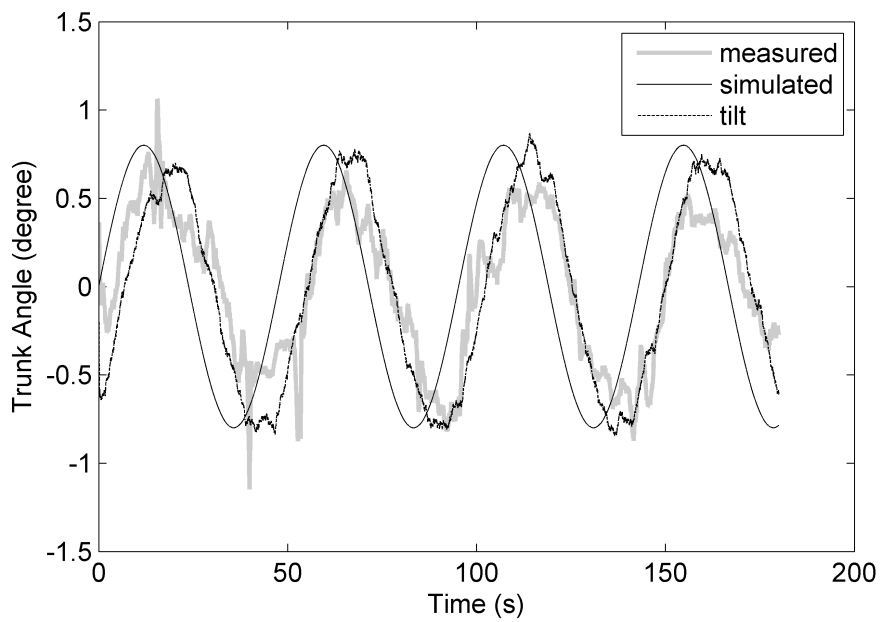
167

Figure D.38 Shank angle for subject 8 and trial 1 for 1 degree, 0.021 Hz perturbation

Figure D.39 Shank angle for subject 10 and trial 1 for 1 degree, 0.021 Hz perturbation

Figure D.40 Shank angle for subject 11 and trial 1 for 1 degree, 0.021 Hz perturbation

Figure D.41 Trunk angle for subject 1 and trial 1 for 1 degree, 0.021 Hz perturbation

Figure D.42 Trunk angle for subject 2 and trial 1 for 1 degree, 0.021 Hz perturbation

Figure D.43 Trunk angle for subject 3 and trial 1 for 1 degree, 0.021 Hz perturbation
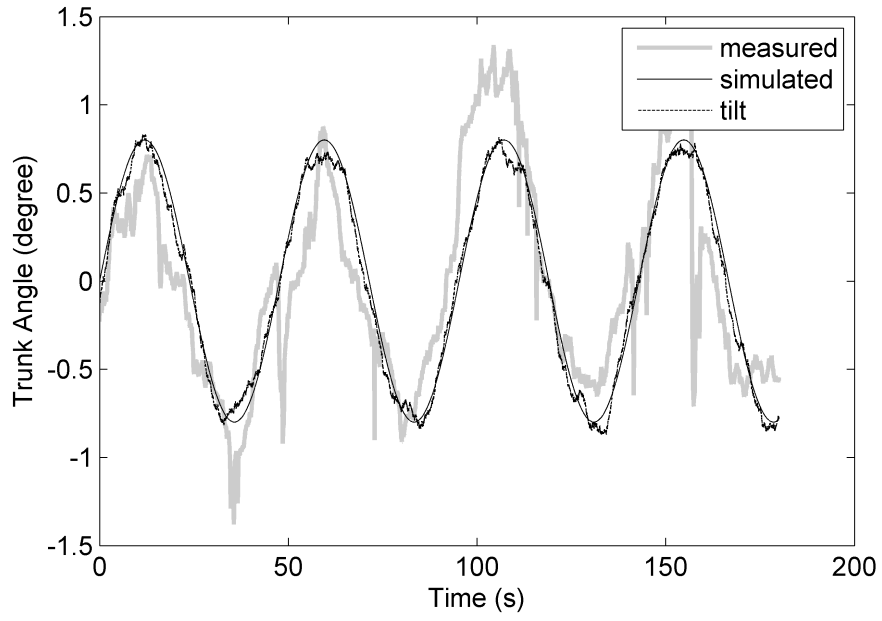
Figure D.44 Trunk angle for subject 4 and trial 1 for 1 degree, 0.021 Hz perturbation
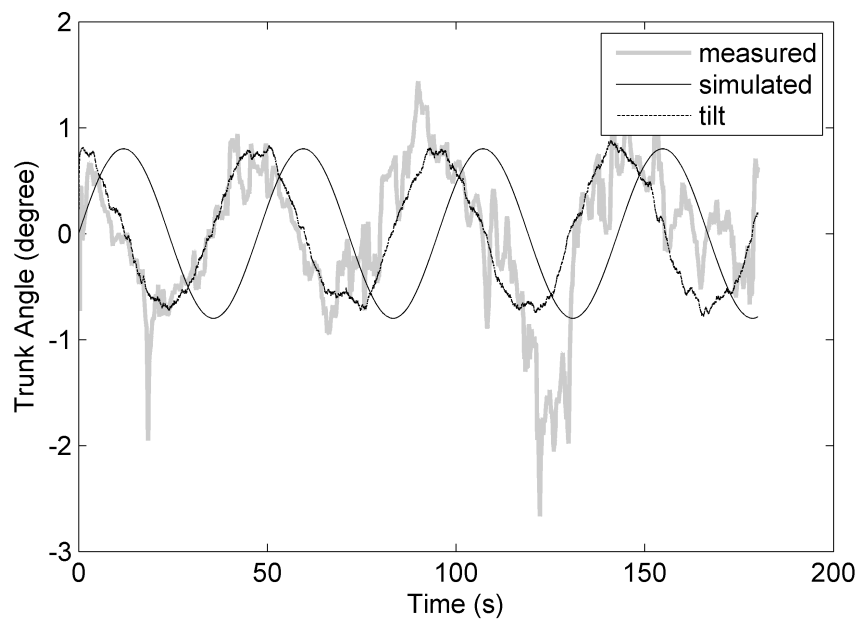

Figure D.45 Trunk angle for subject 5 and trial 1 for 1 degree, 0.021 Hz perturbation
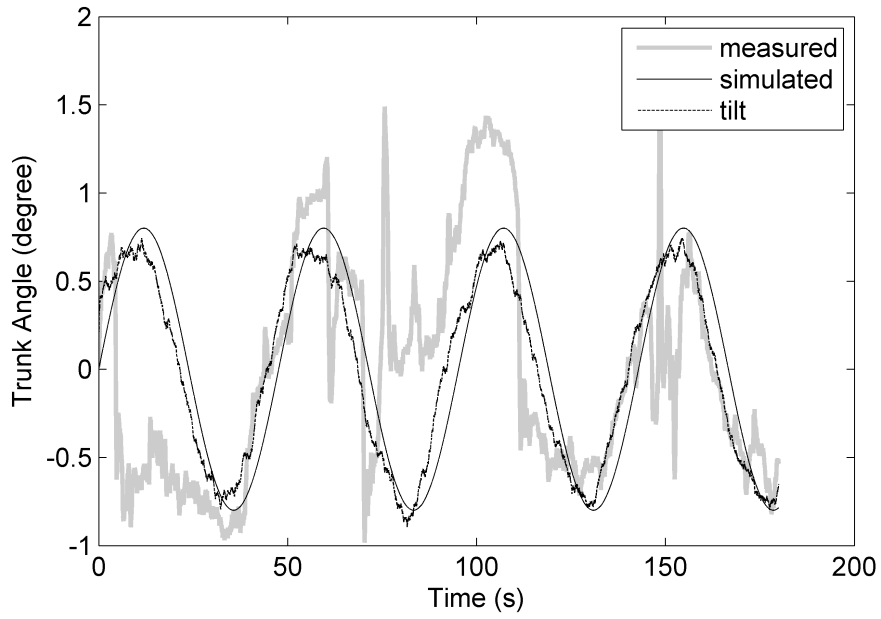
171

Figure D.46 Trunk angle for subject 6 and trial 1 for 1 degree, 0.021 Hz perturbation
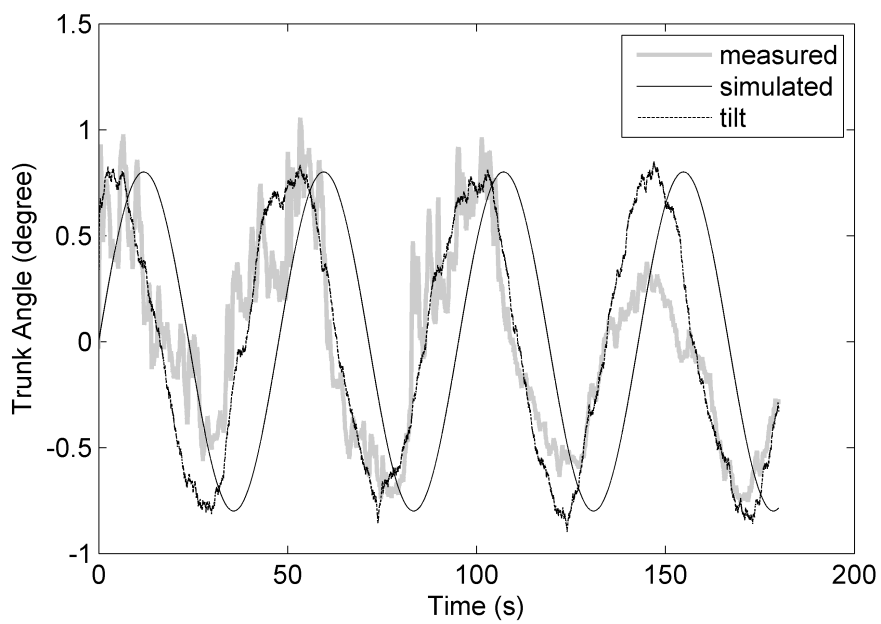

Figure D.47 Trunk angle for subject 7 and trial 1 for 1 degree, 0.021 Hz perturbation
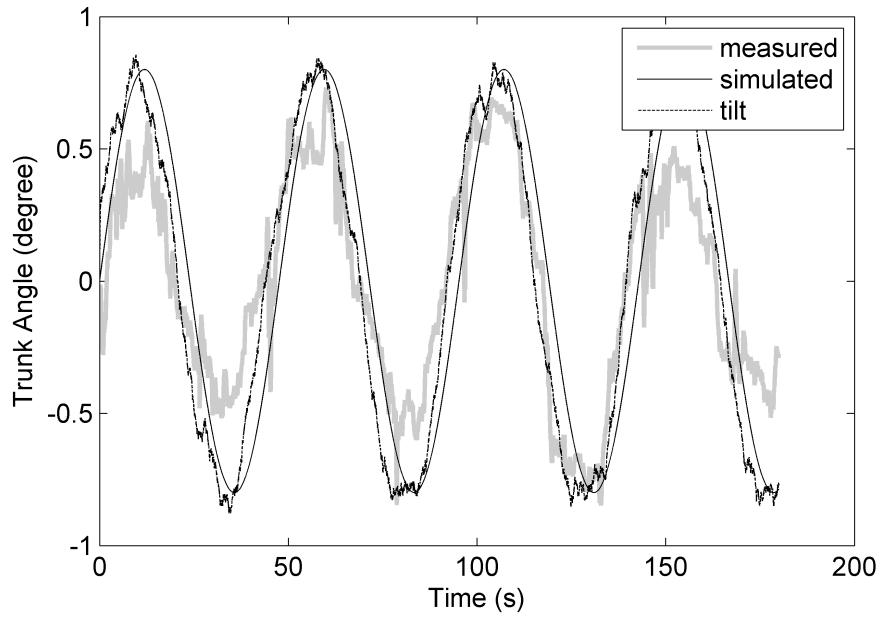
Figure D.48 Trunk angle for subject 8 and trial 1 for 1 degree, 0.021 Hz perturbation
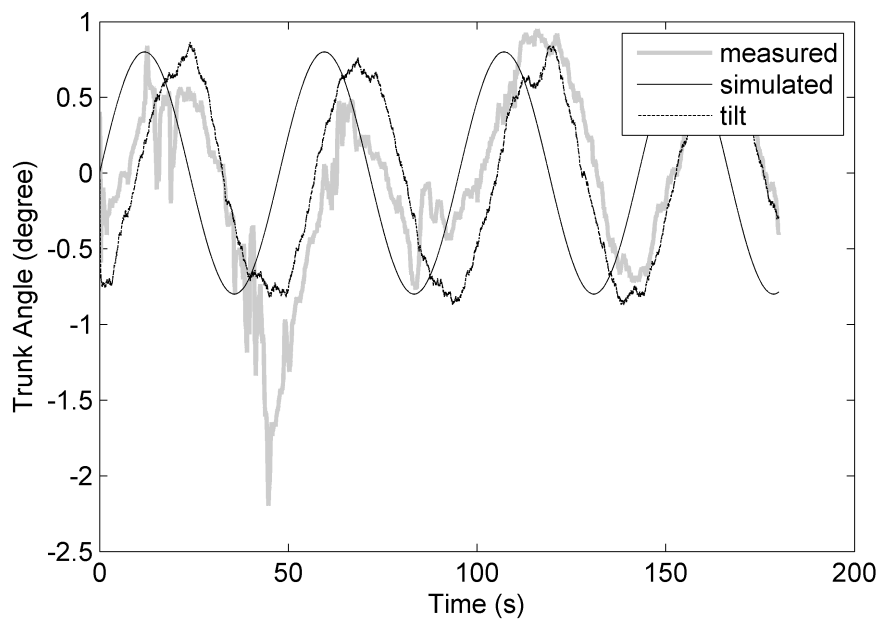

Figure D.49 Trunk angle for subject 10 and trial 1 for 1 degree, 0.021 Hz perturbation
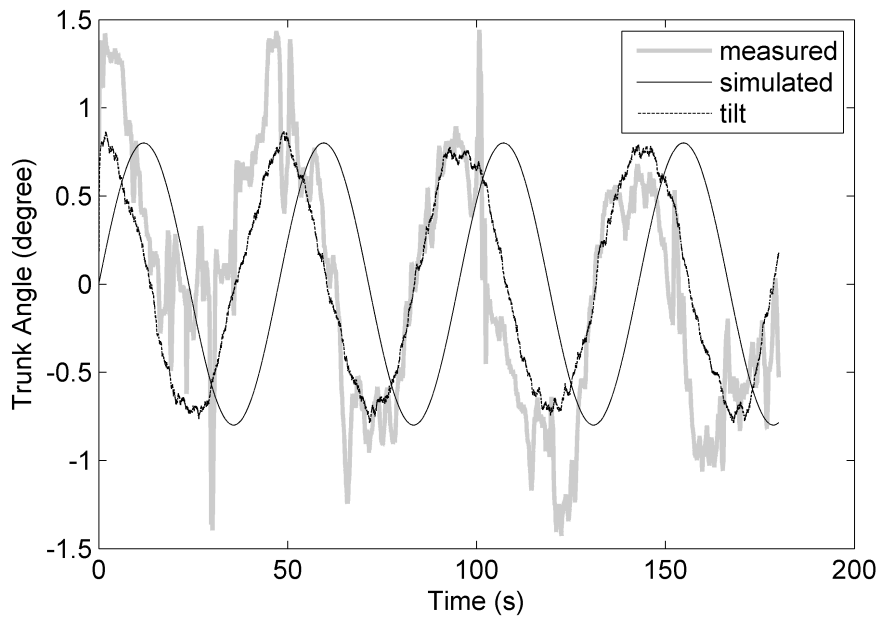
173

Figure D.50 Trunk angle for subject 11 and trial 1 for 1 degree, 0.021 Hz perturbation

Figure D.51 Head angle for subject 1 and trial 1 for 1 degree, 0.021 Hz perturbation

Figure D.52 Head angle for subject 2 and trial 1 for 1 degree, 0.021 Hz perturbation
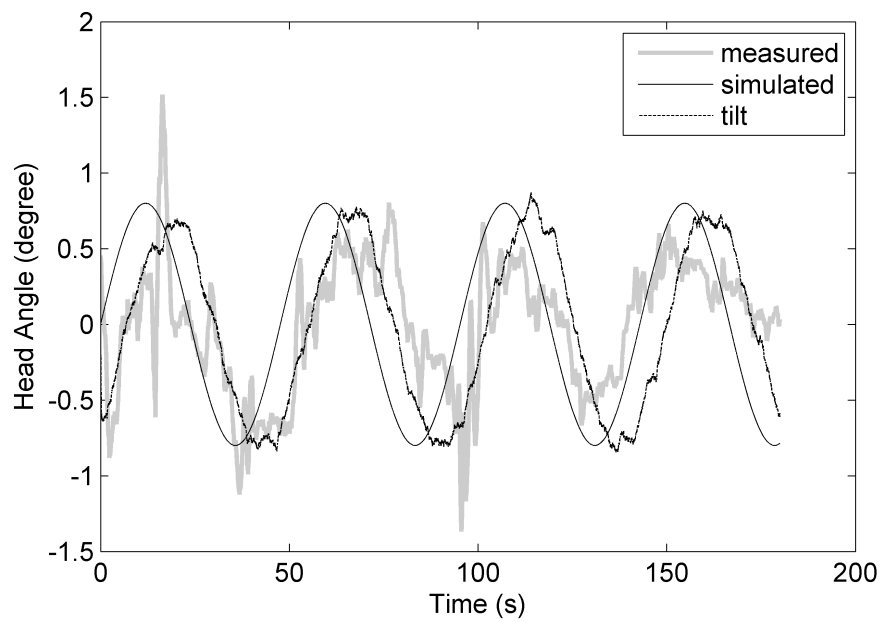
Figure D.53 Head angle for subject 3 and trial 1 for 1 degree, 0.021 Hz perturbation
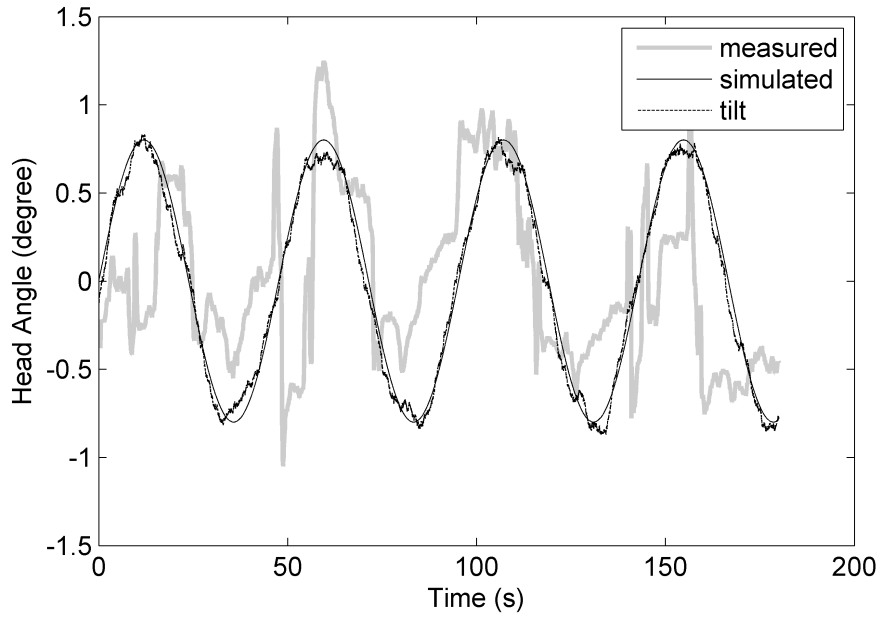
Figure D.54 Head angle for subject 4 and trial 1 for 1 degree, 0.021 Hz perturbation
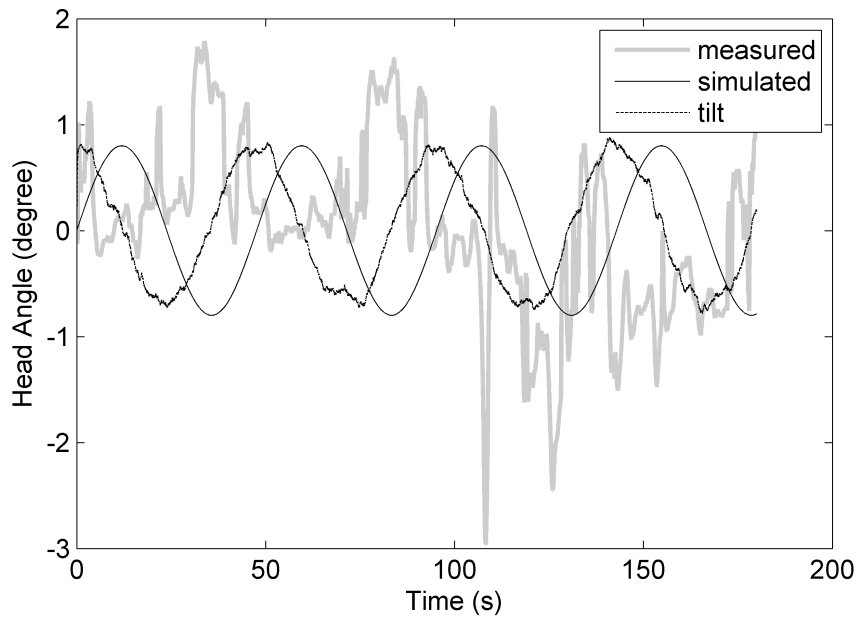
Figure D.55 Head angle for subject 5 and trial 1 for 1 degree, 0.021 Hz perturbation

176
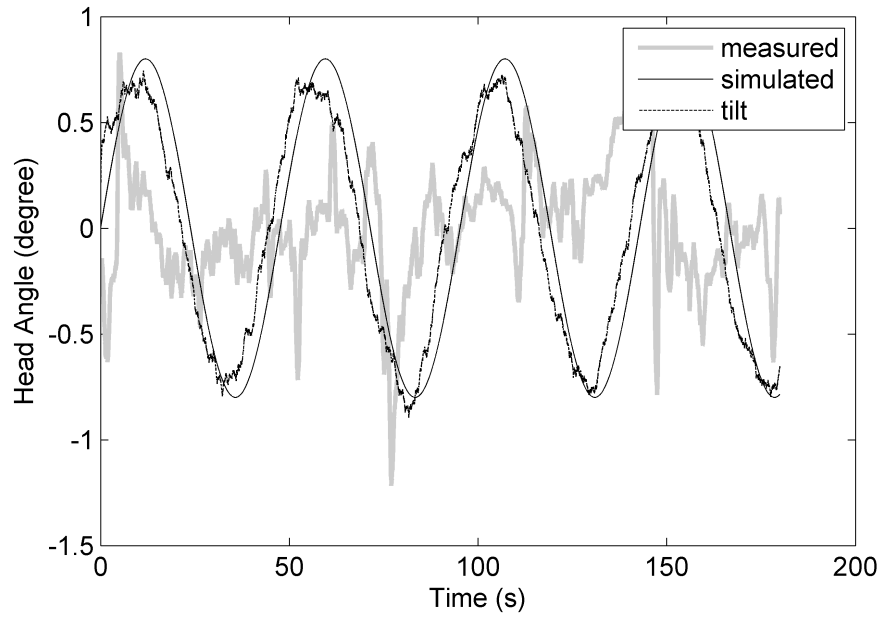
Figure D.56 Head angle for subject 6 and trial 1 for 1 degree, 0.021 Hz perturbation
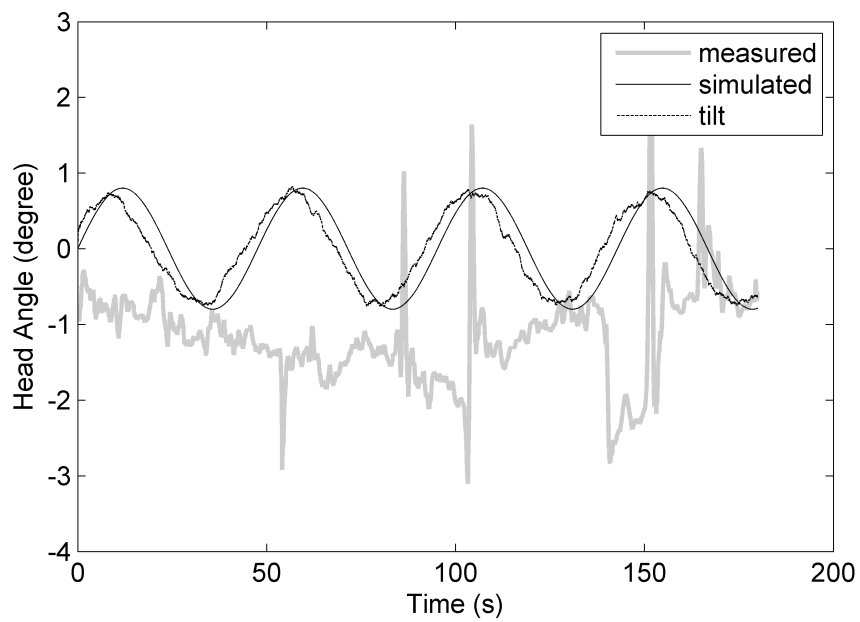

Figure D.57 Head angle for subject 7 and trial 1 for 1 degree, 0.021 Hz perturbation

Figure D.58 Head angle for subject 8 and trial 1 for 1 degree, 0.021 Hz perturbation

Figure D.59 Head angle for subject 10 and trial 1 for 1 degree, 0.021 Hz perturbation
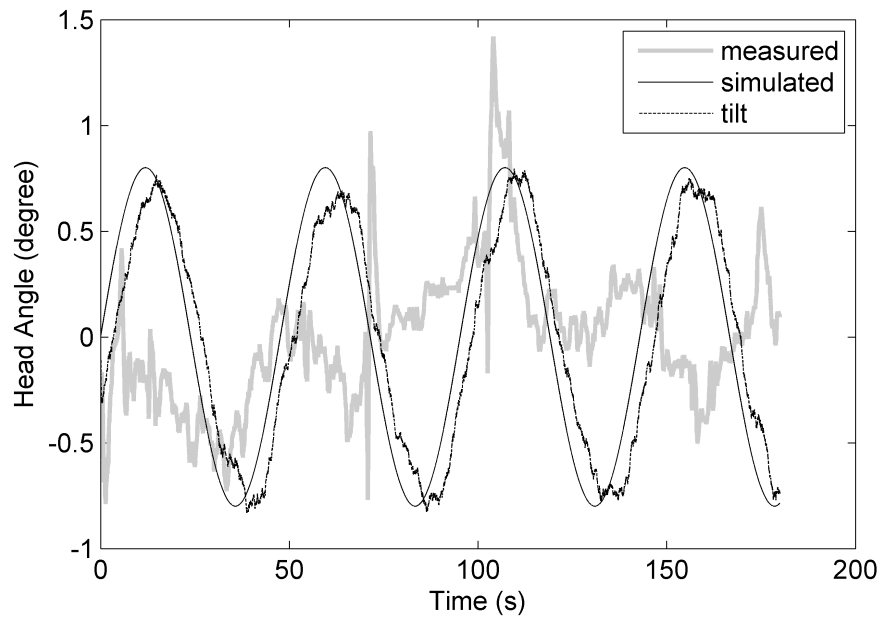
Figure D.60 Head angle for subject 11 and trial 1 for 1 degree, 0.021 Hz perturbation
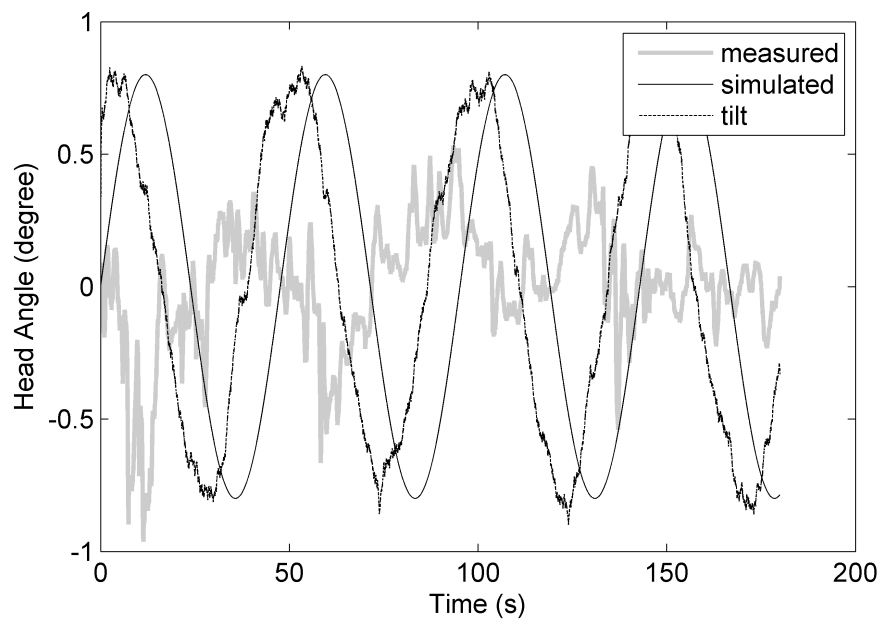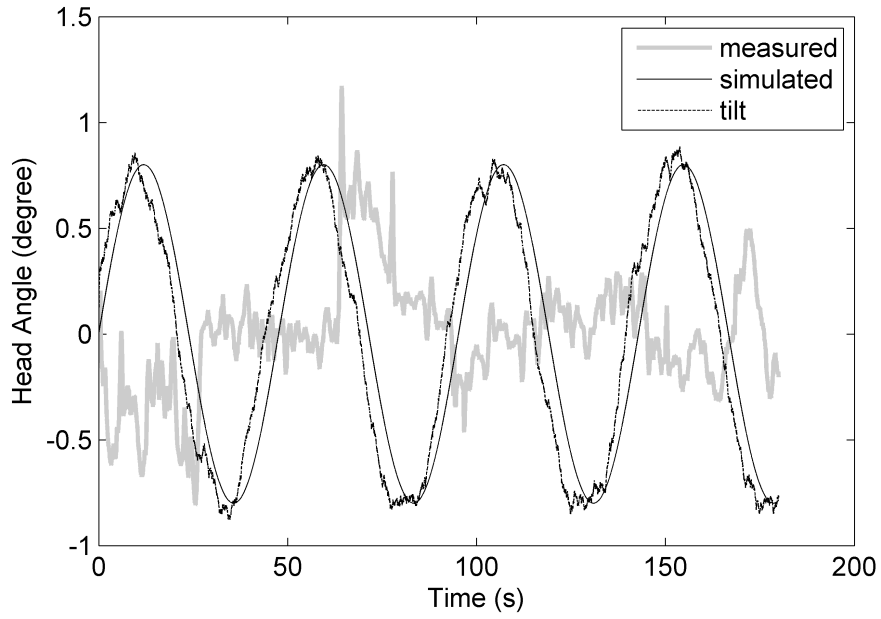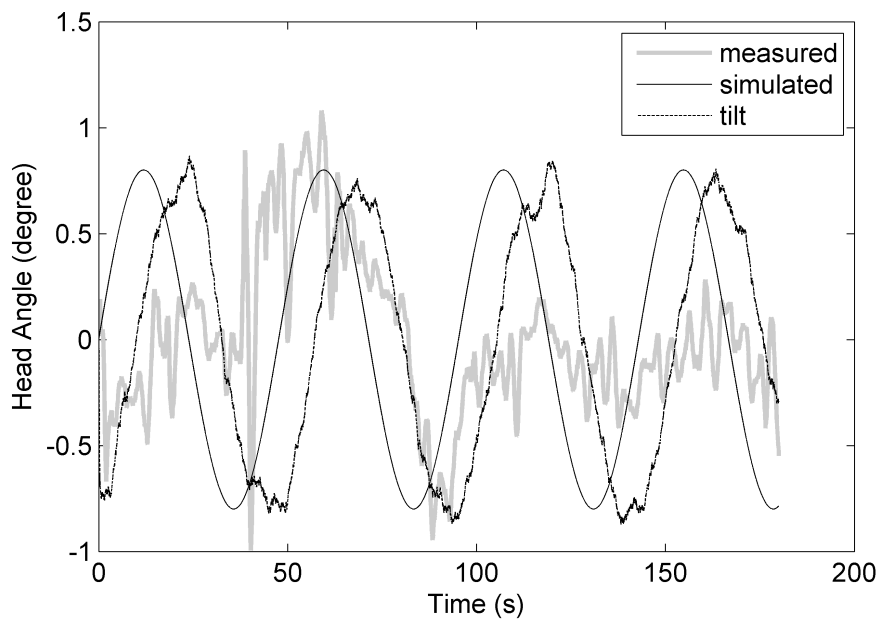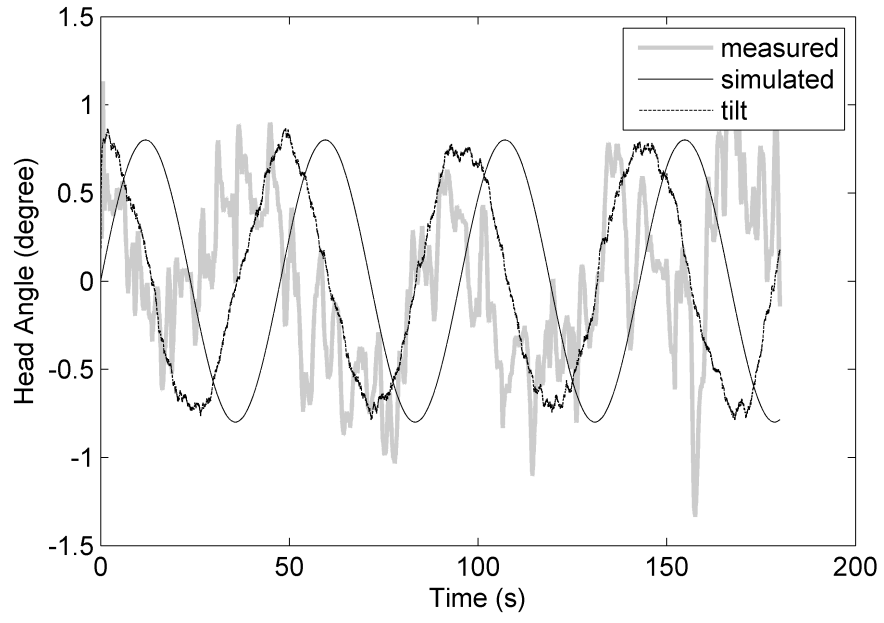
APPENDIX E

MTX SPECIFICATIONS

	MVN BIOMECH Awinda	MVN BIOMECH Link
	Completely wireless, extremely lightweight. Ideal for subject interchangeability	*High update rate. Ideal for high dynamic movement tracking*
System contents	• MVN Studio BIOMECH license • 17 wireless motion trackers (MTw) • 1 spare/prop MTw • Full-body set of straps (incl. M/L/XL T-shirt) • Awinda Station (for data transmission, docking and sync) • Awinda Dongle • MVN Ethernet Camera • Transport backpack	• MVN Studio BIOMECH license • 17 motion trackers (MTx) • 1 spare/prop MTx • 1 Lycra suit (incl. shorts) (size options: S/M/L/XL/XXL) • Body Pack • WiFi Access Point • Sync Station • MVN Ethernet Camera • Transport suitcase
Trackers	Wireless motion trackers	Wired motion trackers
Tracker placement	Easy fastening with Velcro straps	Tight and secure fastening in Lycra suit
Internal update rate	1000 Hz	1000 Hz
Update rate	60 Hz	240 Hz
Latency	30 ms	20 ms
Buffer time (retransmissions)	10 s	120 s
Battery life	6 Hours	10 Hours
Dimensions		
Motion trackers	47 x 30 x 13 mm (20 g)	36 x 24.5 x 10mm (10 g)
Body pack	N/A	160 x 72.5 x 25 mm (150 g)
Battery	N/A	94.7 x 58.5 x 25 mm (70 g)
Communication		
Range open space	Up to 50 m	Up to 150 m
Range office space	Up to 20 m	Up to 50 m
Wireless protocol	Xsens patented Awinda protocol	WiFi 2 and 5 GHz (subject to PC)
Receiver	Awinda Station / Awinda Dongle	WiFi Access Point

MVN BIOMECH Motion Tracker Performance

Orientation

Static accuracy (Roll/Pitch)	0.2 deg
Static Accuracy (Heading)	0.5 deg
Dynamic Accuracy	1 deg RMS

Tracker components

	Angular velocity	Acceleration	Magnetic field
Dimensions	3 axes	3 axes	3 axes
Full scale	± 2000 deg/s	± 160 m/s2	± 1.9 Gauss

APPENDIX F

FORCE PLATE SPECIFICATIONS

Model Designation	FP4060-10-1000	FP4060-10-2000	FP4060-10-4000
Width, mm (in)	400 (15.75)	400 (15.75)	400 (15.75)
Length, mm (in)	600 (23.62)	600 (23.62)	600 (23.62)
Height, mm (in)	100 (3.94)	100 (3.94)	100 (3.94)
Mass, kg (lb)	30 (66)	30 (66)	30 (66)
Max. Load Fz, N (lb)	5,000 (1,100)	10,000 (2,200)	20,000 (4,400)
Max Load Fx, Fy, N (lb)	2,500 (550)	5,000 (1,100)	10,000 (2,200)
Max. Load Mx, N·m (in·lb)	1,500 (13,300)	3,000 (26,600)	6,000 (53,200)
Max. Load My, N·m (in·lb)	1,000 (8,900)	2,000 (17,800)	4,000 (35,600)
Max. Load Mz, N·m (in·lb)	750 (6,600)	1,500 (13,200)	3,000 (26,400)
Natural Frequency Fz (Hz)	430	430	430
Natural Frequency Fx, Fy (Hz)	580	580	580
Static Resolution* Fz, N (lb)	±0.5 (0.11)	±1 (0.22)	±2 (0.44)
Resolution** Fz, N/LSB (lb/LSB)	0.09 (0.02)	0.19 (0.04)	0.37 (0.08)
Linearity, %FSO†	0.2	0.2	0.2

* Static Resolution is the peak-to-peak noise amplitude of the static signal.

** Resolution is given in terms of the sensitivity of the internal digitization and indicates the amount of signal produced (in N or lb) per LSB (least significant bit) of digitized signal.

† FSO : Full Scale Output

Mounting Locations, mm (in)
Foot Mount ‡ :
A = 24 (0.94), B = 29 (1.13)
C = 552 (21.74), D = 343 (13.50)

Top Mount ‡ :
A = 110 (4.33), B = 67 (2.64)
C = 380 (14.97), D = 266 (10.47)
L = 600 (23.62), W = 400 (15.75)

‡ Foot Mount version require four M8x1.25 bolts and flat washers if they are used with a Bertec Mounting Plate. For the Top Mounting option four spring loaded M8 bolts are an integral part of the force plate.
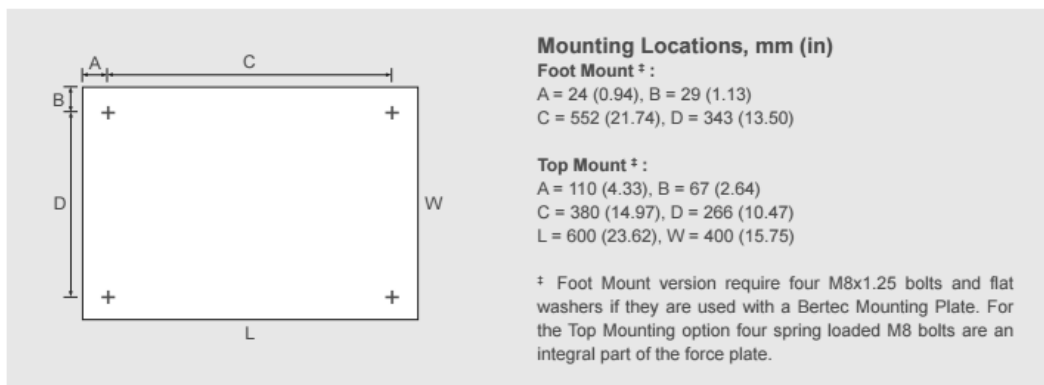
APPENDIX G

PRESSURE PAD SPECIFICATIONS

	MatScan	MatScan VersaTek	HR Mat
Sensor Model	3150	3150E	7101E
Electronics	Evolution® Handle	VersaTek® Cuff VersaTek 2-Port Hub (requires a power connection)	VersaTek® Cuff VersaTek 2-Port Hub (requires a power connection)
# of Sensels™	2,288	2,288	8,448
Active Sensing Area	43.6 x 36.9 cm (17.2 x 14.5 in)	43.6 x 36.9 cm (17.2 x 14.5 in)	48.8 x 44.7 cm (19.2 x 17.6 in)
Platform Thickness at Sensing Area	0.6 cm (0.2 in)	0.6 cm (0.2 in)	0.6 cm (0.2 in)
Sensor Resolution	1.4 sensels™ / cm² 9.2 sensels / in²	1.4 sensels / cm² 9.2 sensels / in²	4 sensels / cm² 25 sensels / in²
Scan Rates	100 Hz	440 Hz (100 Hz in wireless mode)	185 Hz (55 Hz in wireless mode)
Weight (includes all electronics, cables, power supplies)	1.7 kg/ 4.7 lb	3.3 kg/ 7.4 lb	3.5 kg/ 7.7 lb
Connection	USB 2.0*	USB 2.0*	USB 2.0*
Maximum Pressure Range	50-125 psi/ 345-862 kPa (adjustable)	50-125 psi/ 345-862 kPa (adjustable)	50-160 psi/ 345-1103 kPa (adjustable)

CURRICULUM VITAE

PERSONAL INFORMATION

Surname, Name: Akçay, Mustafa Emre

Nationality: Turkish (TC)

Date and Place of Birth: 25.01.1982, İzmir

Marital Status: Married

Phone: 0 312 210 5241

Fax: 0 312 210 2536

EDUCATION

Degree	Institution	Year of Graduation
M.S.	Middle East Technical University	2008
B.S.	Dokuz Eylül University	2004
High School	İzmir Atatürk High School	2000

PROFESSIONAL EXPERIENCE

Year	Place	Enrollment
2004-	METU Mechanical Engineering, Ankara	Research Assistant
2003-2004	DEU Mechanical Engineering, İzmir	Student Assistant

PUBLICATIONS

International Conference Publications

1. Çetin, L., Uyar, E., Akçay, E., Vision Based Reference Generator for Mobile Manipulator, DECOM07 IFAC Workshop Technology Transfer in Developing Countries, İzmir, Turkey, 2007.

2. Akçay, M.E., Gürses,S., Özgören,M.K., A Method for Analysis of Dynamic Posturographic Data, ISPGR konferansı, Trondheim, Norveç, 2012.

3. Çınar, O., Akçay, E., Yıldırım, A., Gürses S., Visual and somatosensory interaction at two different sensory environments tested by tendon vibration technique , ISPGR konferansı, Trondheim, Norveç, 2012.

4. Akçay, M.E., Gürses,S., Özgören, M.K., Decomposition Method for Dynamic Posturographic Data, ISPGR konferansı, Akita, Japonya, 2013.

5. Çınar O., Akçay, E., Yıldırım A., Gürses S., Differences in the fall responses of sedentary subjects versus contact and noncontact sportsmen due to tendon vibration at different sensory conditions, ISPGR konferansı, Akita, Japonya, 2013.

National Conference Publications

1. Uyar, E., Akçay, E.,Varol, E., Cam Temizleme Robotu Tasarımı ve İmalatı, IV. Ulusal Hidrolik Pnömatik Kongresi MMO Yayın No:E/2005/396-1 Sayfa 407-141.

2. Akçay, M.E., Gürses,S., Özgören,M.K., İnsan denge testi için bilgisayar kontrollü iki serbestlik dereceli hidrolik platform tasarımı, benzetimi ve üretimi, TOK 2011, İzmir, Türkiye.